CRANFIELD UNIVERSITY

Renata Jarzebinska

TAPERED OPTICAL FIBRE SENSORS EMPLOYING NANOSTRUCTURED COATINGS

ENGINEERING PHOTONICS GROUP
SCHOOL OF ENGINEERING

PhD Thesis

CRANFIELD UNIVERSITY

SCHOOL OF ENGINEERING

ENGINEERING PHOTONICS GROUP

PhD Thesis

Academic year 2009-2010

Renata Jarzebinska

TAPERED OPTICAL FIBRE SENSORS EMPLOYING NANOSTRUCTURED COATINGS

Supervisors: Dr Stephen W. James

Prof. Ralph P. Tatam

May 2010

ACKNOWLEDGEMENTS

Many thanks to Dr Stephen James for his guidance and support throughout whole studies, for patience and constructive comments upon draft copies of my thesis and for permanent kindliness and understanding during my illness. Thanks to Prof. Ralph Tatam for support and willingness to discuss any problems. Thanks go to the members of Engineering Photonics Group at Cranfield, all of whom helped me in one time or another. Special thanks to Dr Sammy Cheung who taught me clean-room lab work and always had patience to answer silliest questions and help with any big or tiny problem. Big thanks also to Dr Edmond Chehura for his support and willingness to help in solving problems and for many fruitful discussions about the work and remote issues. I must thank Steve Staines without whom and his diligent work my experimental setups would fall apart.

I am grateful to our collaborating group of Environmental Materials of Graduate School of Environmental Engineering of the University of Kitakyushu in Japan for extreme hospitality during my stay in Kitakyushu. Special thanks to Prof. Lee Seung-Woo for the invitation and financial support, and to Dr Sergiy Korposh for fruitful work together in laboratory – despite disastrously damaged samples at the very beginning, and for fantastic time after work – thanks for introducing me to gorgeous Japanese kitchen world!

Above all, I am extremely grateful to my husband – Witold – for permanent optimism and for being strong for us both where I am weak. Many thanks to my family for subtle support and strong belief in me.

ABSTRACT

Tapered optical fibres have been manufactured, characterised and studied. These are compact devices made from single-mode optical fibre. A system for producing tapers has been developed, employing flame heating of the optical fibre and computer controlled rotation stages to stretch the fibre in a controlled and repeatable fashion.

Subsequently tapered fibres were coated with nanostructured films of materials that change their optical properties in response to an external stimulus. An investigation of the effect of depositing chemically sensitive nano-scale films onto tapered optical fibres has been undertaken. Three different methods of deposition were applied: Langmuir-Blodgett technique, electrostatic-self-assembly and – for the first time - chemical grafting. Six different films of materials were deposited onto tapered fibres: 4-[2-(4-dimethylamino-naphtalen-1-yl)-vinyl]-1-octadecyl-quinolinium iodide (merocyanine dye), calix[4]resorcinarene, bilayers of poly(allyamine hydrochloride) (PAH) and anionic tetrakis(4-sulfophenyl)porphine (TSPP), PAH and cyclodextrine, TiO_2 nanoparticles imprinted with ((1-(4-Nitrophenylazo)-2-naphthol (NPAN) compound), polyaniline (PANI). During the deposition process the light was launched into each fibre and the evolution of the transmission spectrum observed.

The coated tapers were subsequently investigated for their potential application as chemical sensors: pH, red-ox, ammonia sensors. The response to a stimulus was investigated by immersing the coated tapered fibre in an environment containing the measurand.

The properties of these devices were also used in combination other photonics concepts, such as fibre Bragg gratings written in the tapered region of a fiber, under investigation within the Engineering Photonics Group to develop new sensor elements.

CONTENTS

INTRODUCTION

1

Among various technologies used in the photonics research field, those based on silica are of great interest [Reed, G. T. 2004 (introduction)]. The most promising applications of silicon photonics are in the fields of low-cost telecommunications and optical sensors [Kersey, A. D. 1996; Lee, B. 2003]. Silica optical fibres are widely used in optical communications, allowing transmission over long distances. The immunity to electromagnetic interference and radio frequency interference, small attenuation, large information capacity and relatively small cross-section make the fibre optic a medium of choice in industrial networks [Davies, M. G. *et al.* 1992; Miya, T. *et al.* 1979; Rolland, C. *et al.* 1992; Udd, E. 1995]. By means of measuring small changes in refractive index the fibre-optic sensors present great application potential as chemical sensors. They can operate in gaseous environment, i.e. for trace chemical detection in enclosed spaces, as well as sensors operating in liquid environment, i.e. for pH measurement, or specific chemical detection. The use of nano-structured coatings deposited onto optical fibres offer a means of controlling the transmission spectrum that changes in response to a specified external stimulus [James, S. W. *et al.* 2006]. Thin film deposition techniques, as Langmuir-Blodgett [Peterson, I. R. 1990], electrostatic self-assembly [Lenahan, K. M. *et al.* 1998], offer the ability to control the coating thickness on the nanometer scale, down to the molecular level. This facilitates the optimisation of light guided in a fibre with coating and ensures the sensing selectivity.

For some applications of optical fibres as sensors, their properties have to be tailored to have specific geometries and dimensions to allow the interaction of the propagating light with the measurand. Examples include side polished optical fibres [Bergh, R. A. *et al.* 1980] and biconical tapers [MacKenzie, H. S. *et al.* 1990]. The reduced diameter of the fibre within the tapered region of a biconical fibre taper allows the evanescent field of the propagating mode of the fibre to extend into the external environment. A particular area of interest is the deposition of functional, nano-scale optical films onto the surface of the tapered fibre. If the deposited materials change their optical properties in response to a particular stimulus, for example a specific chemical species, then the transmission characteristics of the taper will be changed, facilitating the development of new sensing capabilities, with high sensitivity and fast response.

Tapering a fibre using a heat and pull process to sub-wavelength diameter causes the fibre core to either decrease substantially in diameter or to disappear. In this case the initial cladding acts as the core, and the surrounding free space acts as the cladding. Thus the tapering allows the evanescent field of the propagating light to penetrate into the surrounding environment. The resultant ready access to the evanescent field of the propagating mode offers the potential for the development of environmental sensors with a great variety of applications in many fields of research, such as physics, chemistry, biology and materials studies. The deposition of the nano-scale coating of a functional film onto tapered fibre allows for the transmission spectrum control via the interaction of the light propagating in a fibre with the overlay material. The coating may be engineered to change the transmission spectrum in response to an external stimulus and thus sensors for a range of measurands can be manufactured. There are many deposition techniques that can be used for the deposition of functional coatings onto optical fibres, for example the Langmuir-Blodgett technique, the electrostatic-self-assembly technique, and many other chemical as well as physical processes. All mentioned above techniques are easily applied to tapered optical fibres.

Within this project we study the optical response of optical fibres to the increase of the nanostructured coating thickness deposited onto the centre of tapered region. Further investigations applied the sensing potential of the coated tapers as well in solution as in gaseous environment.

1.1 Background

A typical optical fibre is depicted in Fig. 1.1. It is composed of a light guiding region – the core, which is surrounded by a material of lower refractive index called the cladding. Immediately after fabrication the optical fibre is coated with a protective jacket, which protects a fibre from mechanical damage.

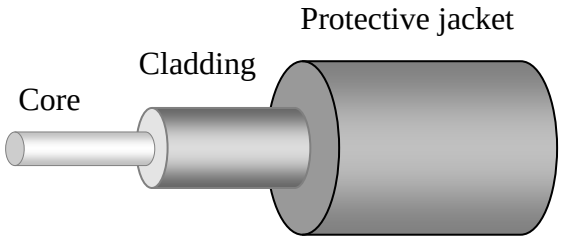

Fig. 1.1. Schematic of an optical fibre.

Fibre tapering process involves reducing the diameter of the cladding, along with that of the core, by heating and pulling the fibre's ends, see Fig. 1.2. The protective jacked is removed from the section that is to be tapered. The result of tapering is a so called fibre taper, which consists of three sections: 1) a segment where the diameter of the fibre gradually decreases (taper transition region); 2) a taper waist where the diameter is small and uniform; 3) a segment where the diameter of the fibre increases gradually (taper transition region). These regions are identified in Fig. 1.2.

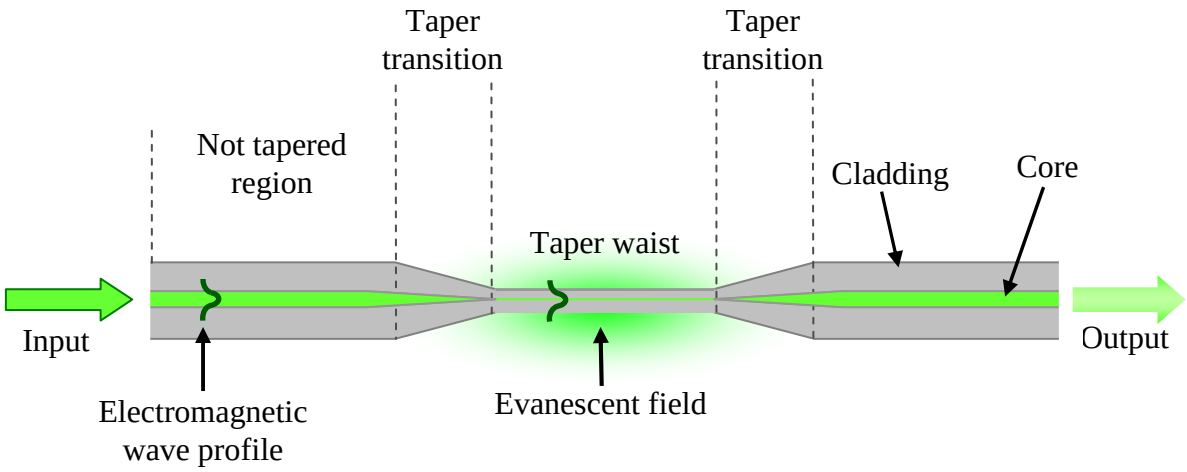

Fig. 1.2. Schematic diagram of a tapered fibre.

The most widely used methods for fabricating tapered fibres are based on flame [Moar, P.N. *et al.* 1999; Villatoro, J. *et al.* 2003] and CO_2 laser heating [Dimmick, T. E. *et al.* 1999; Bayle, F. *et al.* 2006]. Micron-sized tapers with good uniformity of their diameter are achievable using the flame heating method, but there are rigid technical requirements on gas purity, flame stability and on the vicinity of the flame. Air currents in the vicinity of the flame limit the length of the heated region of the fibre and cause non-uniform heating, which affects the taper profile and the uniformity of the taper diameter. This in turn affects the loss of light on the transformation of the local fundamental cladding mode of a tapered region from the fundamental mode of a core. The CO_2 laser technique is a more stable, controllable and safe method of heating a fibre. With this method it is possible to control precisely the length of the fibre to be heated. The main limitation of this approach is the minimum taper diameter attainable for a given CO_2 laser output power.

One approach to sensing using tapered optical fibres is the deposition of functional coatings of thickness on the nanoscale onto the tapered region of a fibre. The functional materials change their optical properties in response to an external stimulus, providing the prospect for the development of chemical sensors. Nanostructured coatings have been deposited onto optical fibres using various techniques such as: electrostatic self-assembly [Corres, J. M. *et al.* 2007], Langmuir-Blodgett [Rees, N. D. *et al.* 2002] and dip coating

[Cusano, A. *et al.* 2005]. These techniques have been used to create various optical structures and sensing configurations, for example, Fresnel interferometers by coating the cleaved ends of a fibre [Arregui, F. J. *et al.* 1999], and coupled waveguide structures [Flannery, D. *et al.* 1999] by coating a side-polished fibre. The techniques have also been successfully used to deposit nano-scale coatings onto optical fibre grating devices, in which core-cladding coupling occurs, such as long period gratings and tilted fibre Bragg gratings [Rees, N. D. *et al.* 2002; Cusano, A. *et al.* 2005; Del Villar, I. *et al.* 2005; Chehura, E. *et al.* 2006] and tapered optical fibres [Diez, A. *et al.* 2001; Pilla, P. et al, 2007]. Sensors for pH [Flannery, D. *et al.* 1999], humidity [Corres, J. M. *et al.* 2007], hydrogen [Zalvidea, D. *et al.* 2004; Zalvidea, D. *et al.* 2006; Cusano, A. *et al.* 2006], in biology for antibodies detection [Corres, J. M. *et al.* 2006] have been demonstrated using those techniques.

Tapered optical fibres with micrometer scale diameters have found a great variety of applications as sensors [Bariain, C. *et al.* 2000; Villatoro, J. *et al.* 2004; Monzon-Hernandez, M. *et al.* 2006; Diez, A. *et al.* 2001; Monzon-Hernandes, D. *et al.* 2006; Allsop, T. *et al.* 2005]. A large proportion of the light guided by the tapered region propagates outside the fibre, as an evanescent wave. Thus the effective index of the guided mode shows high sensitivity to changes in the refractive index of the surrounding region, which may be utilised in interferometric sensors [Lacroix, S. *et al.* 1988; Lacroix, S. *et al.* 1987; Gonthier, F. *et al.* 1987], or in coupled mode based systems, such as gratings written in tapered core fibres [Gonzalez-Segura, A. *et al.* 2007] or overlay waveguides [James, S. *et al.* 2006]. The tapered fibres written with the Bragg gratings are reported in section 5.5. The transmission of the fibre is sensitive to the absorption characteristics of the surrounding environment, which may be exploited for evanescent wave spectroscopy.

1.2 Aims and objectives

The main objectives of the project are the manufacture of microscale optical fibre tapers, the characterisation of their properties, study of the optical response of transmission

spectrum to the deposition of a nanostructured coatings and demonstration of their application as sensors. The goals in the realisation of the project are:

1. Design and construction of a system for tapering fibres.
2. The development of data acquisition and control system, to allow the control of the fabrication parameters
3. Manufacturing and physical characterisation (using ESEM and optical microscopy) of the optical fibre tapers.
4. Characterisation of the optical properties of the tapered fibre devices.

The novelty of the project investigation comprises:

5. The deposition of nano-scale coatings of chemically sensitive materials and study of the optical response of the transmission spectrum to the deposition.
6. Demonstration of the application of tapered fibres coated with nanostructured chemically sensitive films as sensors, with the aim of red-ox sensing and pH changes of a surrounding medium, i.e. a gas or solution, as well as for gas detection of chosen chemical species such as ammonia.
7. The fabrication and spectral characterisation of grating structures within tapered fibre devices.

1.3 Thesis organisation

The thesis is divided into six chapters. Chapter 1 presents the background of the work undertaken within the project and its main objectives. Chapter 2 provides historical introduction of the fibre optic technology and introduces tapers optical fibres, with their manufacture techniques and applicability to various thin film deposition methods. Chapter 3 offers theoretical approach describing waveguiding properties of fibres. In chapter 4 experimental setups and methods used to produce and characterise the spectral responses of tapered optical fibres are introduced. Chapter 5 presents the experimental results and Chapter 6 contains a discussion of the results and suggestions for future study.

References

Allsop, T., Floreani, F., Jedrzejewski, K., Marques, P., Romero, R., Webb, D., Bennion, I., "Refractive index sensing with long-period gratings fabricated in biconical tapered fiber", *Electronics Letters*, Vol. 41, No. 8, pp. 471-472, 2005

Arrregui, F.J., Yanjing, L., Matias, I.R., Claus, R.O., "Optical fiber humidity sensor using a nano Fabry-perot cavity formed by the ionic self-assembly method [and applications as breathing monitor]", *Sensors and Actuators B (Chemical)*, Vol. B59, No. 1, pp. 54-59, 1999

Bariain, C., Matias, I.R., Arregui, F.J., Lopez-Amo, M., "Tapered optical-fiber-based pressure sensor", *Optical Engineering*, Vol. 39, No. 8, pp. 2241-2247, 2000

Bayle, F., Meunier, J.-P., "Efficient fabrication of fused-fiber biconical taper structures by a scanned CO_2 laser beam technique", *Applied Optics*, vol. 44, No. 30, pp. 6402-6411, 2005

Bergh, R. A., Kotler, G., Shaw, H. J., "Single-mode fiber optic directional coupler", *Electronics Letters*, Vol. 16, No. 7, pp. 260-261, 1980

Chehura, E., Murphy, R.P., James, S.W., Tatam. R.P, "Tilted Fibre Bragg Gratings With Nano-structured Ovarlays", 18th International Conference of Fibre Optic Sensors, published in the *Technical Digest*, OSA, Mexico, October, 2006

Corres, J.M., Bravo, J., Matias, I.R., Arreegui, F.J., "Tapered Optical Fiber Biosensor for the Detection of anti-Gliadin Antibodies", *IEEE Sensors 2007 Conference*, 2007

Corres, J.M., Del Villar, I., Matias, I.R., Arregui, F.J., "Fiber-optic pH-sensors in long-period fibre gratings using electrostatic self-assembly", *Optics Letters*, Vol. 32, No. 1, pp. 29-31, 2007

Cusano, A., Consales, M., Cutolo, A., Penza, M., Aversa, P., Giordano, M., Guemes, A., "Optical probes based on optical fibers and single-walled carbon nanotubes for hydrogen detection at cryogenic temperatures", *Applied Physics Letters*, Vol. 89, No. 20, pp. 201106-1-3, 2006

Cusano, A., Iadicicco, A., Pilla, P., Contessa, L., Campopiano, S., Cutolo, A., Giordano, M., "Cladding mode reorganisation in high-refractive-index-coated long-period gratings: effects on the refractive-index sensitivity", *Optics Letters*, Vol. 30, No. 19, pp. 2536-2538, 2005

Davies, M. G., O'Dowd, R. F., "A new large-signal dynamic model for multielectrode DFB lasers based on the transfer matrix method", *IEEE Photonics Techmology Letters*, Vol. 4, No. 8, pp. 838-840, 1992

Del Villar, I., Matias, I.R., Arregui, F.J., Achaerandio, M., "Nanodeposition of materials with complex refractive index in long-period fiber gratings", *Journal of Lightwave Technology*, Vol. 23, No. 12, pp. 4192-4199, 2005

Diez, A., Andres, M.V., Cruz, J.L., "In-line fiber-optic sensors based on the excitation of surface plasmon modes in metal-coated tapered fibres", *Sensors and Actuators B (Chemical)*, Vol. 73, No. 2-3, pp. 95-99, 2001

Dimmick, T.E., Kakarantzas, G., Birks, T.A., Russell, St.J., "Carbon dioxide laser fabrication of fused-fiber couplers and tapers", *Applied Optics*, Vol. 38, No. 33, pp. 6845-6848, 1999

Flannery, D., James, S.W., Tatam, R.P, Ashwell, G.J, "Fibre-optic chemical sensing with Langmuir-Blodgett overlay waveguides", *Applied Optics*, Vol. 38, No. 36, pp. 7370-7374, 1999

Gonthier, F., Lapierre, J., Veilleux, C., Lacroix, S., Bures, J., "Investigation of power oscillations along tapered monomode fibers", *Applied Optics*, Vol. 26, No. 3, pp. 444-449, 1987

Gonzalez-Segura, A., Andres, M. V., Barrios, P. Rodriguez, A., "Fast response vibration sensor based on Bragg gratings written in tapered core fibers", *Measurement Science & Technology*, Vol. 18, No. 10, pp. 3139-3143, 2007

James, S. W., Tatam, R. P., "Fibre optic sensors with nano-structured coatings", Journal of Optics A: Pure and Applied Optics, Vol. 8, No. 7, pp. S430-444, 2006

Kersey, A. D., "A Review of Recent Developments in Fiber Optic Sensor Technology", *Optical Fibre Technology*, Vol. 2, No. 3, pp. 291-317, 1996

Lacroix, S., Gonthier, F., Black, R. J., Bures, J., "Interferometric properties of tapered monomode fibres", ECOC 87: 13th European Conference on Optical Communication. Technical Digest, Vol. 1, pp. 219-22, 1987

Lacroix, S., Gonthier, F., Black, R. J., Bures, J. "Tapered-fibre interferometric wavelength response - the achromatic fringe", *Optics Letters*, Vol. 13, No. 5, pp. 395-397, 1988

Lee, B., "Review of the present status of optical fiber sensors", *Optical Fibre Technology*, Vol. 9, No. 2, pp. 57-79, 2003

Lenahan, K. M., Wang, Y. X., Liu, Y. J., Claus, R. O., Heflin, J. R., Marciu, D., Figura, C., "Novel polymer dyes for nonlinear optical applications using ionic self-assembled monolayer technology", *Advanced Materials*, Vol. 10, No. 11, pp. 853-855, 1998

Mackenzie, H. S., Payne, F. P., "Evanescent field amplification in a tapered single-mode optical fiber", *Electronics Letters*, Vol. 26, No. 2, pp. 130-132, 1990

Miya, T., Terunuma, Y., Hosaka, T., Miyashita, T., "Ultimate low-loss single-mode fiber at 1.55 μm", *Electronics Letters*, Vol. 15, No. 4, pp. 106-108, 1979

Moar, P.N., Huntington, S.T., Katsifolis, J., Cahill, L.W., Roberts, A., Nugent, K.A., "Fabrication, modelling, and direct evanescent field measurement of tapered optical fibre sensor", *Journal of Applied Physics*, Vol. 85, No. 7, pp. 3395-3398, 1999

Monzon-Hernandez, D., Minkovich, V.P., Villatoro, J., High-Temperature Sensing With Tapers Made of Microstructured Optical Fiber", *IEEE Photonics Technology Letters*, Vol. 18, No. 3, pp. 511-513, 2006

Monzon-Hernandez, D., Villatoro, J., "High-resolution refractive index sensing by means of a multiple-peak surface plasmon resonance optical fiber sensors", *Sensors and Actuators B*, Vol. 115, No. 1, pp. 227-231, 2006

Peterson, I. R., "Langmuir-Blodgett films", *Journal of Physics D-Applied Physics*, Vol. 23, No. 4, pp. 379-395, 1990

Pilla, P., Giordano, M., Korwin-Pawlowski, M.L., Bock, W.J., Cusano, A., „Sensitivity characteristics tuning in tapered long-period gratings by nanocoatings", *IEEE Photonics Technology Letters*, Vol. 19, no. 19, pp. 1517-1519, 2007

Rees, N.D., James, S.W., Tatam, R.P., Ashwell, G.J., "Optical fibre long-period gratings with Langmuir-Blodgett thin-films overlay", *Optics Letters*, Vol. 27, No. 9, pp. 686-688, 2002

Rolland, C.,Tarof, L.E., Somani, A., "Multigigabit networks: the challenge", *IEEE LTS*, Vol. 3, No. 2, pp. 16-26, 1992

Udd, E., "An overview of fiberoptic sensors", *Review of Scientific Instruments*, Vol. 66, No. 8, pp. 4015-4030, 1995

Villatoro, J., Monzon-Hernandez, Luna-Moreno, M., "In-line optical fiber sensors based on cladded multimode tapered fibres", *Applied Optics*, Vol. 43, No. 32, pp. 5933-5938, 2004

Villatoro, J., Monzon-Hernandez, D., Mejia, E., "" Fabrication and modelling of uniform-waist single-mode tapered optical fiber sensors, *Applied Optics*, Vol. 42, No. 13, pp. 2278-2283, 2003

Ward, J.M., O'Shea, D.G., Shortt, B.J., Morrissey, M.J., Deasy, K., Chromaic, S.G.N., "Heat-and-pull rig for taper fabrication", *Review of Scientific Instruments*, Vol. 77, No. 8, 2006

Zalvidea, D., Diez, A., Cruz, J.L., Andres, M.V., "Wavelength mutiplexed hydrogen sensor based on palladium-coated fiber-taper and Bragg grating", *Electronics Letters*, Vol. 40, No. 5, 2004

Zalvidea, D., Diez, A., Cruz, J.L., Andres, M.V., "Hydrogen sensor based on palladium-coated fiber-taper with improved time-response", *Sensors and Actuators B (Chemical)*, Vol. 144, pp. 268-274, 2006

REVIEW OF APPLICATIONS OF OPTICAL FIBRES 2

Optical communication technology dates back two centuries, when French engineer Claude Chappe invented “optical telegraph called semaphore” for communication on land in 1790 in France. In 1835 Samuel Morse invented the telegraph and the era of electrical communications started. The use of cables for the transmission of Morse coded signals was implemented in 1844. Since that time the technology of transmitting information over large distances experienced huge steps forward. In the following years a new technology slowly arose that would solve the problem of optical transmission, although it was a long time before it was used for communications. It depended on the phenomenon of total internal reflection, which can confine light in a material surrounded by other materials with lower refractive index, such as glass in air. British physicist John Tyndall popularized light guiding in a demonstration he first used in 1854 - guiding light in a jet of water flowing from a tank. By the turn of the century, inventors realized that bent quartz rods could carry light, and patented them as dental illuminators. The development of the root optical technology led to the invention of the first optical telephone system – precursor of fibre-optics, called Photophone patented by Alexander Graham Bell in 1880 in Washington.

Fibre optic technology experienced rapid progress in the second half of the twentieth century, when it was realized that an increase of several orders of magnitude of bit rate

transmission over distance would be possible if optical waves were used as an information carrier. One of the earliest successes was the development of a fiberscope, which is a flexible bundle of optical fibres with eye piece at one end and a lens at the other. It was reported in 1954 by Abraham van Heel of the Technical University of Delft in Holland and Harold. H. Hopkins and Narinder Kapany of Imperial College in London, which separately announced imaging bundles in Nature [Van Heel, A. C. S. 1954; Hopkins, H. H. *et al*. 1954]. By this time all fibres were "bare," with total internal reflection at a glass-air interface. The key step was development of glass-clad fibres, where the core was covered with a transparent cladding of lower refractive index, by van Heel [Van Heel, A. C. S. 1954]. This protected the total-reflection surface from contamination, and greatly reduced crosstalk between fibres. Meanwhile, telecommunications engineers were seeking more transmission bandwidth and optical fibres had attracted attention. The main problem was the transmission attenuation, which at that stage was too high to make optical fibres useful in telecommunication systems. A team at Standard Telecommunications Laboratories (STL) in United Kingdom initially headed by Antoni E. Karbowiak was working on the reduction of the attenuation. A successful result on transmission improvement was announced in 1972 (Maurer, R. D., patent no. 3659915, “Fused silica optical waveguide”, 1972; Keck, D. B, Schulz, P. C., patent no. 3711262, “Optical fibers”, 1973). It was an outcome of few years of collaborative work between STL, Corning Glass Works (now Corning Inc.) and British Post Office Research Laboratories. Over the next several years, fibre losses dropped dramatically, aided both by improved fabrication methods and by the use of longer wavelengths, where fibres have lower attenuation.

In modern optical fibre telecommunication systems ultra low loss fibres are used. Due to the signal intensity loss in the long distance communisation systems an optical amplification must be used. It is accomplished by placing repeaters that receive and amplify the transmitted signal to its original intensity. Today it is done by erbium doped optical fibre amplifiers by inserting a length of 10 m of such fibre every 100 km of a main fibre, thus the signal to noise ratio is greatly improved. The great progress that has been made in the use of silica fibres for optical communications, as passive elements guiding the light, was accompanied by their application as active elements of optical systems,

providing amplification, routing and filtering of signals. By providing reliable manufacturing techniques, possibilities have been opened up for integration of devices that are useful and cheap, portable and capable of being integrated with as many functions as required. Assembled into building blocks, these objects offer great potential for developing micro- and nano-scale photonic circuits for another important application - in optical sensing. When a fibre is stretched, squeezed, heated or cooled or subjected to some other change by its local environment a measurable change in light transmission can be easily observed. Optical fibre sensors are capable of measuring a great variety of physical measurands (e.g. strain, pressure and temperature, flow, acoustic and seismic vibrations, light intensity, wavelength, phase, polarization), and chemical measurands, (e.g. contamination). Fibre optic sensors may be classified as intrinsic when the effect of measurand on the light being transmitted takes place in the fibre and extrinsic when the light modulation occurs outside the fibre. The basis of sensing a particular measurand can be different in different fibre sensors, which can be specially designed or affected in some way in order to enhance the sensitivity.

Optical fibre based temperature sensing was proposed and investigated widely by [Scheggi, A. M. *et al*. 1985; Gahler, C. *et al*. 1991; Zhang, Z. Y. *et al*. 1998; Stokes, J. *et al*. 2002; Khaliq, S. *et al*, 2002; Hajime, S. *et al*. 2007;] and many other groups. Fibre optic sensors have been also developed to measure temperature and strain simultaneously with very high accuracy [Patrick, H. J. *et al*. 1996; Wood K. *et al*. 2000; Trpkovski, S. *et al*. 2003; Chojnowski, P. *et al*. 2006; Jihong, G. *et al*. 2007; Mondale, S. K. *et al*. 2008 Soto, M. A. *et al*. 2009]. Their big advantages over other types of strain sensors are their intrinsic safety when used in explosive environments, their multiplexing capabilities (multiple sensors in a single fibre can be uniquely identified and interrogated), wide temperature operating range and are not subject to corrosion. They are capable of being used in harsh environments, for example in high-voltage, high-power machinery also in harsh weather conditions, e.g when mounted on wings of an airplane for damage and structure health monitoring as well as for strain and load detection [Takeda, N. 2008; Takeda, N. *et al*. 2007; Frazao, O. *et al*. 2009]. Fibre optic sensors are also utilized in the civil engineering area for strain monitoring in buildings. Buildings with integrated fibre optics sensors are also called “smart structures” where the strain in different parts of the structure on aging

conditions, vibrations and internal condition for the presence of particular specimens as chemical sensors is monitored. Rare-earth doped silica fibres found application in navigation systems as fibre optic gyroscopes and inertial products [Shorthill, R. W. *et al*. 1979; Burns, W. K. et al, 1984; Kim, B. Y. *et al*. 1984].

In order to facilitate the integration of devices that are useful and cheap, they must be portable and be capable of being integrated with as many functions as required. It is becoming increasingly important to find materials that can act as links between different devices based on different phenomena and operations. It is crucial to process those linkers at the micro-scale. Thus, there is a requirement to find materials and techniques which enable the creation and control of micro-scale objects. Assembled into building blocks, those objects, present a great potential for developing micro-scale photonic circuits for application in optical sensing. Over the last few years, much effort has been devoted to the fabrication of waveguides with subwavelength dimensions, made of various materials and by various techniques. Owning to their excellent uniformity and other physical properties (as strength, flexibility) tapered optical fibres have already found direct potential applications as optical couplers and wavelength division multiplexers [Osullivan, N. M. *et al*. 1992; Oakley, K. P. *et al*. 1994; Ashby, S. *et al*. 1998; Velankar, Y. P. *et al*. 2003;], filters [Lacroix, S. *et al*. 1986; Daxhelet, X. *et al*. 2001; Villatoro, J. *et al*. 2005; Hsu, K.-Ch. *et al*. 2009], polarizers [Diez, A. *et al*. 1998; Jaroszewicz, L. R. *et al*. 2001; Zhang, S. *et al*. 2009]. Another common application of tapered fibres is for use with high-powered lasers enhancing their performance [Dejneka, M. J. *et al*. 2002; Filippov, V. *et al*. 2008, Filippov, V. *et al*. 2009]. Apart from the use of tapered fibres as microelements, there are a great number of other applications as: polarization controllers, isolators, phase modulators, optical fibre amplifier, which are widely studied and documented in literature. Tapered optical fibres are also used in the sensing field. The use of tapered optical fibres for sensing physical parameters (stress, pressure, humidity) begun in 1980s [Gerdt, D. W. *et al*. 1987; Romolini, A. *et al*. 1998; Matias, I. R. *et al*. 2007]. This was later extended to analysis of chemical species, both organic and inorganic, enabled by functional coatings [Henry, W. M., 1994; Shadaram M. *et al*. 1997; Arregui, F. J. *et al*. 2000; Villatoro J. *et al*. 2005] and subsequently applied in the study of biological samples such as bio-molecules and cells

[Golden, J. P. *et al*. 1994; Cytron, S. *et al*. 2002; Hong, H. S. *et al*. 2003; Goldberg, I. *et al*. 2004; Corres, J. M. *et al*. 2008; Gravina, R. *et al*. 2009].

Recently much effort has been devoted to developing nanostructured sensitive materials for the building of evanescent wave-based sensors. Long period gratings (periodic index modulation of the refractive index of the fibre core), hollow core fibres, plastic fibres or tapered optical fibres have been used in order to be coated by a sensitive overlay for their use in sensing applications [James, S. W. *et al*. 2007; Del Villar, I. *et al*. 2008; Shadaram, M. *et al*. A comprehensive review on optical fibres coated with nanostructured films can be found in ref. [James, S. W. *et al*. 2006]. It has been shown that the deposition of a thin overlay induces important wavelength shifts in the transmission spectrum of fibre devices. The functional overlay influence on the transmission characteristics of optical fibres with long period gratings (LPGs) imprinted into a core has been widely studied by [Rees, N. D. *et al*. 2002; Del Villar, I. *et al*. 2005, Del Villar, I. *et al*. 2006, Cusano, A. *et al*. 2006, Gu, Z. *et al*. 2007; James, S. W. *et al*. 2007; Del Villar, I. *et al*. 2008; Cheung, C. S. *et al*. 2008] and revealed strong dependence of the central wavelengths of the attenuation bands on the thickness of an overlay. The influence of the coating on the properties of the modes has been thoroughly studied and theoretically described in the work of [Del Villar, I. *et al*. 2005; Del Villar, I. *et al*. 2006; Cusano, A. *et al*. 2006], where detailed discussion on the influence of the coating on the effective indices of the cladding modes is provided. It has been also presented in the theory section in chapter 3. The influence of functional nanocoatings on the transmission spectrum has been demonstrated also in side polished optical fibres [Flannery, D. *et al*. 1997], where the mode propagating in the core of the polished fibre and a mode of the coating layer are phase matched, resulting in energy transfer between the waveguides. The output power spectrum of tapered optical fibres exhibit also substantial dependence on the thickness of the sensitive nanocoatings deposited onto a narrowed region of a fibre [Corres, J. M. *et al*. 2006; Jarzebinska, R. *et al*. 2009]. For the tapers it is anticipated that the propagating mode evanescent field will extend into the surrounding environment and expected that the mode characteristics will be influence significantly by the deposition of a coating. Due to evanescent field interaction with the external medium the spectrum attenuation peaks experience a displacement to higher wavelengths. The common thing for all mentioned optical devices coated with

functional nanofilms is the need for nm scale control over film thickness in order to optimize sensors' sensitivities. For this purpose few coating techniques have been successfully utilized, like electrostatic-self-assembly, Langmuir-Blodgett technique.

2.1. Tapered optical fibres and their application

In this chapter, the basic principles and properties of tapered optical fibres are described. The main approaches to the fabrication of tapered fibres that have diameters on the micrometer scale are outlined, and the applications of tapered fibres are reviewed. Methods that may be used for coating such devices with nano-materials are outlined and their use as environmental sensors is presented.

Fibre tapering process involves reducing the diameter of the cladding, along with that of the core, by heating and pulling the fibre's ends. The result of tapering is a so called fibre taper, which consists of three sections: 1) a segment where the diameter of the fibre gradually decreases (taper transition region); 2) a taper waist where the diameter is small and uniform; 3) a segment where the diameter of the fibre increases gradually (taper transition region). These regions are identified in Fig. 2.1.

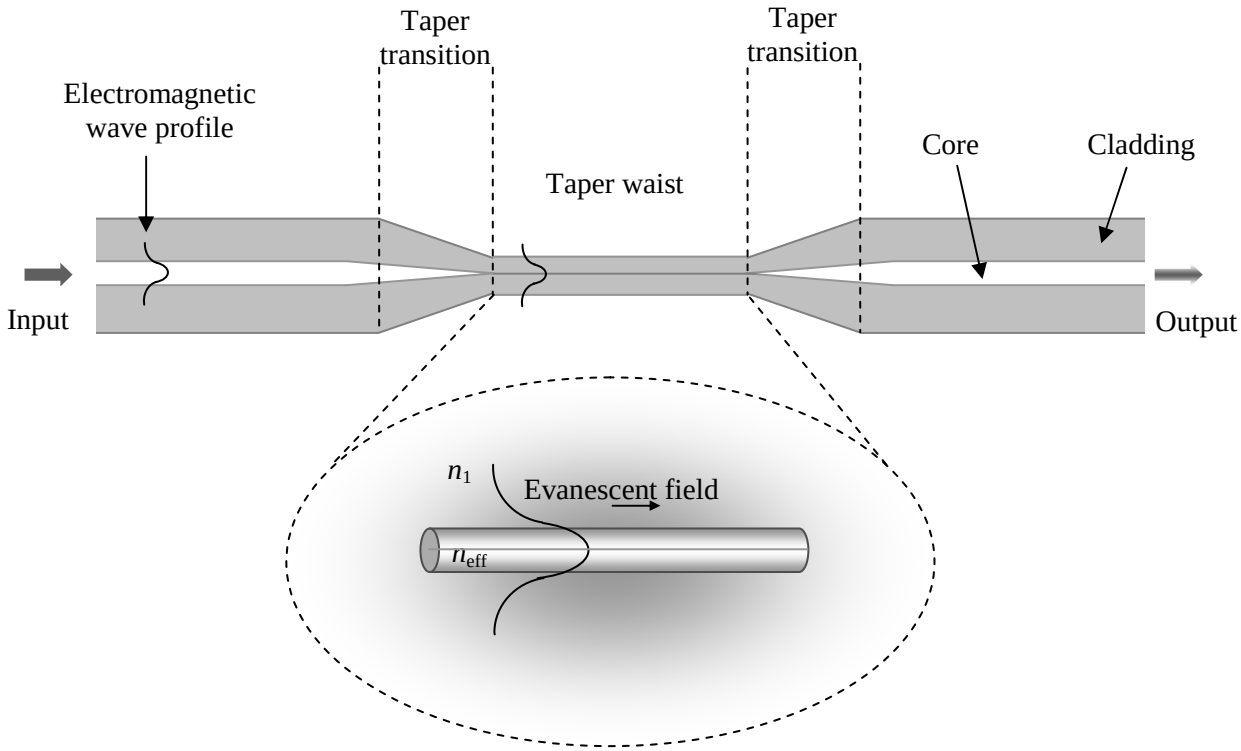

Fig. 2.1. Schematic diagram of a tapered fibre; n_1 is refractive index of the surrounding medium, n_{eff} - effective refractive index of a core mode.

2.1.1. Fibre taper fabrication techniques

Tapering is a technique where an optical fibre is heated, using a flame or other heat source, and stretched. As a result a narrow tapered waist is created, as depicted in the schematic diagram in Fig. 2.2.

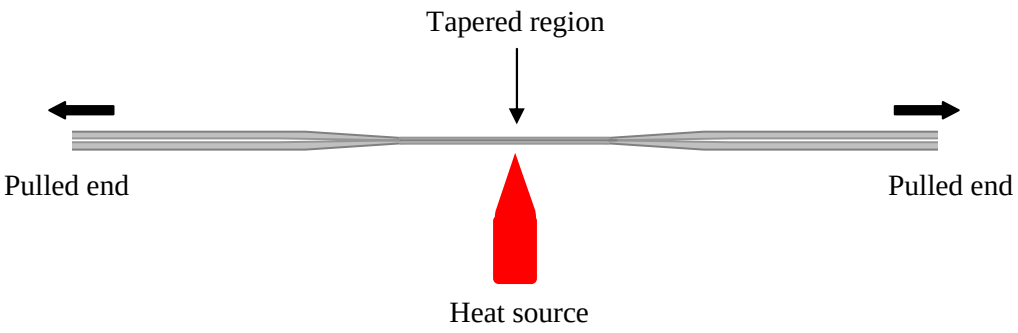

Fig. 2.2. Schematic diagram of the one-step drawing method.

The most common method used to taper optical fibres involves a heat-and-draw process, where a flame or a CO_2 laser beam is used as a heat source. The main objective of all techniques is to obtain tapers of uniform diameter with controllable parameters. Achieving these properties with flame heating based techniques introduces considerable requirements on the control of gas purity, on the flow rate and on the location of the flame. One of the most important aspects of the fabrication process is the thermal energy exchange between the heated section of fibre and the environment. If this is not carefully controlled then it can cause instability of the fibre temperature. Flame based heating can be difficult to control. Heating using the radiation from a CO_2 laser is more stable and controllable [Bayle, F. *et al.* 2005; Ward, J. M. *et al.* 2006].

Micro-taper fabrication methods

1. Burner technique

The reported travelling burner based approaches [Allsop, T. *et al.* 2005; Moar, P. N. *et al.* 1999; Villatoro, J. *et al.* 2003] consist of a heating element, which is a gas burner, mounted on a translation stage (see Fig. 2.3).

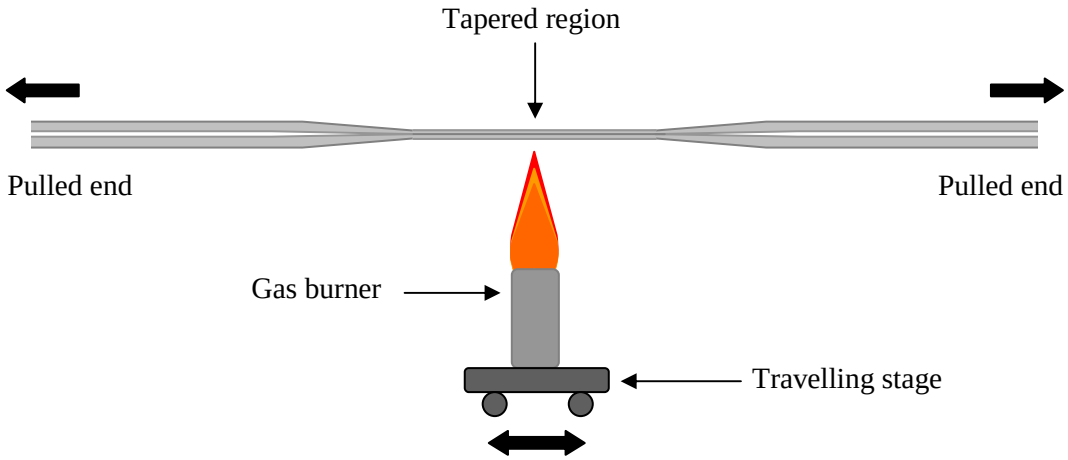

Fig. 2.3. Schematic diagram of the heating section of the taper fabrication rig used in the gas burner based technique [Villatoro, J. *et al.* 2003].

A flame, produced by mixture of methane and oxygen [Moar, P. N. *et al.* 1999] or butane and oxygen [Villatoro, J. *et al.* 2003] with the temperature of approximately 1250°C, heats a section of an optical fibre. The flame of millimetre dimensions oscillates, at a constant velocity of 2-3mm/s, over the distance from 1.5mm [Ding, J.-F. *et al.* 2005] up to several tens of milimeters [Mora, J. *et al.* 2002; Brambilla, G. *et al.* 2004] along the fibre. This ensures the constant heating of the section of the fibre to be tapered and manufacture of tapers with uniform waist diameter and taper transition of well defined length and shape [Birks, T. *et al.* 1992]. At the same time as the flame heats the fibre, the fibre is pulled with the constant speed of 5-6 mm/min [Ding, J.-F. *et al.* 2005] in opposite directions along the fibre axis. This technique facilitates the fabrication of tapers with smooth walls and low optical loss ~ 10^{-2} dB/mm [Brambilla, G. *et al.* 2004]. However, the control of the size of the taper diameter is limited by this technique, where the turbulence of the flame and air currents in the flame vicinity can produce random perturbations in waist diameters.

An alternative approach is to use a CO_2 laser for a heat source as the radiation from this laser (λ=10.6μm) is strongly absorbed by silica.

2. CO_2 laser beam technique

The use of a CO_2 laser can be the means of alleviation of "flame technique" problems. Here air currents or flame turbulence has no consequences on the precision of tapers' manufacture. Using this method it is possible to control accurately the length of the fibre to be heated. In comparison with the burner based approach, the CO_2 laser based technique is clean and free of inertia. The methods reported in [Dimmick, T. E. *et al.* 1999; Bayle, F. *et al.* 2005; Ward, J. M. *et al.* 2006] use a CO_2 laser beam (λ=10.6μm) as the heat source for tapering fibres. The laser power used ranged from 0-13W [Grellier, A. J. C. *et al.* 1998; Dimmick, T. E. *et al*. 1999; McLachlan, A. D. *et al*. 1987]. The light was focused onto the fibre by a lens, and scanned at a constant velocity of few mm/s by a mirror over a small distance (millimetres or tens of millimetres) along the fibre; see Fig. 2.4. At the same time as the laser heats the fibre, it is stretched in opposite directions. Control over the waist diameter and transition regions was achieved by varying the laser sweep throughout the taper manufacture process.

The physical process of heating a fibre using a laser beam relies on absorption of the radiation and heating from the inside. For a flame based technique the physical process involves surface heating. During laser heating, the temperature of the fibre depends on the laser power as well as on the absorption coefficient and cooling rate [Bayle F. *et al*. 2005]. This requires, as a consequence, that the laser power must be adjusted throughout the tapering process. Precise adjustments and control of the parameters of the tapering process allows the fabrication of long, uniform tapers [Bayle F. *et al*, 2005].

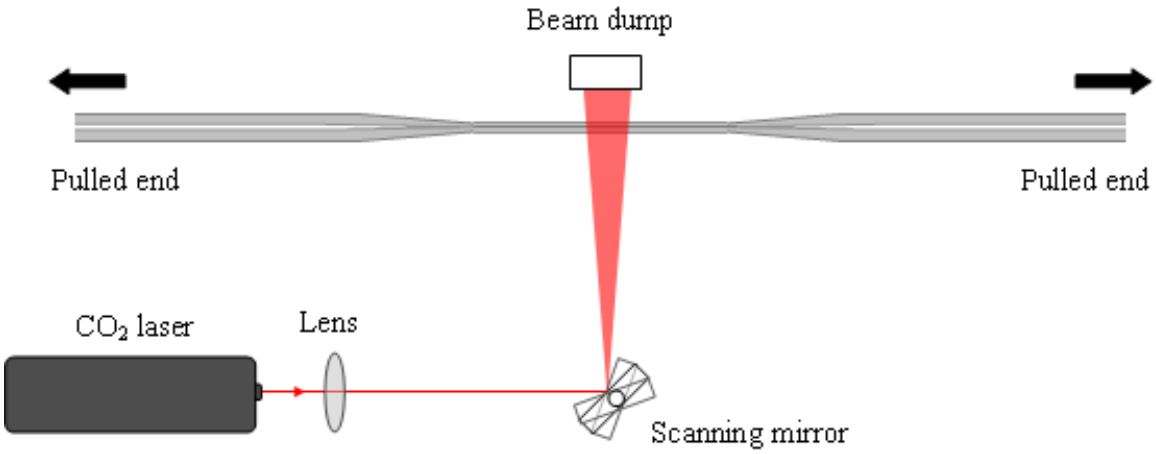

Fig. 2.4. Schematic diagram of a heating part of the taper fabrication rig used in the CO_2 laser based technique [Ward, J.M. *et al.* 2006].

After the tapering of an optical fibre three parameters of tapers are taken into account in prediction of their operation: total length of a taper (i.e. length of transition zones together with uniform diameter length), the length of the uniform diameter of a taper and the transmission loss. The length of the transition zones influences the angle of the contracting zones which controls the coupling of light between propagating mode of the single mode fibre and the modes of the tapered zone. The more efficient transfer from the mode of untapered fibre to the fundamental mode of the central part of the taper the smaller transmission loss of the guided light. The summarizing comparison is presented in Table 2. 1.

	Burner technique	**CO_2 laser based technique**
Total taper length (mm)	20 - 110	20 - 35
Length of taper uniformity (mm)	4 - 10	5 - 6
Transmission loss (dB)	0.02 - 0.15	0.01 – 0.02

Table 2.1. Comparison between tapers' parameters obtained using the two techniques: gas burner and CO_2 laser based technique.

2.2. Tapered fibre devices coated with nanostructured materials

Tapered optical fibres present a large potential for application as sensors in biology, chemistry, medicine, and have already found great applications as biosensors [Marazuela, M. D. *et al*, 2002, Corres, J. M. *et al*, 2007]. Decreasing locally the fibre diameter causes growth of the transversal dimensions of the fundamental mode, which propagates outside of the taper waist as an evanescent field (see Fig. 2.1). The evanescent field extends into the ambient medium and can be used for detection of its change. The transmission characteristics of the tapered fibres change in response to the deposition of a functional coating onto the surface of the tapered region of a fibre [Warken, F. *et al*, 2007]. If the optical properties of the coating layer are sensitive to one chemical species, or if it is designed to interact with species of a chosen shape (microstructured or molecularly imprinted coatings), then species specific chemical sensing is possible [Corres, J. M. *et al*, 2006; Zalvidea, D. A. *et al*, 2006, Corres, J. M. *et al*, 2007]. Several methods can be used for the deposition of the sensitive coatings like evaporation [Zalvidea, D. *et al*, 2006], Langmuir-Blodgett (LB) [Peterson, I. R. 1990] and electrostatic self-assembly (ESA) [Decher, G. *et al*, 1992].

2.3. Deposition techniques

Within this project, three different deposition techniques have been used for six different films of materials coating onto tapered optical fibres:

— Langmuir-Blodgett deposition of 4-[2-(4-dimethylamino-naphtalen-1-yl)-vinyl]-1-octadecyl-quinolinium iodide and calix-4-resorcinarene,

— layer-by-layer (Lbl) self assembly for: bilayers of poly(allyamine hydrochloride) (PAH) and anionic tetrakis(4-sulfophenyl)porphine (TSPP), PAH and cyclodextrine, TiO_2 nanoparticles imprinted with ((1-(4-Nitrophenylazo)-2-naphthol (NPAN) compound),

— and, for the first time applied for the coating of optical fibres, the chemical grafting technique for polyaniline (PANI) deposition.

2.3.1 Langmuir-Blodgett (LB) thin film deposition

The Langmuir-Blodgett (LB) technique is well known and extensively described in the literature, for example [Blodgett, K. 1935; Peterson, I. R. 1990] therefore a brief review on the main points is given here. In the LB method a monolayer, a single layer of molecules, of an amphihilic material is formed on the surface of water in a self-orientation process. Amphihilic molecules contain spatially separated hydrophilic (water attracting) and hydrophobic (water repelling) tail-groups. When such molecules arrive at the air-water interface, the hydrophilic parts, called also polar groups, tend to be solvated within the subphase whereas the nonpolar (hydrophobic) tails tend to stay apart. This results in molecular self-orientation with the hydrophobic tails remaining above the water surface and the hydrophilic heads submerged in the water, Figure 2.5(a).

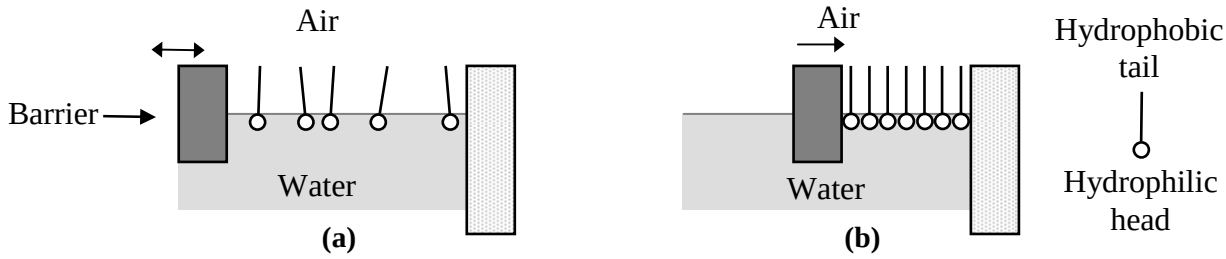

Fig. 2.5. Amphihilic molecules at the air-water interface; (a) spread material, (b) compressed monolayer.

In order to obtain a good quality film when the material is deposited onto a substrate, monolayer of floating molecules should be in the solid state phase. The initial condition after spreading the solution of molecule onto the water surface is depicted in Figure 2.5(a). A monolayer of a material is formed by applying the molecules to the surface of the subphase and the solvent is allowed to evaporate leaving molecules dispersed across the whole of the water surface. In order to achieve a regular two-dimensional solid monolayer

the surface area is being reduced by means of moving barrier and the molecules are pushed closer together. Further compression reduces the surface area occupied by each molecule close to its cross-sectional area, producing a phase where molecules are densely packed and forming an ordered array. In this phase the floating monolayer can be transferred from the water surface onto the substrate by dipping it vertically through water-air interface, Fig. 2.6.

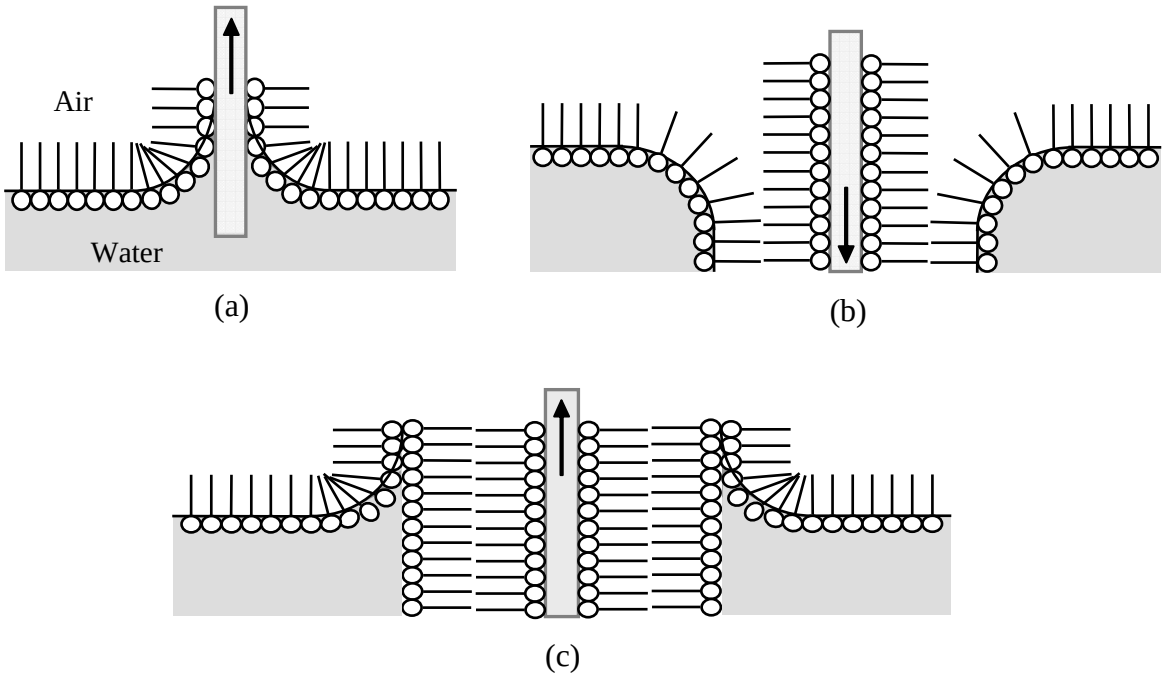

Fig. 2.6. Schematic diagram of LB monolayer deposition; (a) first layer deposition, (b) second layer deposition, (c) third layer deposition.

The LB technique enables: (i) precise control of the monolayer thickness, (ii) homogenous deposition of the monolayer over large areas, (iii) the possibility to make multilayered structures with varying layers composition. An additional advantage of the LB techniques is that monolayers can be deposited on almost any kind of solid substrate. The limitation of the technique is that monolayers material has to be a surfactant that can remain at the water/air subphase and ensure successful transfer to a solid substrate. Thus they are limited to some organic compounds. The stability of the deposited films depends on the used material.

2.3.2. Chemical deposition

Chemical deposition of a material is a controlled condensation of an individual atomic or molecular species by a chemical process. Chemical solution deposition consist in deposition of a material existing in a liquid/solution form, where a substrate acts as a physical support and does not take part in chemical reaction. The polyaniline (PANI) polymerisation is one of such methods of deposition. Creation of PANI proceeds in chemical oxidative polymerization. The material is prepared in an aqueous, acidic medium, in which the formed polymer precipitates during the subsequent reaction. In situ formation of the polymer on a substrate involves immersion of the substrate into a solution containing monomer and oxidant. After a specified period of time a polymer is formed on a substrate as a deposit. It has been shown [Mazur, M. *et al*. 2003] that in case of PANI creation the polymer is starts to form in the bulk of the solution during the first 200s of reaction. Subsequently the formation of the polymer in the bulk of the solution precedes its accumulation the substrate surface. Although the creation of polymer films is complex and places stringent requirements on the polymerization conditions of the reaction, the whole procedure is relatively easy to carry out. In order to achieve a good optical quality polyaniline film - characterized by uniform molecular weight, good and reproducible spectroscopic properties - the proper reaction conditions, namely an acidic environment and low temperature – below 0°C [Cao, Y. *et al.* 1989], should be preserved. The coating thickness is depends on the polymerization time. This technique does not ensure such high film thickness control as LB technique.

2.3.3. Electrostatic layer-by-layer (Lbl) self-assembly deposition

A variety of functional nano-films can be produced using the layer-by-layer self-assembly technique. The method has been introduced by Iler in 1966 [Iler, R. K. 1966], and subsequently developed by Decher and coworkers [Decher, G. *et al.* 1992; Lvov, Y. *et al.* 1993; Ramsden, J. J. *et al.* 1995]. Thin layers are created, based on the electrostatic interactions, by alternate immersion of a charged substrate in positively- and negatively

charged solutions as shown in the Fig. 2.7. Steps 1-4 are repeated until desired number of bi-layers is obtained. The excess of remaining solution is rinsed with water. The thickness of layers is controlled by the number of cycles and depends on molecular weight of molecules, time of deposition of each single layer, charge density, temperature, pH of solutions.

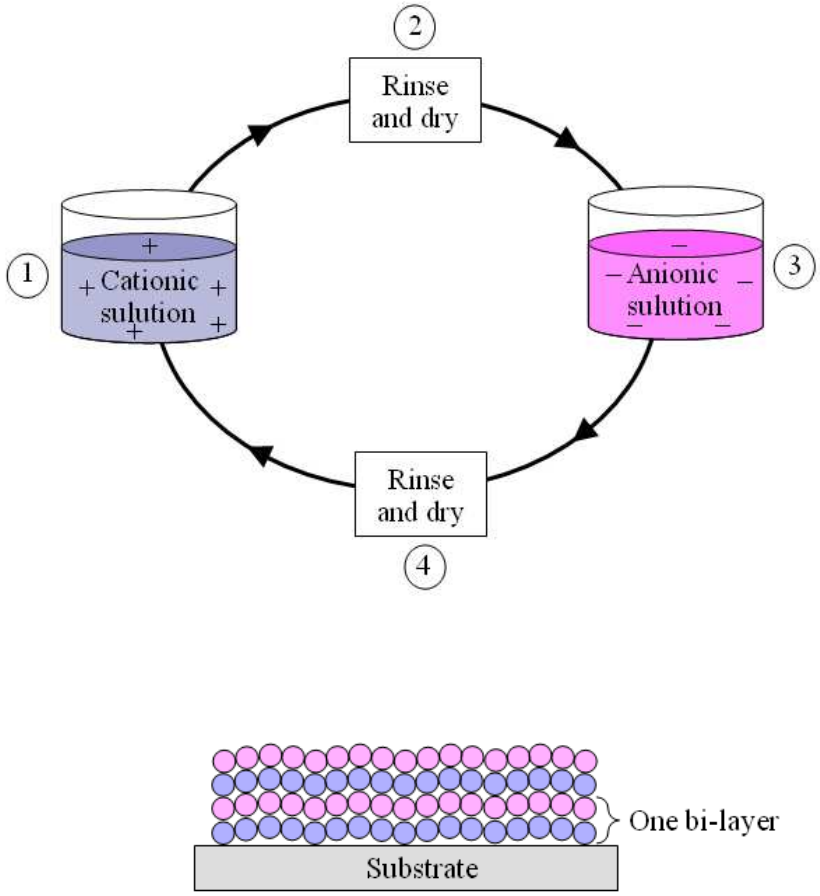

Fig. 2.7. Schematic diagram of a layer-by-layer deposition process (a); steps 1-4 are repeated until desired number of bi-layers on a substrate is obtained (b).

ESA is a method that is used for the deposition of the polymeric nano-assembled composites [Del Villar, I. *et al*. 2008; Corres, J. M. *et al*. 2006], magnetic multilayered films [Liu, Y. *et al*. 1997], electrically conductive films [Liu, Y. *et al*. 1998]. Electrostatic-self-assembly allows for the deposition of nanostructured coatings which are optically homogenous and show low scattering losses and long-term stabilities [Arregui, F. J. *et al*. 2000]. The undeniable advantage of this method is control of coating thickness down to

nm-scale, simplicity and universality. The technique is based on the attraction of opposite charges that allows for incorporation of more than two molecules into multilayer, which offers more versatility than the Langmuir-Blodgett technique. The ESA process is based on the immersion of substrates in as many solutions of polyelectrolytes as desired and facilitated deposition on substrates of various sizes, shapes and materials [Arregui, F. J. *et al*. 1999].

References

Aizawa, M., "Principles and applications of electrochemical and optical biosensors", *Analytica Chimica Acta*, Vol. 250, No. 1, pp. 249-256, 1991

Allsop, T., Floreani, F., Jedrzejewski, K., Marques, P., Romero, R., Webb, D., Bennion, I., "Refractive index sensing with long-period grating fabricated in biconical tapered fibre", *Electronics Letters*, Vol. 41, No. 8, pp. 471-472, 2005

Arregui, F. J., Cooper, K. L., Liu, Y. J., Matias, I. R., Claus, R. O., "Optical fiber humidity sensor with a fast response time using the ionic self-assembly method", *IEICE Transactions On Electronics*, Vol. E83C, No. 3, pp. 360-365, 2000

Arregui, F. J., Fernandez-Valdivielso, C., Ilundain, I., Matias, I. R., "A pH sensor made using cellulosic coating on a biconically tapered singlemode optical fiber", *Proceedings Of The Society Of Photo-Optical Instrumentation Engineers (SPIE)*, 14th International Conference On Optical Fiber Sensors, Vol. 4185, pp. 464-467, 2000

Ashby, S., Charters, R. B., Love, J. D., Ladouceur, F., Elias, M. C., "Wavelength shifts in UV-exposed single-mode fused taper fibre couplers", *Proceedings Of The Society Of Photo-Optical Instrumentation Engineers (SPIE)*, Photosensitive Optical Materials And Devices II, Conference on Photosensitive Optical Materials and Devices II, Vol. 3282, pp. 9-16,
San Jose, 1998

Bayle, F., Meunier, J.-P., „Efficient fabrication of fused-fiber biconical taper structures by a scanned CO_2 laser beam technique", *Applied Optics*, Vol. 44, No. 30, pp. 6402-6411, 2005

Blodgett, K.B., "Films built by depositing successive monomolecular layers on a solid surface", *Journal of American Chemical Society*, Vol. 57, pp. 1007-1002, 1935

Bravo, J., Matias, I. R., Del Villar, I., Corres, J. M., Arregui, F. J., "Nanofilms on hollow core fiber-based structures: an optical study", *Journal of Lightwave Technology*, Vol. 24, No. 5, pp. 2100-2107, 2006

Burns, W. K., Moeller, R. P., Villarruel, C. A., Abebe, M., "All-fiber gyroscope with polarization-holding fiber", Optics Letters, Vol. 9, No. 12, pp. 570-572, 1984

Chojnowski, P., Jedrzejewski, K. P., "Strain and temperature sensor applications of fiber Bragg gratings", *Proceedings of the Society of Photo-Optical Instrumentation Engineers (SPIE)*, Photonics Applications in Astronomy, Communications, Industry, and High-Energy Physics Experiments 2006, Vol. 6347, pp. W3470-W3470, Part 1&2, 2006

Corres, J. M., Arregui, F. J., Matias, I. R., "Sensitivity optimization of tapered optical fiber humidity sensors by means of tuning the thickness of nanostructured sensitive coatings", *Sensors And Actuators B-Chemical*, Vol. 122, No. 2, pp. 442-449, 2007

Corres, J. M., Matias, I. R., Bravo, J., Arregui, F. J., "Tapered optical fiber biosensor for the detection of anti-gliadin antibodies", *Sensors and Actuators B-Chemical*, Vol. 135, No. 1, pp. 166-171, 2008

Cytron, S., Kravchick, S., Selal, B. A., Shulzinger, E., Vasserman, I., Raichlin, Y. I., Katzir, A., "New applications of fiberoptic IR spectroscopy in urologic practice", *Proceedings Of The Society Of Photo-Optical Instrumentation Engineers (SPIE)*, Conference on Biomedical Vibrational Spectroscopy II, Vol. 4614, pp. 55-62, San Jose, 2002

Daxhelet, X., Gonthier, F.,"Optical properties of tapered fiber filters for telecommunication applications", *Proceedings of The Society of Photo-Optical Instrumentation Engineers (SPIE)*, Optical Devices For Fiber Communication II, Vol. 4216, pp. 67-77, 2001

Decher, G., Hong, J.D., Schmitt, J., "Buildup of ultrathin multilayer films by a self-assembly process: III. Consecutively alternating adsorption of anionic and cationic polyelectrolytes on charged surfaces", *Thin Solid Films*, Vol. 210-211 (PART2), pp. 831-835, 1992

Dejneka, M. J., Hanson, B. Z., Crigler, S. G., Zenteno, L. A., Minelly, J. D., Allan, D. C., Miller, W. J., Kuksenkov, D., "La2O3-Al2O3-SiO2 glasses for high-power, Yb3+-doped, 980-nm fiber lasers", *Journal of the American Ceramic Society*, Vol. 85, No. 5, pp. 1100-1106, 2002

Del Villar, I., Matias, I. R., Arregui, F. J., Lalanne, P., "Optimization of sensitivity in long period fiber gratings with overlay deposition", *Optics Experss*, Vol. 13, No. 1, pp. 56-69, 2005

Del Villar, I., Matias, I. R., Arregui, F. J., "Deposition of coatings on long-period fiber gratings: tunnel effect analogy", *Optical and Quantum Electronics*, Vol. 38, No. 8, pp. 655-665, 2006

Del Villar, I., Matias, I. R., Arregui, F. J., "Fiber-optic nanosensors by electrostatic molecular self-assembly", *Current Analytical Chemistry*, Vol. 4, No. 4, pp. 341-355, 2008

Diez, A., Andres, M. V., Culverhouse, D. O., "In-line polarizers and filters made of metal-coated tapered fibers: Resonant excitation of hybrid plasma modes", *IEEE Photonics Technology Letters*, Vol. 10, No. 6, pp. 833-835, 1998

Dimmick, T.E., Kakarantzas, G., Birks, T.A., Russell, P.St.J., "Carbon dioxide laser fabrication of fused-fiber couplers and tapers", *Applied Optics*, Vol. 38, No. 33, pp. 6845-6848, 1999

Filippov, V., Chamorovskii, Y., Kerttula, J., Kholodkov, A., Okhotnikov, O. G., "Single-mode 212 W tapered fiber laser pumped by a low-brightness source", *Optics Letters*, Vol. 33, No.13, pp. 1416-1418, 2008

Filippov, V., Chamorovskii, Y., Kerttula, J., Kholodkov, A., Okhotnikov, O. G., "600 W power scalable single transverse mode tapered double-clad fiber laser", *Optics Express*, Vol. 17, No. 3, pp. 1203-1214, 2009

Flannery, D., James, S. W., Tatam, R. P., Ashwell, G. J., "pH sensor using Langmuir-Blodgett overlays on polished optical fibers", *Optics Letters*, Vol. 22, No. 8, pp. 567-569, 1997

Frazao, O. Oliveira, R., Dias, I. " A simple smart composite using fiber Bragg grating sensors for strain and temperature discrimination", *Microwave and Optical Technology Letters*, Vol. 51, No. 1, pp. 235-239, 2009

Gahler, C., Friedrich, S., Miles, R. O., Melchior, H., "Fiber Optic Temperature Sensor Using Sampled Homodyne Detection", *Applied Optics*, Vol. 30, No. 21, pp. 2938-2940, 1991

Ge, Z., Brown, W., Sun, L., Yang, S.C., "Fiber-optic pH sensor based on evanescent wave absorption spectroscopy", *Analytical Chemistry*, Vol. 65, pp. 2335-2338, 1997

Genies, E.M., Tsintavis, C., "Redox mechanism and electrochemical behaviour of polyaniline deposits", *Journal of Electroanalytical Chemistry*, Vol. 195, No. 1, pp. 109-128, 1985

Gerdt, D.W.; Gilligan, L.H., "Variable coupler fiber optic sensor", *Proceedings of the SPIE*, Conference on Integrated Optical Circuit Engineering V, Vol. 835, pp. 25-31, San Diego, 1987

Goldberg, I., Shushan, A., Brenner, S., Nadler, B., Raichlin, Y., Shulzinger, E., Gerber, L., Katzir, A., "Infrared fiber optic spectroscopy: a novel tool for skin diagnosis", *Proceedings Of The Society Of Photo-Optical Instrumentation Engineers (SPIE)*, Conference on Biomedical Vibrational Spectroscopy and Biohazard Detection Technologies, Vol. 5321, pp. 44-50, San Jose, 2004

Golden, J. P., Anderson, G. P., Rabbany, S.Y., Ligler, F. S., "An evanescent-wave biosensor .2. Fluorescent signal acquisition from tapered fiber optic probes", *IEEE Transactions On Biomedical Engineering*, Vol. 41, No. 6, pp. 585-591, 1994

Gravina, R., Bernini, R., "Polymer optical fiber tapers for biosensing applications", *Proceedings of the SPIE*, Conference on Optical Fibers and Sensors for Medical Diagnostics and Treatment Applications IX, Vol. 7173, pp. 717305-717313, San Jose, 2009

Grummt, U.-W., Pron, A., Zagorska, M., Lefrant, S., „Polyaniline based optical pH sensor", *Analytica Chimica Acta*, Vol. 357, pp. 253-259, 1997

Gu, Z., Xu, Y., "Design optimization of a long-period fiber grating with sol-gel coating for a gas sensor", *Measurement Science & Technology*, Vol. 18, No. 11, pp. 3530-3536, 2007

Hajime, S., Hisashi, I., "Optical fiber temperature sensor using a pair of nonidentical long-period fiber gratings for intensity-based sensing ", *Optics Communications*, Vol. 280, No. 1, pp. 87-90, 2007

Henry, W. M., "An Investigation Of Coated Tapered Optical Fibers", *Sensors And Actuators B-Chemical*, Vol. 22, No. 2, pp. 101-107, 1994

Hong, H. S., Shankar, P. M., Mutharasan, R., "Evanescent sensing of biomolecules and cells", *Sensors and Actuators B (Chemical)*, Vol. B88, No. 1, pp. 67-74, 2003

Hopkins, H. H., Kapany, N. S., "A Flexible Fiberscope, using Static Scanning", *Nature*, Vol. 173, No. 4932, pp. 39-41, 1954

Hsu, K.-Ch., Chen, N.-K., Chou, S.-Y., Liaw, S.-K., Lai, Y., Chi, S., "Bandpass Filter With Variable Bandwidth Based on a Tapered Fiber With External Polymer Cladding", *IEEE Photonics Technology Letters*, Vol. 21, No. 13, pp. 935-937, 2009

Iler, R. K., "Multilayers of colloidal particles", *Journal of Colloid Interface Science*, Vol. 21, pp. 569-594, 1966

James, S. W., Cheung, C. S., Tatam, R. P., "Experimental observations on the response of 1st ans 2nd order fibre optic long period grating coupling bands to the deposition of nanostructured coatings", *Optics Express*, Vol. 15, No. 20, pp. 13096-13107, 2007

James, S. W., Tatam, R. P., "Fibre optic sensors with nano-structured coatings", *Journal of Optics. A-Pure and Applied Optics*, 1st Topical Meeting of the European-Optical-Society on Optical Microsystems - Conference, Vol. 8, No. 7, Special Issue: SI, pp. S430-S444, 2006

Jarzebinska, R. Cheung, C. S., James, S. W., Tatam, R. P., "Response of the transmission spectrum of tapered optical fibres to the deposition of a nanostructured coating", *Measurement Science & Technology*, Vol. 20, No. 3, Article Number: 034001, 2009

Jihong, G., Staines, S., Blake, M., Shibin J., "Novel distributed fiber temperature and strain sensor using coherent radio-frequency detection of spontaneous Brillouin scattering". Conference on Lasers and Electro-Optics (CLEO '07), pp. 2940 - 2940, Baltimore, MD, USA, 2007

Jin, Z., Su, Y., Duan, Y., "An improved optical pH sensor based on polyaniline", *Sensors and Actuators B: Chemical*, Vol. 71, No. 1-2, pp. 118-122, 2000

Khaliq, S., James, S. W., Tatam, R. P., "Enhanced sensitivity fibre optic long period grating temperature sensor", *Measurement Science & Technology*, Vol. 13, No. 5, pp. 792-795, 2002

Kim, B. Y.,, Shaw, H. J., "Phase-reading, all-fiber-optic gyroscope", *Optics Letters*, Vol. 9, No. 8, pp. 378-380, 1984

Lacroix, S., Gonthier, F., Bures, J., "All-Fiber Wavelength Filter From Successive Biconical Tapers", *Optics Letters*, Vol. 11, No. 10, pp. 671-673, 1986

Lindfors, T., Harju, L., Ivaska, A., "Optical pH measurements with water dispersion of polinamiline nanoparticles and their redox sensitivity", *Analytical Chemistry*, Vol. 78, no. 9, pp. 3019-3026, 2006

Lindfors, T., Ivaska, A., "All-solid-state calcium-selective electrode prepared of soluble electrically conducting po;yaniline and di(2-ethylhexyl)phosphate with tetraoctylammonium chloride as cationic additive", *Analytic Chimica Acta*, Vol. 404, No. 1, pp. 111-119, 2000 (**a**)

Lindfors, T., Ivaska, A., "Calcium-selective electrode based on polyaniline functionalized with bis[4-(1,1,3,3-tetramethylbutyl)phenyl]phosphate", *Analytica Chimica Acta*, Vol. 437, No. 2, pp. 171-182, 2001 (**b**)

Lindfors, T., Ivaska, A., "Stability of the inner polyaniline solid contact layer in all-solid-state K+-selective electrodes based on plasticized poly(vinyl chloride)", *Analytical Chemistry*, Vol. 76, No. 15, pp. 4387-4394, 2004 (**c**)

Lindfors, T., Sjöberg, P., Bobacka, J., Lewenstam, A., Ivaska, A., "Characterisation of a single-piece all-solid-state lithium-selective electrode besed on soluble conducting polyaniline", A*nalytica Chimica Acta*, Vol. 385, no. 1-3, pp. 163-173, 1999

Liu, Y.J., Wang, A.B., Claus, R.O., "Layer-by-layer electrostatic self-assembly of nanoscale Fe3O4 particles and polyimide precursor on silicon and silica surfaces", *Applied Physics Letters*, Vol. 71, No. 16, pp. 2265-2267, 1997

Liu, Y.J., Wang, A.B., Claus, R.O., "Layer-by-layer ionic self-assembly of Au colloids into multilayer thin-films with bulk metal conductivity", *Chemical Physics Letters*, Vol. 298, No. 4-6, pp. 315-319, 1998

Lvov, Y., Decher, G., Möhwald, H., "Assembly, structural characterization, and thermal behavior of layer-by-layer deposited ultrathin films of poly(vinyl sulfate) and poly(allylamine) ", *Langmuir*, Vol. 9, No. 2, pp. 481-486, 1993

Maiman, T., "Stimulated Optical Radiation in Ruby", *Nature*, Vol. 187, No. 4736, pp. 493-494, 1960

Marazuela, M.D., Moreno-Bondi, M.C., "Fiber-optic biosensors – an overview", *analytical Bioanalytical Chemistry*, Vol. 372, pp. 664-682, 2002

Matias, I. R., Arregui, F. J., Corres, J. M., Bravo, J., "Evanescent field fiber-optic sensors for humidity monitoring based on nanocoatings", *IEEE Sensors Journal*, Vol. 7, No. 1-2, pp. 89-95, 2007

Mazur, M., Tagowska, M., Palys, B., Jackowska, K., "Template synthesis of polyaniline and poly(2-methoxyaniline) nanotubes: comparison of the formation mechanisms", *Electrochemistry Communications*, Vol. 5, No. 5, pp. 403-407, 2003

Meerholz, K., Heinze, J., "Influence of chain-length and defects on the electrical-conductivity of conducting polymers", *Synthetic Metals*, Vol. 57, No. 2-3, pp. 5040-5045, 1993

Moar, P.N., Huntington, S.T., Katsifolis, J., Cahill, L.W., Roberts, A., Nugent, K.A., "Fabrication, modelling and direct evanescent evanescent field measurements of tapered optical fiber sensor", *Journal of Applied Physics*, Vol. 85, No. 7, pp. 3395-3398, 1999

Mondal, S. K., Mitra, A., Tiwari, U., Pant, J., Jain, S. C., Mishra, V., Poddar, G. C., Singh, N., Kapur, P., "Embedded dual fiber Bragg grating sensor for temperature-load (strain) discrimination", 2008 International Conference on Recent Advances in Microwave Theory and Applications (MICROWAVE-08), pp. 400-403, Jaipur, India, 2008

Oakley, K. P., Osullivan, N. M., Kenny, R. P., Hussey, C.D., "Loss and Spectral Control in Fused Tapered Couplers", *Optical Engineering*, Vol. 33, No. 12, pp. 4006-4019, 1994

Osullivan, N. M., Birks, T. A., Hussey, C. D., "Control of Polariztaion Degradation in Fiber Amplifier WDMS", *Electronics Letters*, Vol. 28, No. 17, pp. 1616-1618, 1992

Paasch, G., Nguyen, P. H., Fisher, A. J., "Potential dependence of polaron and bipolaron densities in conducting polymers: theoretical description beyond the Nernst equations", *Chemical Physics*, Vol. 227, No. 1-2, pp. 219-241, 1998

Patrick, H. J., Williams, G. M., Kersey, A. D., Pedrazzani, J. R., Vengsarkar, A. M., "Hybrid fiber Bragg grating/long period fiber grating sensor for strain/temperature discrimination", *IEEE Photonics Technology Letters*, Vol. 8, No. 9, pp. 1223-1225, 1996

Peterson, I.R. "Langmuir-Blodgett films", *Journal of physics D: Applied Physics*, Vol. 23, pp. 379-395, 1990

Pringsheim, E., Terpetschnig, E., Wolfbies, O.S., "Optical sensing of pH using thin films of substituted polyanilines", *Analytica Chimica Acta*, Vol. 357, No. 3, pp. 247-252, 1997

Pron, A., Osterholm, J.-E., Smith, P., Heeger, A.J., Laska, J., Zagorska, M., "Processable conducting polyaniline", *Synthetic Metals*, Vol. 57, No. 1, pp. 3520-3525, 1993

Ramsden, J.J., Lvov, Y.M., Decher, G., "Determination of optical constants of molecular films assembled via alternate polyion adsorption", *Thin Solid Films*, Vol. 254, No. 1-2, pp. 246-251, 1995

Rees, N. D., James, S. W., Tatam, R. P, "Optical fiber long-period gratings with Langmuir-Blodgett thin-film overlays", *Optics Letters*, Vol. 29, No. 9, pp. 686-688, 2002

Romolini, A., Falciai, R., Schena, A., "Biconically-tapered optical fiber probes for the measurement of esophageal pressure", *Sensors And Actuators A-Physical*, Vol. 70, No. 3, pp. 205-210, 1998

Scheggi, A.M., Bacci, M., Brenci, M., Conforti, G., Falciai, R., Mignani, A.G., "Compact temperature measurement system for medical applications", *Proceedings of the SPIE - The International Society for Optical Engineering*, Fiber Optic Sensors Conference, Vol. 586, pp. 110-13, Cannes, France, 1985

Shadaram, M., Espada, L., Martinez, J., Garcia, F., "Modeling and performance evaluation of ferrocene-based polymer clad tapered optical fiber gas sensors", *Optical Engineering*, Vol. 37, No. 4, pp. 1124-1129,1998

Shadaram, M., Martinez, J., Garcia, F., Tavares, D., "Sensing ammonia with ferrocene-based polymer coated tapered optical fibers", *Fiber And Integrated Optics*, Vol. 16, No. 1, pp. 115-122, 1997

Shorthill, R.W., Morris, G.J., Weaver, L.D., "Optical fiber gyroscope", *Proceedings of the 8th IFAC Symposium*, Automatic Control in Space Conference, pp. 247-250,1979

Soto, M. A., Bolognini, G., Di Pasquale, F., "Enhanced Simultaneous Distributed Strain and Temperature Fiber Sensor Employing Spontaneous Brillouin Scattering and Optical Pulse Coding", *IEEE Photonics Technology Letters*, Vol. 21, No. 7, pp. 450-452, 2009

Stokes, J., Palmer, G., "A fiber-optic temperature sensor", *Sensors*, Vol. 19, No. 8, pp. 28-31, 2002

Takeda, N., Okabe, Y., Mizutani, T., "Damage detection in composites using optical fibre sensors", *Proceedings of the Institution of Mechanical Engineers Part G-Journal of Aerospace Engineering*, Vol. 221, No. G4, pp. 497-508, 2007

Takeda, N., "Fiber optic sensor-based SHM technologies for aerospace applications in Japan" *Proceedings of the Society of Photo-Optical Instrumentation Engineers (SPIE)*, Smart Sensor Phenomena, Technology, Networks, and Systems 2008 Conference, Vol. 6933, pp. 93302-93302, San Diego, USA, 2008

Tatam, R. P., "Planar Doppler velocimetry using optical fibres", *Proceedings of the Society of Photo-Optical Instrumentation Engineers* (SPIE), Conference on Interferometry XII - Applications, Vol. 5532, pp. 50-60, Colorado, 2004

Trpkovski, S., Wade, S. A., Baxter, G. W., Collins, S. F., "Dual temperature and strain sensor using a combined fiber Bragg grating and fluorescence intensity ratio technique in Er3+-doped fiber", *Review of Scientific Instruments*, Vol. 74, No. 5, pp. 2880-2885, 2003

Van Heel, "A new method of transporting Optical Images without Aberrations", *Nature*, Vol. 173, No. 4392, pp. 39-39, 1954

Velankar, Y. P., Shadaram, M., "Tapered optical fiber for WDM applications", *Proceedings Of The Society Of Photo-Optical Instrumentation Engineers (SPIE)*, Applications Of Photonic Technology 6 - Closing The Gap Between Theory, Development, And Application, 6th International Conference on Applications of Photonic Technology, Vol. 5260, pp. 298-302, Montreal, 2003

Villatoro, J., Monzon-Hernandez, D., Mejia, E., "fabrication and modelling of uniform-waist single-mode tapered optical fiber sensor", *Applied Optics*, Vol. 42, No. 13, pp. 2278-2283, 2003

Villatoro, J., Luna-Moreno, D., Monzon-Hernandez, D., "Optical fiber hydrogen sensor for concentrations below the lower explosive limit", *Sensors And Actuators B-Chemical*, Vol. 110, No. 1, pp. 23-27, 2005

Villatoro, J., Monzon-Hernandez, D., Luna-Moreno, D., "In-line tunable band-edge filter based on a single-mode tapered fiber coated with a dispersive material", *IEEE Photonics Technology Letters*, Vol. 17, No. 8, pp.1665-1667, 2005

Ward, J.M., O'Shea, D.G., Shortt, B.J., Morrissey, M.J., Deasy, K., Chromaic, S.G.N., "Heat-and-pull rig for taper fabrication", *Review of Scientific Instruments 2006*, Vol. 77, No. 8, 2006

Wood, K., Brown, T., Rogowski, R., Jensen, B., "Fiber optic sensors for health monitoring of morphing airframes: I. Bragg grating strain and temperature sensor", Smart Materials & Structures, Vol. 9, No. 2, pp. 163-169, 2000

Zhang, S., Kopp, V. I., Churikov, V., Zhang, G., "PANDA-based in-fiber linear polarizers", *Proceedings of the SPIE*, Vol. 7212, pp. 72120D-72128D, Conference on Information: Optical Components and Materials VI, San Jose, 2009

Zhang, Z. Y., Grattan, K. T. V., Palmer, A. W., Meggitt, B. T., "Thulium-doped intrinsic fiber optic sensor for high temperature measurements (> 1100 degrees C)", *Review of Scientific Instruments*, Vol. 69, No. 9, pp. 3210-3214, 1998

THEORETICAL APPROACH 3

In this section a theoretical analysis of light propagation through optical fibres is presented. Subsequently the phenomena occurring in tapered fibres and their mathematical description is introduced followed by the waveguiding properties of tapered optical fibres coated with an overlay film.

3.1. Waveguiding properties of optical fibres

A typical optical fibre is depicted in Fig. 1.1. Light propagation along an optical fibre waveguide is described exactly by Maxwell's equations. However the classical geometric optics provides an approximate description of electromagnetic propagation. Classical geometric optics does not take into account the wave nature of light. Therefore we use the classical approach just to depict in a conceptually simple way the light propagation within an optical fibre, which is based on the phenomenon of total internal reflection. The concept is depicted in Fig. 3.1, which shows a light ray from a higher refractive index n_1 medium incident on a medium of lower refractive index n_2. The propagation of the ray is governed by the Snell's law. When the incident angle is smaller than the total internal reflection angle, θ_c, a part of ray power is transmitted into the second medium (dotted-line). There is also a reflected wave that propagates in the original medium (dashed line). When a ray is incident on an interface at an angle less than the critical angle, θ_c, refraction produces a

wave travelling parallel to the interface (solid-line). This wave has a field distribution that consists of a standing wave pattern in the first medium and a surface wave (evanescent wave) in the second medium, as shown in Fig. 3.1(a). The evanescent wave has a very small range and it disappears rapidly at a distance of few wavelengths into the second medium. When the incident angle is bigger than θ_c then the ray is totally-internally reflected back to the first medium (dashed-line).

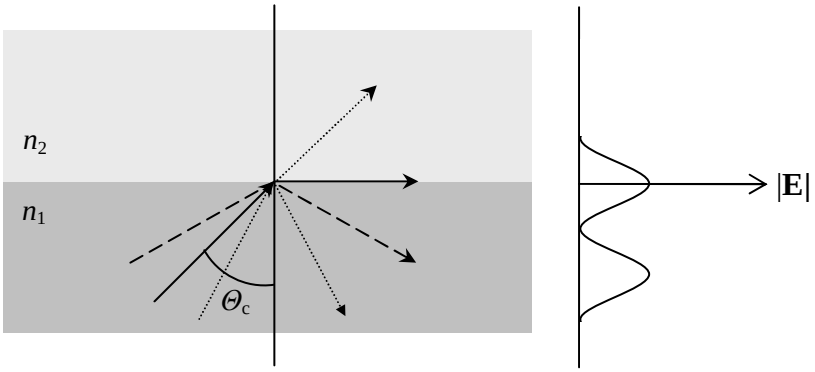

Fig. 3.1. (a) Light incident on a dielectric interface ($n_1 > n_2$), solid line arrow represents a ray incident under critical angle θ_c, dotted ray transmits to the second medium, dashed ray is totally reflected back to the first medium; (b) transverse field distribution.

The propagation of light in an optical fibre is the most conveniently described by modes of a waveguide. Physically, a mode is a three-dimensional electromagnetic field profile characterized by a propagation constant β or phase velocity $\upsilon_{p,}$ which satisfies

$$\upsilon_{pj} = \frac{\omega}{\beta_j} \tag{3.1}$$

where υ_{pj} is phase velocity of the *j*th mode, ω is the angular frequency, β_j - propagation constant of the *j*th mode.

Mathematically, modes are solutions to the source-free Maxwell's equations with the boundary conditions imposed by the waveguide geometry. Based on these, characteristic equations describing the fields in the cylindrical step-index dielectric waveguide, i.e.

eigenvalue equations, are derived [Snyder, A. *et al.* 2000]. Detailed theoretical consideration is included in appendix A.

3.2. Waveguiding properties of tapered optical fibres

For practical reasons optical fibres are divided into two major groups: single-mode fibres and multi-mode fibres; see Fig. 3.2. The division is based on the number of modes *N* that can propagate in the core. In the single-mode fibre only one mode is capable of being guided. Such a fibre has a small core diameter, typically 10μm or less. Fibres with large core diameters, 50μm or greater, are multimode fibres. Hundreds or thousands of modes can be supported in these fibres [Hunsperger, R.G. 1994; Pask, C. *et al*. 1975].

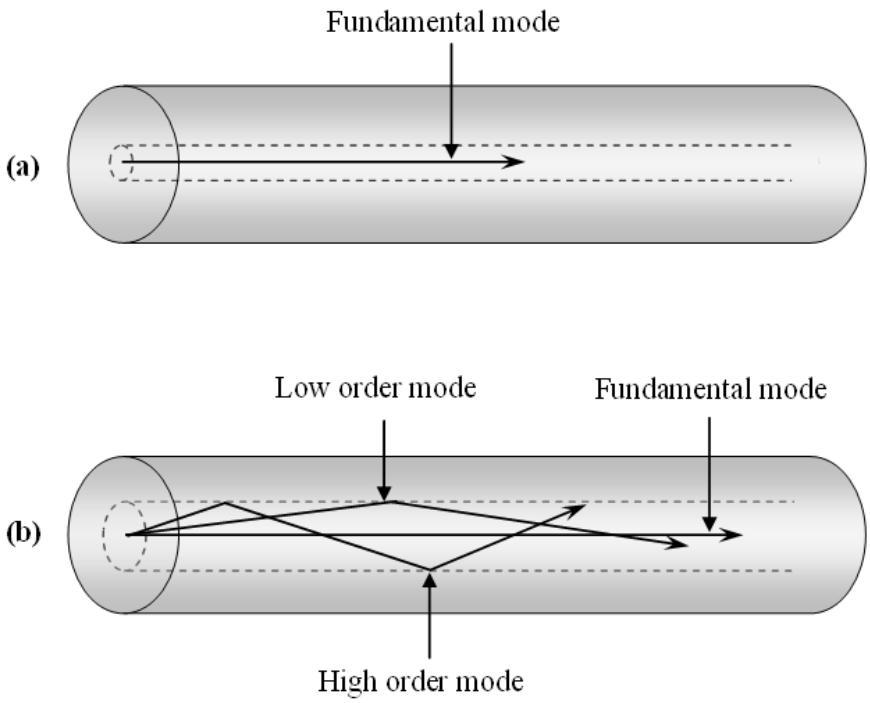

Fig. 3.2. Two major types of fibres; (a) single-mode fibre, (b) multi-mode fibre. The fundamental mode has the biggest propagation constant and is subject to the smallest number of reflections on the interface; its path is the most parallel to fibre long axis.

The fundamental mode of a fibre propagates with the largest propagation constant and subjects the smallest number of reflections from the core-cladding boundary. For

simplicity it is marked as straight line in the Fig. 3.2 in order to distinguish it from other modes.
Within this work the results for a single-mode tapered optical fibre are presented therefore larger emphasis is put on the description of single-mode fibres.

In a single-mode optical fibre, the mode field diameter is larger than the core diameter, and thus a fraction of power of the fundamental mode is guided in the cladding in the form of an evanescent wave [Hunsperger, R. G. 1994; Snyder, A. W. *et al*. 2000]. Figure 3.3 shows the electric field distribution in a single-mode optical fibre.

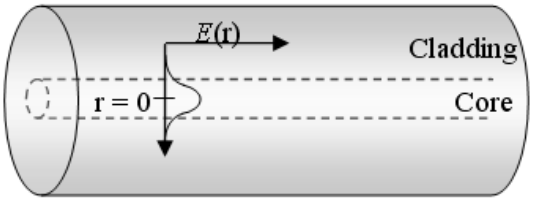

Fig. 3.3. Distribution of modal field in a single-mode fibre, r is radius distance from the long axis of the fibre, *E*(r) is modal electric field.

Tapering of a single-mode optical fibre leads to a loss of power from the fundamental core mode because of the change in the diameter along a fibre. Typical power loss was measured to be within the range 3 -10% of the initial overall transmittance [Orucevic F. *at al*. 2008; Warken, F. *at al*. 2007]. Many extensive studies have been undertaken in order to describe and explain the phenomena occurring in tapered fibres [Love, J. D. *et al*. 1991; Black, R. J. *et al.* 1991 (**a**); Black, R. J. *et al.* 1991 (**b**); Leon-Saval, S. G. *et al.* 2004].

According to the analysis presented in [Love, J. D. *et al.* part 1, 1991], to minimize the power loss through the tapered region, a small core taper angle (below 10^{-3} rad) should be used. The smaller the taper angle the longer the transition zones are. When the length of the transition is larger than the local coupling length between fundamental mode and higher order cladding modes then the power loss is small. In this case, the fundamental mode of the single mode fibre couples to the fundamental mode of the tapered region. If

the taper angle is small enough to ensure negligible attenuation of the power carried in the fundamental core mode, then the taper is termed adiabatic. In nonadiabatic tapers the fundamental core mode of the single mode fibre may couple to numerous cladding modes of the tapered region, which exists because of the high index contrast between the silica and the surrounding media [Fielding, A. F. *et al*. 1999; Black, R. J. *et al*. 1991]. The perturbation introduced by tapering causes that the mode field continues to expand as the core diameter decreases and finally reaches completely into the cladding. When the length of the transition part is smaller than local coupling length between fundamental mode and higher modes then significant coupling occurs. It has been shown [Black, R. J. *et al.* 1991 (**a**); Kieu, K. Q. *et al.* 2006] that nonadiabatic fibre tapers can be made such that coupling occurs mainly between the fundamental mode of the single mode fibre and the first two modes of the tapered part - HE_{11} and HE_{12}. The higher order modes propagate along the tapered region and, at the second taper transition, couple back to the fundamental mode LP_{01} of the single mode optical fibre. Interference between the modes produces a periodic oscillation in the transmission spectrum as a result of their different propagation constants [Love, J. D. *et al*. 1991; Black, R. J. *et al.* 1991 (**a**); Kieu, K. Q. *et al.* 2006]. The intensity at the output of the fibre depends on the relative phase $\Delta\phi = \Delta\beta \cdot l$ of the two participating modes. $\Delta\beta$ is the difference of propagation constants of the two modes and l is the interaction length along the taper. If $\Delta\beta$ or/and l change the spectral response of the fibre will change. A change in $\Delta\beta$ occurs when, for instance, the refractive index n_c of the surrounding media changes. In this case changes in the surrounding refractive index result in a differential change in the effective refractive indices n_{eff} of the two modes propagating in the tapered region which are related to the propagation constants by

$$\beta = \frac{2\pi}{\lambda} n_{\text{eff}} , \tag{3.2}$$

where λ is the free space wavelength.

3.3. Waveguiding properties of coated tapered optical fibres

The phenomenon of the coupling of the fundamental LP_{01} mode to the HE_{11} and HE_{12} modes and back which occurs the taper waist of non-adiabatic tapers has been studied in this project towards prospective sensors creation. The differential response of the propagating modes within the taper waist to the index change in the surrounding environment has classified uncoated tapered single-mode optical fibres as good candidates for sensing applications, measuring parameters such as temperature, refractive index of surrounding media [Kieu, K. Q. *et al.* 2006]. As an extension of those studies we investigate the applicability of tapered optical fibres as pH sensors and to measure the concentration of chosen chemical species. For this purpose the tapered region of a single-mode optical fibre is coated with thin film of sensitive material. The tapered fibre's transmission spectrum is monitored as the increase of the thickness of the coating changes its optical properties. Thus the optical response of the tapers to the environmental stimulus is studied. See Fig. 3.4.

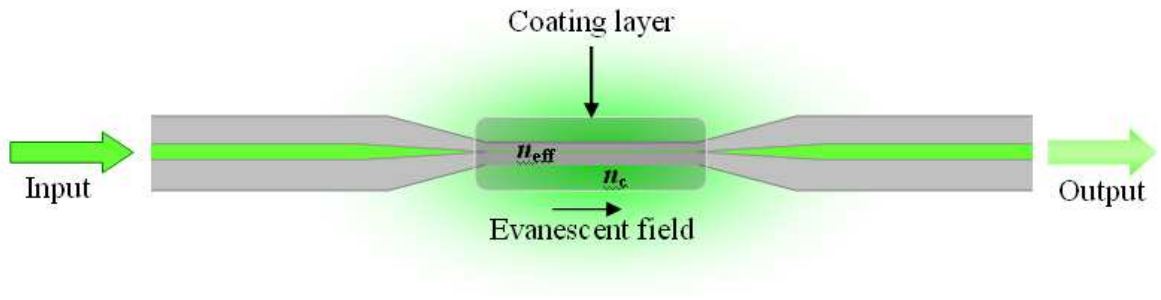

Fig. 3.4. Schematic diagram of a tapered region of an optical fibre with a coating layer, n_{eff} effective index of mode propagating in the tapered region of a fibre, n_c refractive index of mode propagating in the coating layer.

Theoretical predictions of the optical response of tapered single-mode optical fibres are obtained using the matrix method of Ghatak [Ghatak, A. K. *et al.* 1987]. This technique was originally developed for the determination of propagation characteristics of planar multilayer waveguides, and has been extended by transformation to cylindrical coordinates to allow the analysis of optical fibres by Sharma et al. [Sharma, A. *et al.* 1990].

Theoretical analysis of the propagation characteristics of guided modes using the Ghatak method involves a 2 x 2 matrix multiplication process [Ghatak, A. K. *et al.* 1987]. The basis of the theoretical considerations is a layered structure as shown in Fig. 3.5.

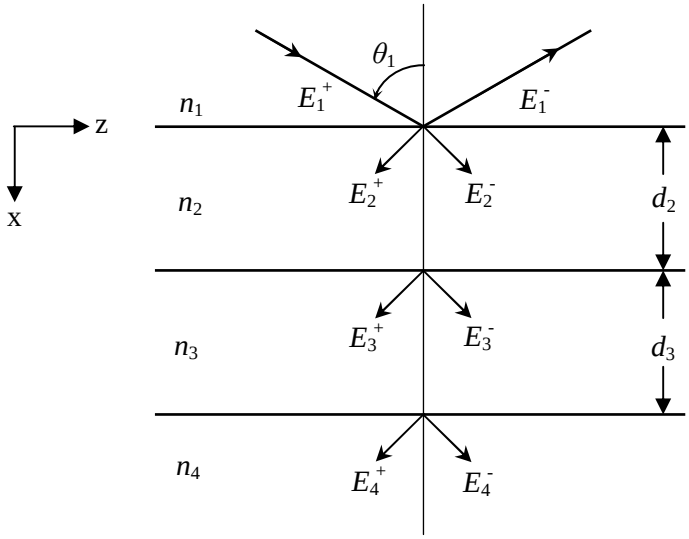

Fig. 3.5. Schematic diagram of the incidence of the plane wave at an angle θ_1 in a multilayer medium.

For a plane wave incident at an angle θ_1, as depicted in Fig. 3.5, the electric field in each medium can be written in the form:

$$\varepsilon_i = \hat{e}_i^+ E_i^+ e^{i\Delta_i} \exp[i(\omega t - k_i \cos\theta_i x - \beta z)] + \hat{e}_i^- E_i^- e^{-i\Delta_i} \exp[i(\omega t + k_i \cos\theta_i x - \beta z)] \quad (3.3)$$

where

$$\Delta_1 = \Delta_2 \ , \ \Delta_3 = k_3 d_2 \cos\theta_3$$

$$\Delta_4 = k_4 \cos\theta_4 (d_2 + d_3) \quad (3.4)$$

$$k_i = k_0 n_i = \frac{\omega}{c} n_i \quad (3.5)$$

and

$$\beta = k_1 \sin\theta_1 = k_2 \sin\theta_2 = ... = k_4 \sin\theta_4 \quad (3.6)$$

which is an invariant of the system. $\hat{e}_i^+$ and $\hat{e}_i^-$ represent the unit vectors along the direction of the electric field, and E_i^+ and E_i^- represent the electric field amplitudes of waves propagating in the downwards and upwards directions (see Fig. 3.5), respectively. On applying the boundary conditions at the interfaces one can obtain

$$\begin{pmatrix} E_i^+ \\ E_i^- \end{pmatrix} = S_1 \begin{pmatrix} E_2^+ \\ E_2^- \end{pmatrix} = \ldots = S_1 S_2 S_3 \begin{pmatrix} E_4^+ \\ E_4^- \end{pmatrix} \tag{3.7}$$

where

$$S_i = \frac{1}{t_i} \begin{pmatrix} e^{i\delta_i} & r_i e^{i\delta_i} \\ r_i e^{-i\delta_i} & e^{-i\delta_i} \end{pmatrix} \tag{3.8}$$

and r_i and t_i represent, respectively, the amplitude reflection and transmission coefficients at the *i*th interface; $\delta_i = k_i d_i \cos\theta_i$. For TE polarisation

$$\begin{aligned} r_i &= \frac{n_i \cos\theta_i - n_{i+1} \cos\theta_{i+1}}{n_i \cos\theta_i + n_{i+1} \cos\theta_{i+1}} \\ t_i &= \frac{2n_i \cos\theta_i}{n_i \cos\theta_i + n_{i+1} \cos\theta_{i+1}} \end{aligned} \tag{3.9}$$

and for TM polarisation

$$\begin{aligned} r_i &= \frac{n_{i+1} \cos\theta_i - n_i \cos\theta_{i+1}}{n_{i+1} \cos\theta_i + n_i \cos\theta_{i+1}} \\ t_i &= \frac{2n_i \cos\theta_i}{n_{i+1} \cos\theta_i + n_i \cos\theta_{i+1}} \end{aligned} \tag{3.10}$$

Assuming that the second, third and fourth media (in Fig. 3.5) correspond to a multiple layer device and the first medium is a substrate, one can use the above matrix to determine

the propagation characteristics of a planar waveguide. If the excitation efficiency η is evaluated as a function of the propagation constant β, i.e.:

$$\eta(\beta) = \left|\frac{E_3^+}{E_1^+}\right|^2 \quad \text{or} \quad \eta(\beta) = \left|\frac{E_3^-}{E_1^+}\right|^2 \tag{3.11}$$

then one would obtain resonance peaks at discrete values of β, which correspond to the modes supported by the layer [Ulrich, R. 1970]. The values of β at which peaks appear give the real value of the propagation constants of the mode, while the full width at half maximum (FWHM) represents the power attenuation coefficient which is twice the imaginary part of the propagation constant [Ulrich, R. 1970].

To apply the above method to study the propagation characteristics of a cylindrical optical fibre, some modifications must be introduced. A convenient transformation of the optical properties of the cylindrical fibre to a planar geometry has been derived by Sharma et al [Sharma, A. *et al.* 1990]. It was found that the expression for the propagation constant distribution may be found from the equivalent expression for the refractive index distribution, which includes adjustable parameters. Those parameters are obtained by maximizing the stationary expression for β

$$\beta^2 = \frac{\int_{-\infty}^{\infty}\int_{-\infty}^{\infty} dxdy\left[k_0^2 n^2(r)\left|\Psi(r,y)\right|^2 - \left|\nabla\Psi\right|^2\right]}{\int_{-\infty}^{\infty}\int_{-\infty}^{\infty} dxdy\left|\Psi(x,y)\right|^2} \tag{3.12}$$

where $r = \sqrt{x^2 + y^2}$ is the radial variable, $k_0 = \frac{\omega}{c}$ is the free-space wavenumber, Ψ is a modal field of the following form:

$$\Psi(x,y) = \Psi_x(x)\Psi_y(y) \tag{3.13}$$

Ψ_x and Ψ_y are the scalar modes of two slabs with index variations along the x and y directions, respectively. Choosing the following functional form for Ψ_x:

$$\Psi_x(x) = A\cos\left(\frac{px}{a}\right), \qquad |x| \le \sigma a$$
$$\Psi_x = A\cos(px)\exp\left[-p\tan(p\sigma)\cdot\left\{\left(\frac{x}{a}\right)-\sigma\right\}\right], \qquad |x| \ge \sigma a \tag{3.14}$$

where a is core radius, values of p and σ are obtained by solving the equation 3.12. Once the parameters are known, the refractive index distribution can be defined. This distribution may be represented by the following empirical formulae:

$$n^2(x) = n_{x1}^2 = n_1^2 - \frac{(u^2 - p^2)}{(k_0 a)^2} \qquad |x| < \sigma a \tag{3.15}$$

$$n^2(x) = n_{x2}^2 = n_{x1}^2 - \frac{p^2 \sec^2(p\sigma)}{(k_0 a)^2} \qquad |x| > \sigma a \tag{3.16}$$

where

$$p^3 = -1.3528 + 1.6880V - 0.1894V^2 \tag{3.17}$$

$$\sigma = 0.8404 + 0.0251V - 0.0046V^2 \tag{3.18}$$

$$u = \sqrt{V^2 - (1.148V - 0.996)^2} \tag{3.19}$$

subject to the constraint 1.5<V<2.5, where V is the normalised frequency.
This analysis allows for prediction of the effective indices of the modes and subsequently prediction of the transmission spectrum of the chosen waist diameter taper and its response to a change of refractive index changes in the surrounding environment of the taper waist.

The response of taper based sensors is dependent on the taper waist diameter. Tapering of a single mode fibre necessarily couples power from the fundamental mode into higher order modes as described in chapter 3.2. Power also couples back from the higher order modes into the fundamental mode. In case of smaller diameter taper, with the waist diameter size smaller than 20μm the variation of the power loss, from the fundamental into higher order modes, with wavelength has a sinusoidal dependence. The transmission spectrum of such a taper shows characteristic interferometric oscillations and is called “channelled spectrum” and oscillations are known to result from the interference between modes and the

modulation of their envelope is due to the beating of different frequencies [Black, R. J. *at al*. 1991], see Fig. 3.6.

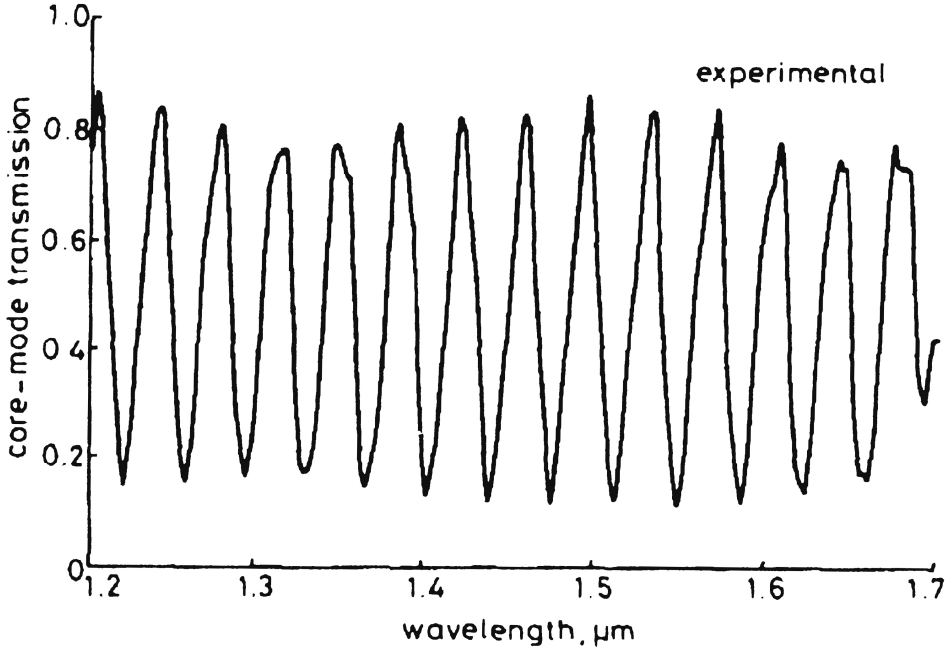

Fig. 3.6. Experimental core-mode transmission of a bitaper as a function of wavelength (insert after [Love, J. D. *et al*. 1991])

The observed oscillations for tapers with diameters below 6μm [Jarzebinska, R. *at al*. 2009] originate from beating of HE_{11} and HE_{12} local modes, which propagate along tapers with different propagation constants β_i, and recombine at the output with a relative phase which depends on the length of the taper. Any change of the refractive index of the surrounding medium causes a change in n_{eff} of the excited modes and thus by the relation in Eq. 3.2 induces a change in their propagation constants. This results in measurable shift of the channelled spectrum. In this project the refractive index modulation has been obtained by means of the deposition of nanostructured coatings and the spectral response of tapers was studied, and the channelled spectrum based sensors proposed.

In case of large diameter tapers, with waist diameters above 20μm interferometric oscillations also occur, but the period of the channeled spectrum is larger than the spectral range offered by the spectrometer used in this project to monitor the spectrum. Therefore it can be said that the transmission spectrum of large diameter tapers does not change in

response to tapering; its shape in general reflects the source transmission. The operation of sensors based on the large diameter tapers is different form those of small diameter- a coupled waveguide response is observed. The underlying effect is similar to that observed previously for nanostructured films deposited onto a side polished optical fibre [Flannery, D. *et al*. 1999; Charters, R. B. *et al*. 1994] when mode of a core of the tapered fibre and a mode of a coating waveguide are phase matched. This results in energy transfer between these two waveguides. The deposition of a nanoscale coating influences the transmission spectrum in a way that characteristic attenuation bands with central wavelengths that are dependent on the optical thickness of the coating are produced. It has been shown theoretically and experimentally [Cusano, A. *et al.* 2005; Del Villar, I. *et al*. 2004; Del Villar, I. *et al.* 2005 (**d**); Del Villar, I. *et al.* 2006 (**a**)] that as the thickness of an overlay increases core modes shift their effective refractive index to higher values, see Fig. 3.7. There is a moment when the cladding mode with highest refractive index becomes guided in the overlay. If the thickness continues to increase more modes become guided in the overlay. The mode that couples to the overlay is always the highest refractive index mode of the cladding. During this transition a change in effective refractive indices of all cladding modes takes place. After this, each mode has a refractive index of an immediate lower order cladding mode without overlay see Fig. 3.7.

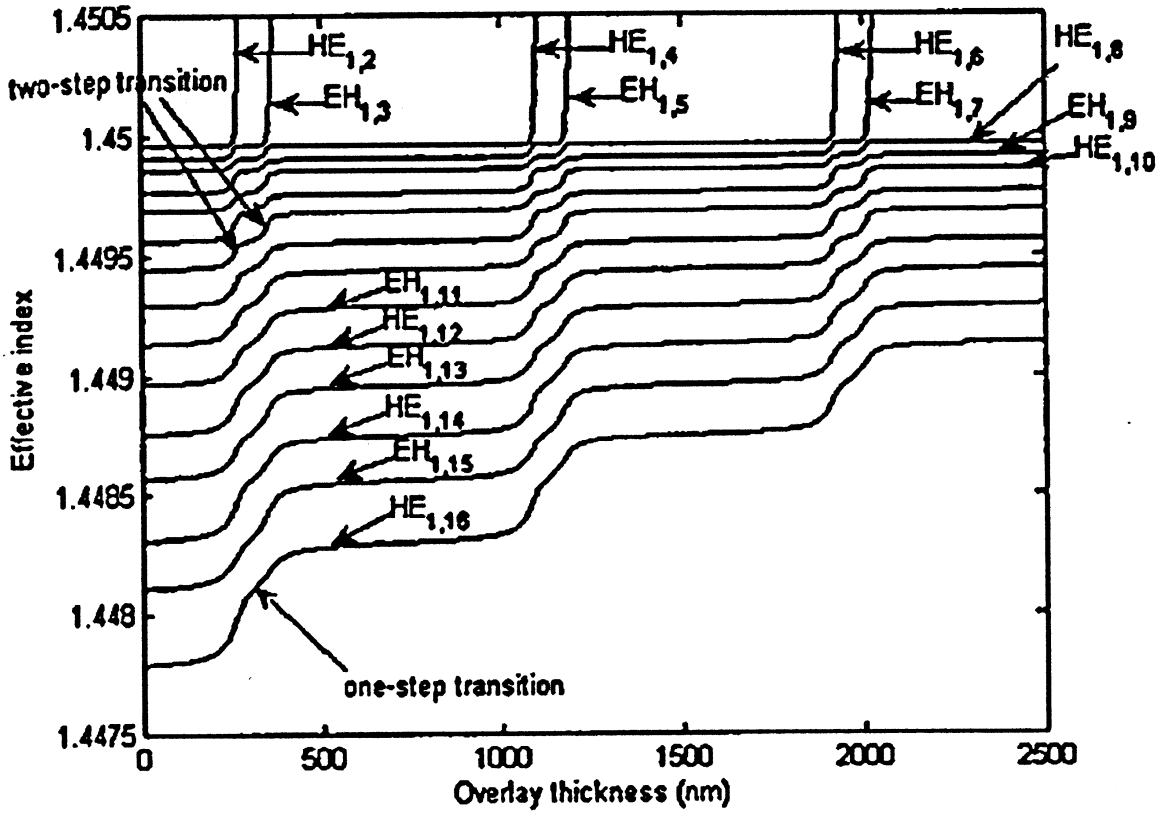

Fig. 3.7. Effective refractive index of the first 15 cladding modes as a function of the overlay thickness (insert after [Del Villar, I. *et al.* 2006]).

The results for these fibres have been explained [Del Villar, I. *et al.* 2005 (**c**); Cusano, A. *et al.* 2006; Del Villar, I. *et al.* 2006 (**b**)] with the theory based on a vectorial analysis of modes and coupled mode theory applied, with LP mode approximation. The theory is an extension of a model for a three-layer cylindrical waveguide proposed by [Erdogan, T. *et al.* 1997]. This has been applied for the analysis of LPGs fibres with several layers deposited. The matrix method for the propagation constants in such waveguide proposed by [Guo, S. *et al.* 2004] was applied by [Del Villar, I. *et al.* 2006 (**e**)] where the interactions between the fundamental core mode HE_{11} and HE_{1j} and EH_{1j} modes of cladding were studied. Once the exact modes are calculated they are introduced to couple-mode equation and the self- and cross coupling coefficients are calculated. Then propagation constants are obtained.

It can be observed in Fig. 3.7 that the transition of the refractive index of each HE_{1j} mode is shifted to immediate lower order cladding mode in two steps. The mode effective index is shifted to an EH mode before it is definitely shifted to the HE of the lower order. This also applies to the resonant wavelengths.

The phenomenon can be explained as a reorganization of modes. There is finite number of allowed effective refractive indices states of modes in an uncoated fibre. Deposition of a thin layer causes the perturbation of the refractive index which leads to appearance of not-allowed (in uncoated fibre) states of modes. This allows for transition to guidance of one cladding mode in the overlay. Guidance occurs at a specific thickness. With the increase of the thickness the distribution of modes recovers it original state. The phenomenon repeats periodically as the thickness increase. This phenomenon was reported to occur also in tapered fibres with an overlay deposited onto tapered region [Jarzebinska, R. *et al*. 2009].

Tapering of a fibre does not lead to dropout bands appearing. The deposition of a specific coating onto tapered region induces their appearance. In the case of tapers it was also observed that the phenomenon occurs periodically with the overlay thickness increase and attenuation bands are always composed of two separate attenuation dropouts. Figure 3.8 and 3.9 depict experimental results published in [Jarzebinska, R. *et al*. 2009] as well as obtained during realisation of this project.

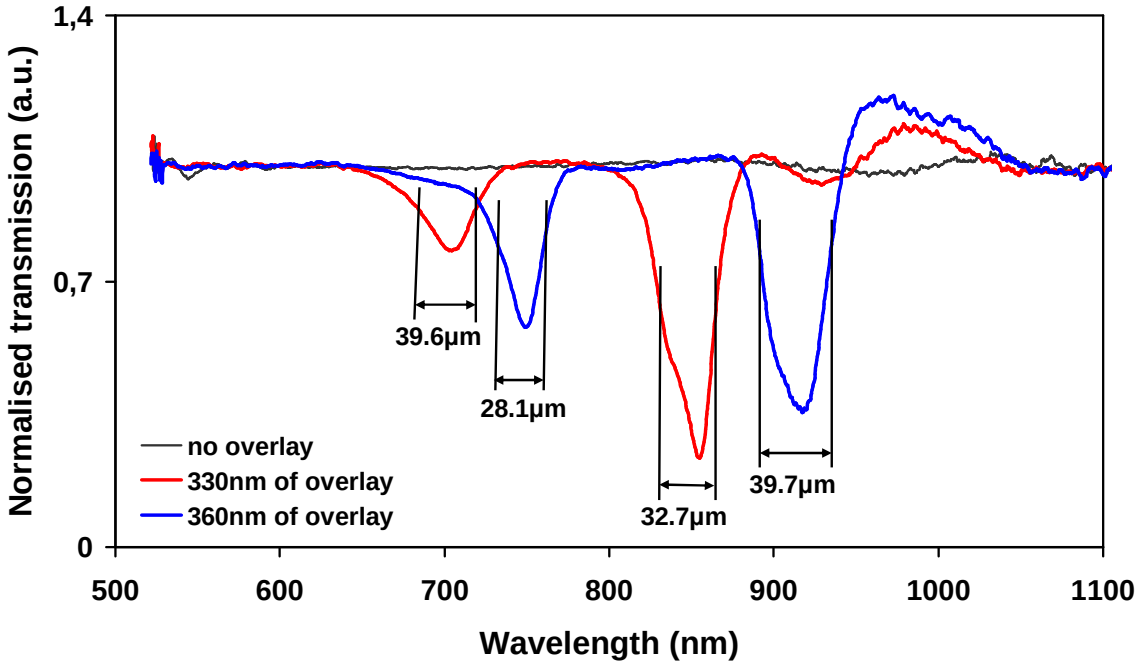

Fig. 3.8. Normalised transmission spectrum of the 37.4µm diameter fibre taper coated with 330nm and 360nm of the quinolinium iodide overlay using Lagmuir-Blodgett technique. Spectral width (FWHM) of transmission losses marked for each dropout band.

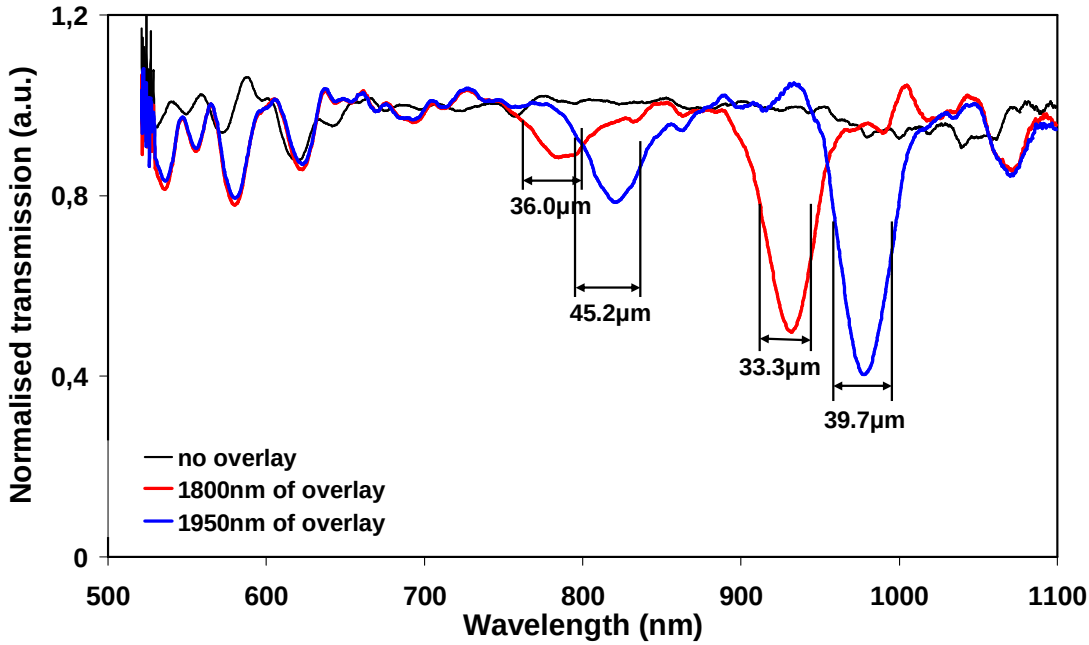

Fig. 3.9. Transmission spectrum of the 26µm diameter fibre taper coated with 1800nm and 1950nm of the quinolinium iodide overlay using Lagmuir-Blodgett technique. Spectral width (FWHM) of transmission losses marked for each dropout band.

This indicates the two-step transition of refractive indices of modes takes place. Therefore the scalar analysis, where hybrid modes – HE - are considered, is the appropriate approach for the description of the phenomenon.

The presented in this section phenomenon of the coupling of the fundamental LP_{01} mode to the HE_{11} and HE_{12} modes which occurs in the taper waist of non-adiabatic tapers has been studied in this project towards prospective sensors creation. The differential response of the propagating modes within the taper waist to the index change in the surrounding environment has been used for studies of the applicability of tapered optical fibres as pH sensors and to measure the concentration of chosen chemical species both in liquid as well as in gaseous environment. Mathematical description of the waveguiding properties of tapered fibres is used for theoretical predictions of the optical response of tapered single-mode optical fibres coated with an overlay film.

References

Black, R.J., Bures, J., Lapierre, J., "Finite-cladding fibres: HE_{12} and local-normal-mode coupling evolution", *IEE Proceedings J (Optoelectronics)*, Vol. 138, No. 5, pp. 330-336, 1991 (**a**)

Black, R.J., Lacroix, S., Gonthier, F., Love, J.D., "Tapered single-mode fibres and devices. Part2: Experimental and theoretical quantification", *IEE Proceedings J (Optoelectronics)*, Vol. 138, No. 5, pp. 355-364, 1991 (**b**)

Charters, R.B., Staines, S.E., Tatam, R.P., "In-line fiber-optic components using Langmuir-Blodgett-films", *Optics Letters*, Vol. 19, No. 23, pp. 2036-2038, 1994

Cusano, A., Iadicicco, A., Pilla, P., Contessa, L., Campopiano, S., Cutolo, A., Giordano, M., "Mode transition in high refractive index coated long period gratings", *Optics Express*, Vol. 14, No. 1, pp. 19-34, 2006

Del Villar, I., Corres, J.M., Achaerandio, M., Arregui, F.J., Matias, R.I., "Spectral evolution with incremental nanocoating of long period fiber gratings", *Optics Express*, Vol. 14, No. 25, pp. 11972-11981, 2006 (**a**)

Del Villar, I., Matias, I.R., Arregui, F.J., "Long-Period Fiber Gratings With Overlay of Variable Refractive Index", *IEEE Photonics Technology Letters*, Vol. 17, No. 9, pp. 1893-1895, 2005 (**c**)

Del Villar, I., Matias, I.R., Arregui, F.J., "Influence on cladding mode distribution of overlay deposition on long-period fiber gratings", *Journal of Optical Society of America A*, Vol. 23, No. 3, pp. 651-658, 2006 (**b**)

Del Villar, I., Matias, I.R., Arregui, F.J., "Fiber-Optic Nanostructures by Electrostatic Molecular Self-Assembly", *Current Analytical Chemistry*, Vol. 4, pp. 341-355, 2008

Del Villar, I., Matias, I.R., Arregui, F.J., "Deposition of coatings on long-period fiber gratings:tunnel effect analogy", *Optical and Quantum Electronics*, Vol. 38, pp. 655-665, 2006 (**e**)

Del Villar, I., Matias, I.R., Arregui, F.J., Lalanne, P., "Optimization of sensitivity in Long Period Fiber Gratings with overlay deposition", *Optics Express*, Vol. 13, No. 1, pp. 56-69, 2005 (**d**)

Erdogan, T., "Cladding mode resonances in short and long period gratings filters", *Journal of optical Society of America*, Vol. 14, pp. 1760-1773, 1997

Fielding, A.F., Edinger, K., Davis, C.C., "Experimental observation of mode evolution in single-mode tapered optical fibers", *Journal of Lightwave Technology*, Vol. 17, No. 9, pp. I649-656, 1999

Flannery, D.; James, S.W.; Tatam, R.P.; Ashwell, G.J., "Fiber-optic chemical sensing with Langmuir-Blodgett overlay waveguides", *Applied Optics*, Vol. 38, No. 36, pp. 7370-7374, 1999

Ghatak, A.K., Thyagarajan, K., Shenoy, M.R, „Numerical analysis of planar optical waveguides using matrix approach", *Journal of Lightwave Technology*, Vol. LT-5, No. 5, pp. 660-667, 1987

Gloge. D, "Weakly guiding fibers", *Applied Optics*, Vol. 10, pp. 2252-2258, 1971

Guo, S., Albin, S, Rogowski, S, "Comparative analysis of Bragg fibers", *Optics Express*, Vol. 12, pp. 198-207, 2004

Hunsperger, R.G. "Photonic devices and systems", Marcel Dekker Inc., New York, 1994

Jarzebinska, R. Cheung, C. S., James, S. W., Tatam, R. P., "Response of the transmission spectrum of tapered optical fibres to the deposition of a nanostructured coating", *Measurement Science & Technology*, Vol. 20, No. 3, Article Number: 034001, 2009

Kieu, K.Q., Mansuripur, M., "Tuning of fiber lasers by use of a single-mode biconic fiber taper", *Optics Letters*, Vol. 31, No. 16, pp. 2435-2437, 2006

Leon-Saval, S.G., Birks, T.A., Wadsworth, W.J., Russel, P.St.J., Mason, M.W., "Supercontinuum generation in submicron fibre waveguides", *Optics Express*, Vol. 12, No. 13, pp. 2864-2869, 2004

Love, J.D., Henry, W.M., Stewart, W.J., Black, R.J., Lacroix, S., Gonthier, F., "Tapered single-mode fibres and devices. Part1: Adiabaticity criteria", *IEE Proceedings J (Optoelectronics)*, Vol. 138, No. 5, pp. 343-354, 1991

Orucevic, F., Lefevre-Seguin, V., Hare, J., "Transmittance and near-field characterization of sub-wavelength tapered optical fibers", *Optics Express*, Vol. 15, No. 21, pp. 13624-13629, 2007

Pask., C., Snyder, A. W., Mitchell, D. J., "Number of modes on optical-waveguides", *Journal Of The Optical Society Of America*, Vol. 65, No. 3, pp. 356-357, 1975

Sharma, A., Kompella, J., Mishra, P.K., "Analysis of fibre directional couplers and coupler half-blocks using a new simple model for single-mode fibers", *Journal of Lightwave Technology*, Vol. 8, No. 2, pp. 143-151, 1990

Synder, A., Love, J.D., "Optical Waveguide Theory", Kluwer Academic Publishers Group, London, 2000

Ulrich, R. "Theory of prism-film coupler by plane-wave analysis", *Journal of Optical Society of America*, Vol. 60, pp. 1337-1350, 1970

Warken, F., Vetsch, E., Meschede, D., Sokolowski, M., Rauschenbeutel, A., "Ultra-sensitive surface absorption spectroscopy using sub-wavelength diameter optical fibers", *Optics Express*, Vol. 15, No. 19, pp. 11952-11958, 2007

METHODOLOGY

4

In this section the experimental setups and the methods used to produce and characterise the spectral responses of tapered optical fibres are presented. In order to systematize the work that has been undertaken the project is presented in the form of the flowchart shown in Fig. 4.1. The development of the project was as follows: 1. manufacture and characterisation of tapered optical fibres, 2. deposition of functional coatings onto the tapered region of an optical fibre using the appropriate deposition technique, 3. study of a coated tapered fibre as a potential sensor to a specified stimulus.

In the last part of the section the mathematical model used to predict the development of the transmission spectrum of tapered fibres in response to increasing overlay thickness is presented.

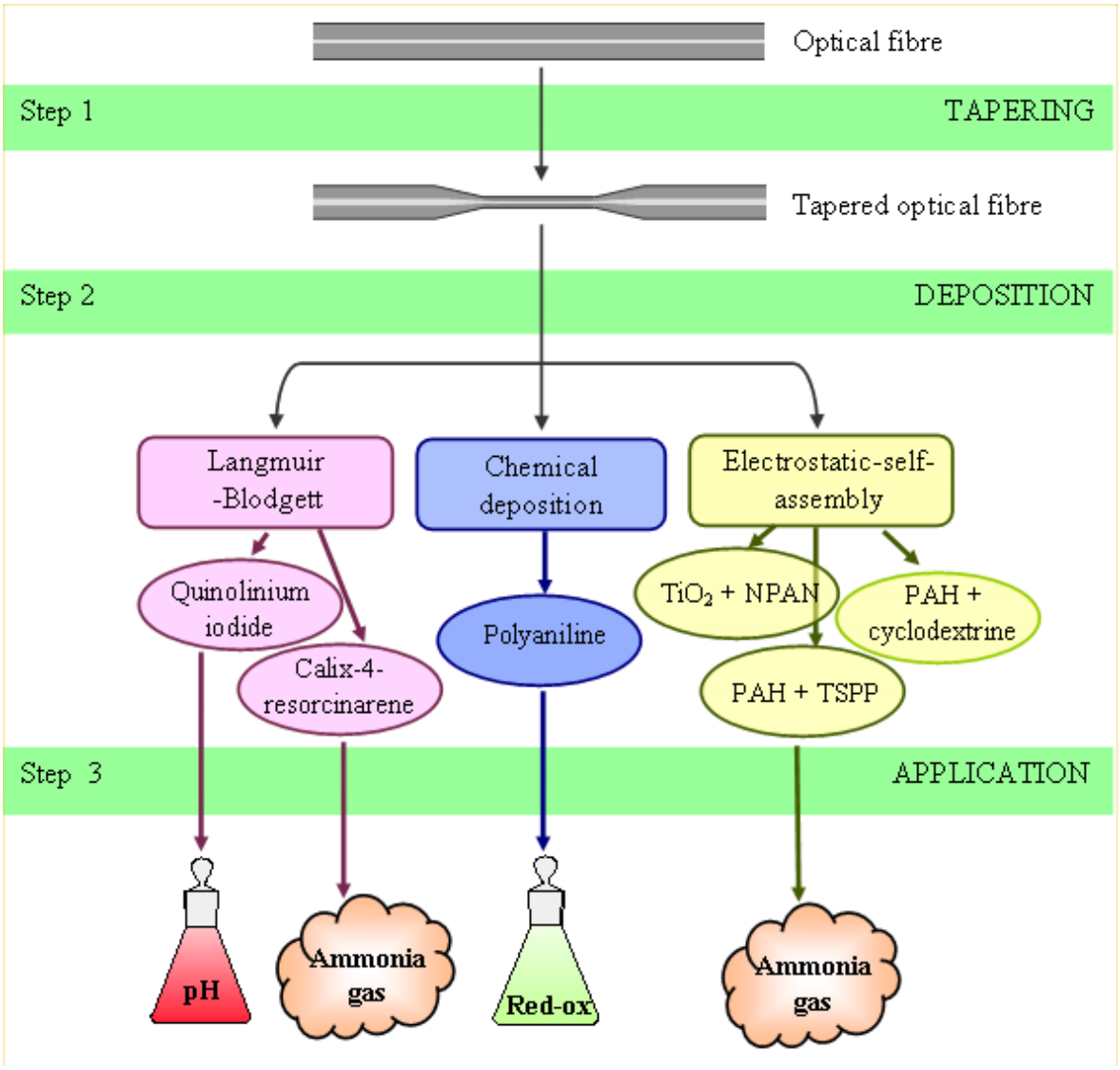

Fig. 4.1. Schematic diagram of the work undertaken within the project.

4.1 Fabrication and characterisation of tapers

The setup shown in Fig. 4.2, using a gas burner as a source of heat, was constructed to facilitate the fabrication of optical fibre tapers. The gas burner contained a butane (65%)/propane (35%) mixture. The burner was equipped with a nozzle enabling manual flame length control. The width of a flame was ~6mm. Using this experimental setup,

optical fibre tapers with micron scale diameters in the range 3µm – 60µm have been fabricated.

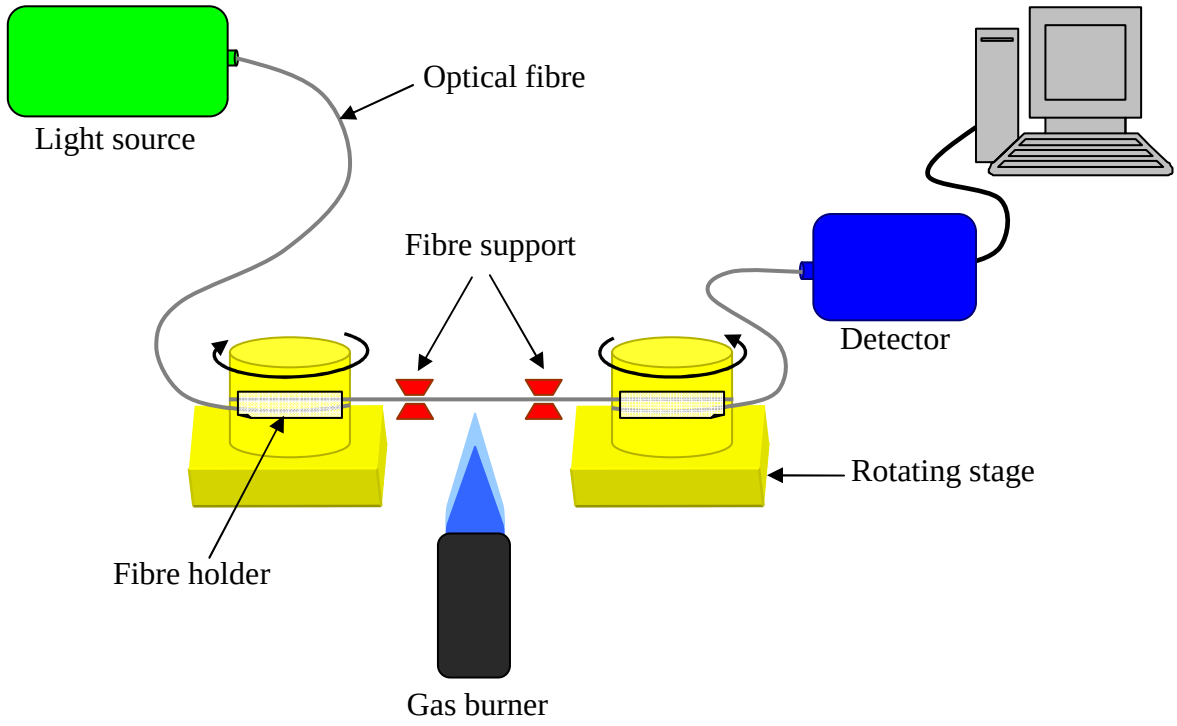

Fig. 4.2. Schematic diagram of the setup used for fibre tapering.

One type of telecommunication fibre was studied - single mode fibre, Fibrecore SM750, with cladding/core diameters of 125/5µm, and cut-off wavelength of 635nm.

To prepare the fibres for the tapering process, the protective polyacrylate buffer coating was removed from a section of length larger than that which was to be tapered, using a mechanical stripper. The reason for stripping the coating from a fibre is to avoid impurities remaining on a tapered region after heating it with a flame. The remaining impurities could cause local overheating and excessive local melting of a fibre during the tapering process due to their burning, and have an influence on the transmission spectrum of a tapered fibre. The stripped length of fibre was then thoroughly cleaned by wiping with a tissue soaked in acetone and next - with isopropanol, choosing a clean section of the same tissue or using a new one. The length of optical fibre containing the stripped section was inserted in fibre

supports. The supports ensured parallel to the stretching plane position of the tapered section during pulling. Subsequently the optical fibre was stretched between the two rotation stages and secured using scotch tape to brass cylinders protruding from the rotating parts of stages. The optical fibre was wound by one full turn around each cylinder so that the fibre section to be tapered could be placed under tension. The typical tapering length was ~1.5cm for a taper of a waist diameter lying within the range of 20-30μm, and ~3cm for a 5μm taper. The typical length of a stripped region was ~2cm long.

After the attaching the to the rotation stages, the fibre was ready for tapering. The gas burner is positioned such that when not operating it is below the level of the optical fibre to be tapered. When the fibre is ready for tapering, the burner is switched on and the gas is lit and raised up ~10cm to heat a fibre and rotating stages switched on. The size of the flame was ~6mm. A fibre was placed in a flame in the point where the flame temperature is the highest i.e. top of the inner cone of a flame, see Fig. 4.3.

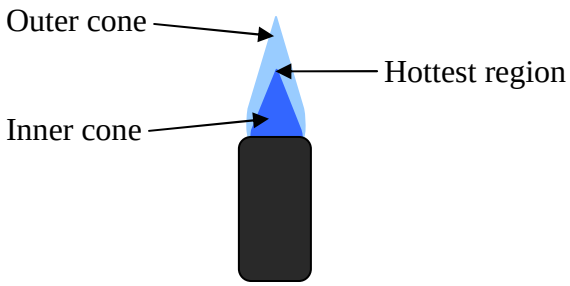

Fig. 4.3. Schematic diagram of a structure of a flame.

During heating, the ends of the fibre were drawn in opposite directions by driving the rotation stages at a constant linear speed of approximately 100μm/s. The speed was experimentally worked out, based on the transmission intensity of the guided light, to be the most effective in the setup. The stages were driven by separate controllers (Oriel Instruments, Encoder Mike Controller, model 18011) with a resolution of 0.1μm/s and range 0.5 – 200.0μm/s. The tapering process lasted from 50 to 120 seconds, depending on the desired taper diameter. After fabrication, each taper was carefully mounted on a

straight holder which secured the fibre and enabled easy handling and operation, see Fig. 4.4. The holder is called “straight” in order to distinguish it from another one – the “cross” holder – described thereinafter. The dimensions of the holder were designed to secure the taper holding close to tapered region. On the other hand the holder ensured the mounting of a fibre far enough from the tapered waist so the polyacrylate buffer coating was clamped in order to prevent the breakage of uncoated silica.

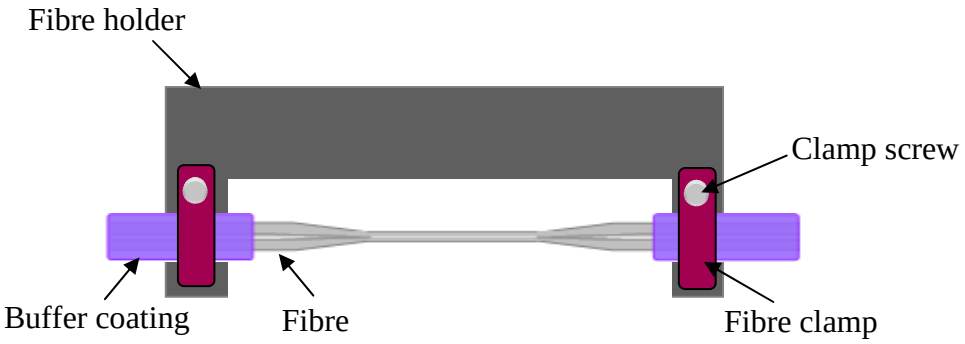

Fig. 4.4. Schematic diagram of a fibre holder.

Following tapering, the dimensions of the fibres are characterized using optical and scanning electron microscopes. For a fast estimate of the diameter and to allow a qualitative view of the fibre (check for the presence of inner fractures), an optical microscope (Vickers Photoplan) with image shearing readout unit (Vickers Instruments) is used. The taper size was measured in ten points along the uniform waist diameter and the average value was calculated. Microscope resolution was 0.01μm. For more precise studies of the waist diameter an Environmental Scanning Electron Microscope (FEI ESEM XL30, 1.5nm resolution) is used.

— ESEM is a modified version of the Scanning Electron Microscope, SEM, where a sample is studied in high vacuum environment by exposure to a high-energy beam of electrons emitted from an electron gun. Generated secondary electrons, produced in inelastic interaction of electron beam with valence electrons of the sample material, and back scattered electrons are collected by detectors to form images of the sample. In SEM imaging the samples must be electrically conductive. Nonconductive specimens,

like silica, tend to get charged, which causes scanning faults and other image artefacts. These problems are overcome in the ESEM, where the specimen remains in an electrically conductive gaseous environment which prevents negative charge accumulation on the sample [Stokes, D. J. 2008].

The cross-section of a tapered fibre was studied via the Focus Ion Beam technique (FEI Strata 200xP FIB) that was used to cut a waist and to scan its surface.

— An FIB system operates in a similar fashion to an SEM instead of using an electron beam, the FIB system uses a finely focused beam of gallium ions that can be operated at low beam currents for imaging or high beam currents for site specific sputtering or milling [Yao, N. 2007].

The optical characteristics of the tapered fibres were studied, in particular the response to the deposition of nanostructured coatings. The coated fibres were then assessed for use as chemical sensors. The criteria for materials selection were based on the aimed sensors' working environment, namely: liquid and gaseous.

In the following sections the techniques used for the coating of tapered optical fibres are presented. The transmission spectrum was monitored during the deposition process and during subsequent assessment of their performance as sensors using the configuration depicted in Fig. 4.5. Transmission spectra were recorded by coupling the output from a tungsten halogen lamp (LS-1, Ocean Optics) into one end of the fibre and coupling the distal end to fibre optic CCD spectrometer (S2000, Ocean Optics, Inc., bandwidth: 530-1100nm, resolution: 0.3nm).

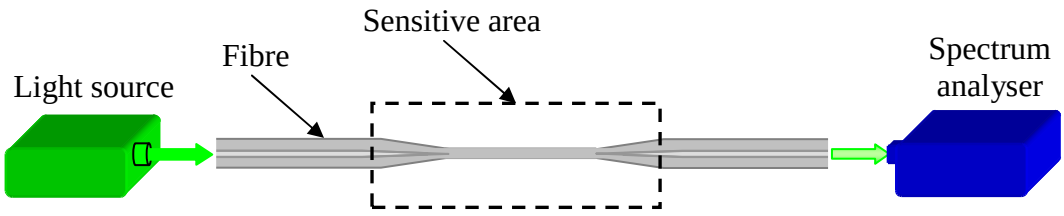

Fig. 4.5. Schematic diagram of arrangement of the experimental setup, in a configuration with a spectrum analyser.

4.2. Langmuir-Blodgett deposition technique

Prior to the deposition of materials onto tapered fibres using the LB technique, solutions of the materials were submitted for spectroscopic analysis. The aim of this is to examine whether or not absorption in the deposited material contributes to the spectral response of tapers to the overlay deposition. Absorption spectra were acquired on a Perkin Elmer Lambda 7 spectrophotometer (total wavelength range: 200 – 900nm) in School of Applied Sciences of Cranfield University, UK. The materials were dissolved in the mixture of solvents: $CHCl_3$ and CH_3OH (ratio 1:1). The spectrum of the solvent mixture was used as the baseline for subsequent measurements of spectra of the solutions. The baseline was subtracted form each spectrum.

The LB technique facilitates deposition of the material one molecular layer at a time onto a substrate in controlled way [[Blodgett, K. 1935; Peterson, I. R. 1990]]. The technique has been introduced in chapter 2.3.1. A two compartment Nima Technology LB trough was used. Each compartment has a subphase area of 30x20cm and a maximum monolayer containment area of 565cm^2. One compartment was filled with deionised water. A monolayer of the material is formed by applying the molecules on the water/air subphase in the form of the chloroform solution. A solvent was allowed to evaporate by leaving for 10min before the experiment began. The molecules dispersed across the whole water surface and oriented with the hydrophilic parts immersed in water and hydrophobic parts remaining upwards – above the water surface. Thus a floating monolayer with randomly oriented molecules was produced. Reducing the surface area by moving a barrier molecules start to be pushed closer together as the hydrophobic tails of molecules start to lift above the surface. Constant reduction of the surface area causes change in the surface pressure of the monolayer that can be monitored as surface pressure isotherm. Further compression reduces the area occupied by each molecule close to its crossectional area and thus produces solid phase. In this state molecules are ready to be transferred to a solid substrate, i.e. a fibre. The fibre containing the taper was mounted on a cross-holder and positioned vertically so its long axis was aligned with the dipping direction, see Fig. 4.6.

The cross-holder was mounted on the motor-driven track chains by screwing both arms of the holder on track chains.

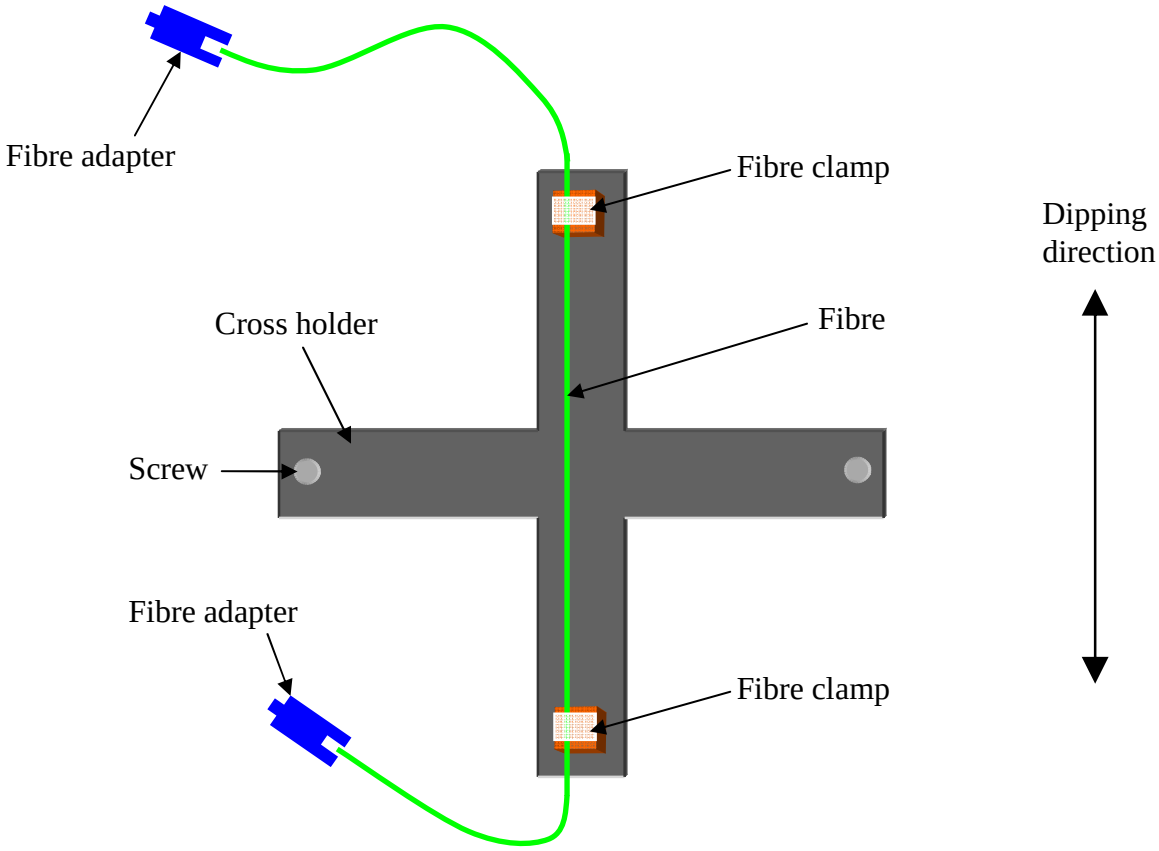

Fig. 4.6. Schematic diagram of a cross-holder (dimensions: 10 x 10cm) with a fibre mounted and fibre adapters facilitating connection to a light source and spectrophotometer.

The fibre was alternately raised and lowered through the floating monolayer at the air-water interface to deposit a coating (see Fig. 4.7). Both ends of a taper were ~50cm long and terminated with bare-fibre adapters, which enabled fibre connection to the source and spectrophotometer, facilitating the recording of the transmission spectrum during coating deposition. Fibre adapters' design provides a simple and easy method to quickly interconnect any standard fibre connector to testing bare fibre. Mounting procedure requires stripping off a bit of buffer coating, cleaning the glass fibre and inserting it into

the ferrule while depressing the clamping button. Fibre is held mechanically and removable. Transmission spectra were recorded using the fibre coupled CCD spectrometer after the deposition of each monolayer, with the taper below and above the water surface for alternate layers.

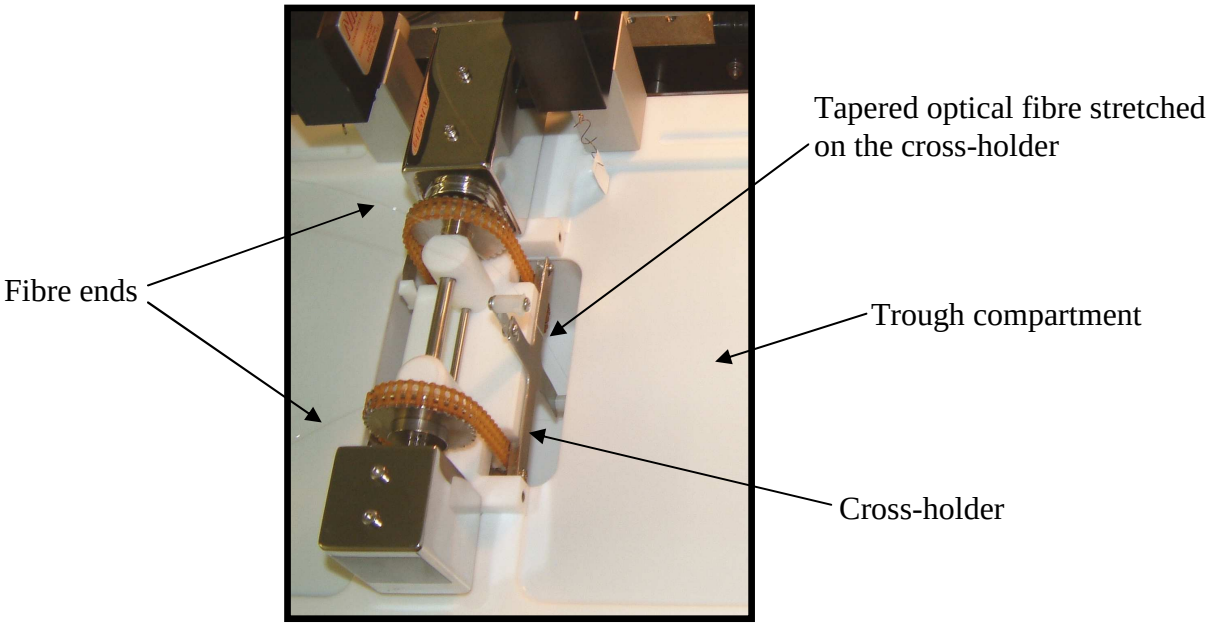

Fig. 4.7. Photograph of the tapered optical fibre mounted on the cross-holder and placed in the bath separating two compartments of the trough.

4.2.1. Materials used for Langmuir-Blodgett deposition

Two materials suitable for LB deposition were selected for the deposition onto tapered devices. The first of the materials, belonging to merocyanine dye family, was 4-[2-(4-dimethylamino-naphtalen-1-yl)-vinyl]-1-octadecyl-quinolinium iodide), which was chosen for chemical sensing in solutions. The second material was calix[4]resorcinarene, which belongs to a large family of calixarens. This material was chosen for sensing in the gas phase.

The 4-[2-(4-dimethylamino-naphtalen-1-yl)-vinyl]-1-octadecyl-quinolinium iodide) structure is depicted in Fig. 4.8.

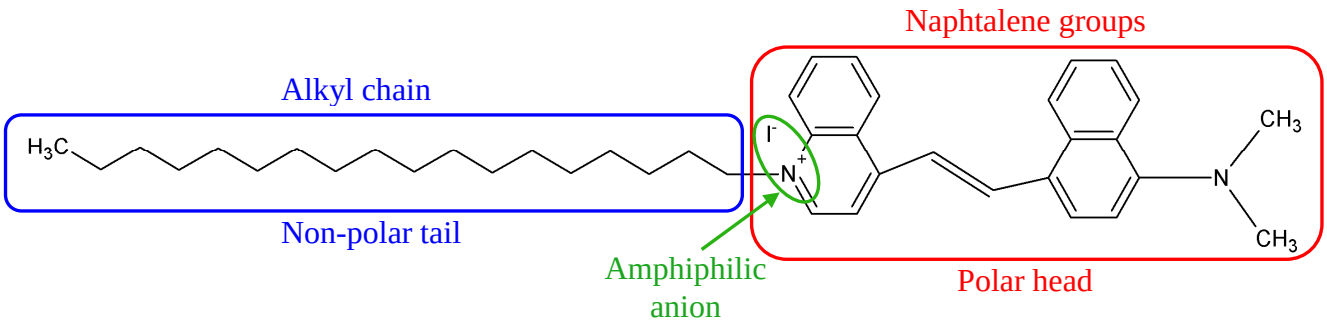

Fig. 4.8. Molecular structure of the 4-[2-(4-dimethylamino-naphtalen-1-yl)-vinyl]-1-octadecyl-quinolinium iodide.

The molecule structure contains an alkyl chain, two naphthalene rings and amphihilic anion, which dissolves in water leaving the species at the air water interface where they form an organized monolayer when compressed. The quinolinium iodide molecule contains also the amine group, which in water undergoes ionization according to formula:

$$R - NH_2 + H_2O \rightarrow R - NH_3^+ + OH^-$$

The $-NH_3^+$ group within the molecule is anticipated to be pH sensitive. Thus for the first time the pH sensitivity of the molecule has been studied. Langmuir-Blodgett films of iodide salts have found application for the deposition to thickness suitable for waveguiding and second harmonic generation [Ashwell, G. J. *et al.* 1996, Ashwell, G. J. *et al.* 2002]. We believe this to be the first use of 4-[2-(4-dimethylamino-naphtalen-1-yl)-vinyl]-1-octadecyl-quinolinium iodide) for LB film deposition as well as for its chemical sensing application. The molecule was synthesized in the Nanomaterials group of Prof. G. Ashwell, of the School of Chemistry, Bangor University.

The second of the materials used was calix[4]resorcinarene. The calix[4]resorcinarene structure contains four resorcinol aromatic rings interconnected to form a larger ring, see Fig. 4.9. Calix[4]resorcinarenes make up a platform for creation of more complicated molecular host systems. They form a conical cavity that can be extended by suitable substitution (in the position R and/or X, see Fig. 4.9) and sensitization of the

substituted groups.

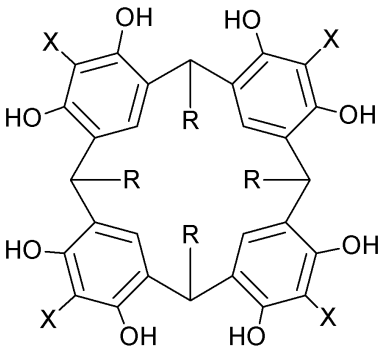

$R=C_{11}H_{23}$
X=H

Fig. 4.9. Molecular structure of the calix[4]resorcinarene.

The cavity of resorcinarenes provides a site for the binding of organic/inorganic ions [Pietraszkiewicz, M. *et al.* 2000, Turshatov, A. A. *et al.* 2004] and organic neutral molecules [Stone, M. M. *et al.* 2002]. The molecule has been investigated previously as a coating for vapours sensing of various volatile organic compounds (ethanol, benzene, toluene, ethylbenzene, ethyl acetate, acetone, hexane, and cumene) [Rusanova, T. Y. *et al.* 2009]. It was found that the proposed sensor was characterized by a short response time – 15s - and reproducible measurements. Calix[4]resorcinarene is an amphihilic molecule and so is proved to form well ordered monolayers that have been deposited on substrates as thin films by Langmuir-Blodgett technique [Hassan, A. K. *et al.* 1999, Sugden, M. W. et al. 2008]. Recently it has been reported that by using an optical fibre with long period coated with a calix[4]resorcinarene nanostructured coating, chemical vapour sensing (toluene, benzene, cyclohexane and hexane) can be performed [Topliss, S. M. *et al.* 2010]. The sensor proposed in this project utilises a calix[4]resorcinarene nanostructured coating formed on a tapered section of an optical fibre using the LB technique in order to facilitate the sensing of ammonia vapours. The material was synthesized by Dr. Frank Davies from Cranfield Health, Cranfield University.

Quinolinium iodide deposited onto fibre tapers

A chloroform solution of the quinolinium iodide salt (0.1mg/ml) was spread onto the pure water subphase of one compartment of a Nima Technology LB trough. The deposition was carried at a surface pressure of 26.0mN/m and a transfer rate of 10 mm/min at the room temperature of 21°C. All spectra were measured by coupling the output from the tungsten-halogen lamp into a fibre and connecting the distal end to Ocean Optics CCD spectrometer of resolution 0.3nm and recorded. The spectrum was recorded when the tapered region of a fibre was above and below the water. This is important as the required thickness of the coating to allow the mode transition to an overlay strongly depends on the surrounding refractive index [James, S. W. *et al.* 2007]. Thus for the quinolinium iodide coated taper the spectrum recorded with a taper below the water was used since the application of the sensor is measurement of pH in different water solutions.

In general, the response of the quinolinum iodide coated tapers to pH was characterised immediately after deposition of the coating. In cases where the experiments were not carried out on the same day, the coated tapers were stored at room temperature immersed in water, in order to prevent drying up of the material. pH measurements were carried at the room temperature of 21°C and were undertaken by immersing the coated taper in buffer water solutions, which covered the pH range of 3-11. The buffer solutions were poured into the solution gap (see Fig. 4.10) of the experimental vessel and a fibre was immersed. The volume of the solution gap was ~3ml. Chemicals were acquired from Aldrich Chemicals. The pH buffers were in a powder form, and were prepared according to producer instructions. The setup is depicted in Fig. 4.10.

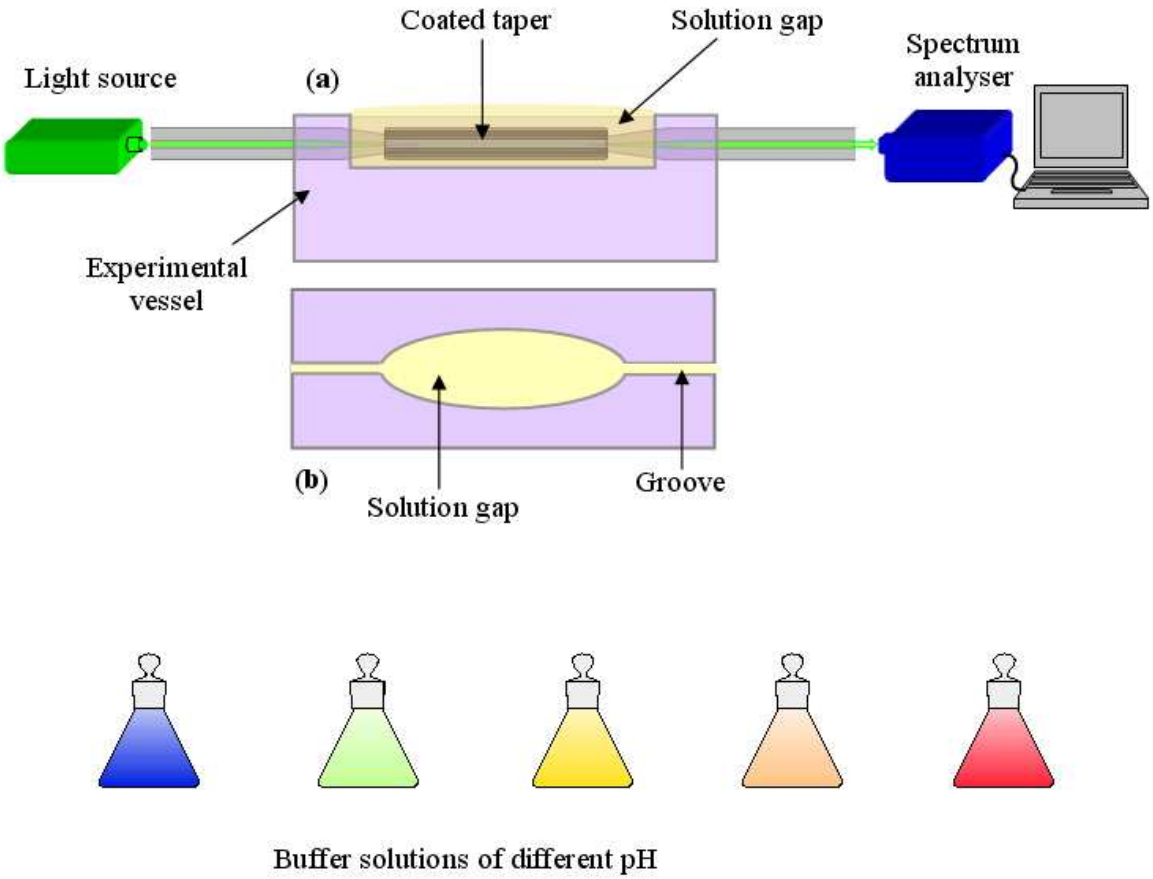

Fig. 4.10. Schematic diagram of the pH experiments setup; a) side view of the experiment vessel with a gap filled with solution and the coated tapered region of a fibre immersed in it; b) top view of the experiment vessel with the solution gap and fibre groove marked.

The coated taper was immersed in pH solutions for 15min for each pH. Before exposure to a subsequent pH solution a fibre was immersed in deionized water for 15min and rinsed thoroughly afterwards. Each series of measurements of the whole pH range for each taper was repeated three times. Both ends of a fibre were long enough to facilitate leading outside the experimental vessel and light coupling into a fibre and lead out to a spectrometer.

Calix[4]resorcinarene deposited tapers

A chloroform solution of the calix[4]resorcinarene was spread onto the water/air surface of the Nima Technology LB trough from the 0.1mg/ml chloroform solution. The deposition was carried at a surface pressure of 26.0mN/m and a transfer rate of 30 mm/min at room temperature, 21°C. All spectra were measured by coupling the output from the tungsten-halogen lamp into a fibre and connecting the distal end to Ocean Optics CCD spectrometer of resolution 0.3nm and recorded. For the calix[4]resorcinarene coated tapers the spectrum recorded with a taper above the water was used since the destination of the sensor is gas sensing.

After the deposition of the calix[4]resorcinarene film onto tapered fibres the ammonia sensitivity of the sensor was investigated. In case the experiments were not carried out on the same day the coated tapers were stored at room temperature in air. These experiments were carried out in a gaseous environment, see Fig. 4.11. The coated tapers were placed in a sealed glass container of volume of 3 liters. Ammonia drops of volume 20μl were injected, at room temperature of 21°C and atmospheric pressure, inside the chamber. The analyte vaporised inside the chamber and the response of the sensor to the vapour concentration was recorded. Drops were placed inside the container using a micro-syringe through a pipe in the container cover which was sealed immediately after each injection. The ammonia solution (d = 0.88g/cm^3, HiPerSolv for HPLC) was acquired from BDH Laboratory Supplies.

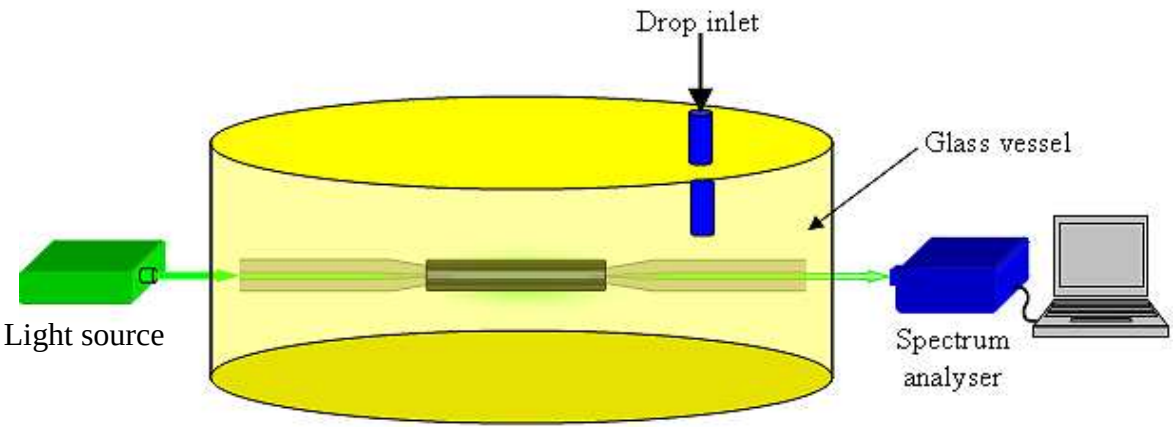

Fig. 4.11. Schematic diagram of the ammonia sensing setup.

The volume of the glass container and volume of each ammonia drop was known, thus the ammonia vapour concentration was calculated. Both ends of a fibre were led out of the experimental vessel through the cover, which was subsequently sealed and the light was coupled into the fibre. All spectra were recorded using the CCD spectrometer.

4.3. Chemical deposition of polyaniline (PANI)

For the chemical deposition of an overlay onto tapered region of a fibre the polyaniline (PANI) molecule was used. The compound was chosen for chemical sensing in solutions. Polyaniline belongs to a family of conducting polymers. This polymer exists in a number of chemical forms that differ in their oxidation and protonation states, see Fig. 4.12

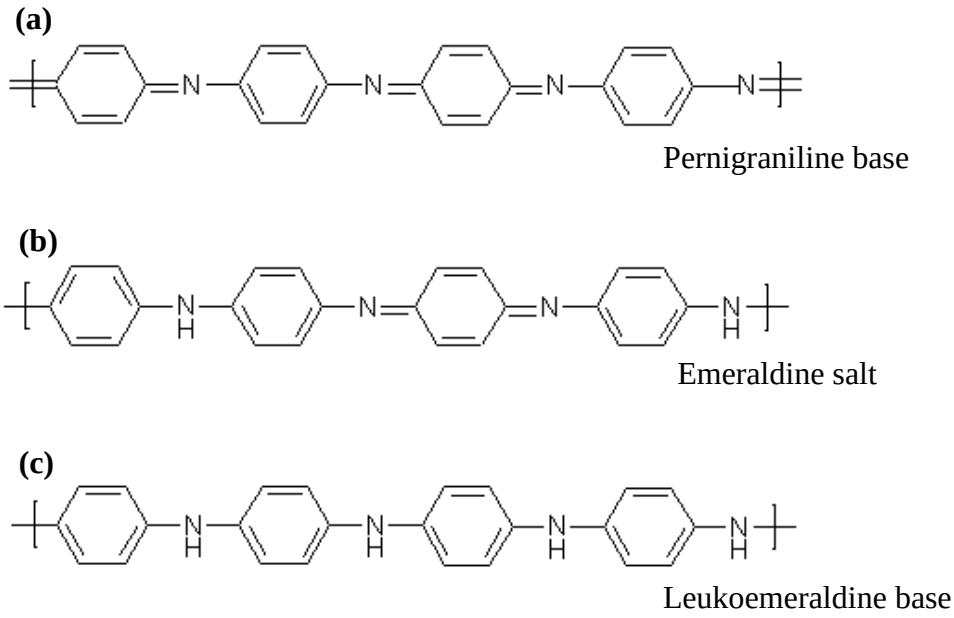

Fig. 4.12. Molecular structure of accessible oxidation states of polyaniline; (a) fully oxidized pernigraniline base, (b) half oxidized emeraldine salt, (c) fully reduced leukoemeraldine base.

The only conducting form of polyaniline is the protonated polymer - emeraldine salt. The charged form of the polymer shows the well known “capacitive behaviour” [Meerholz, K. *et al*, 1993, Paasch, G. *et al*, 1998]. This state is caused by the redox process [Neudeck, A. *et al*, 1999] and can be used in pH sensing based on the change of the oxidation states inside the polymer layer. The acid-base equilibrium must be established between emeraldine salt and both base forms within entire material before measurements can be conducted [Lindfors, T. *et al.* 2004]. Polyaniline is usually prepared in aqueous, acidic media in which the formed polymer precipitates during the reaction. It has been confirmed that for good reproducible spectroscopic properties the synthesis must be carried out below 0°C [Cao, Y. *et al.* 1989].

The material is capable of film forming and as being pH [Wallace, G. G. *et al.* 2003, Lindfors, T. *et al.* 2006] and red-ox [Genies, E. M. *et al.* 1985] sensitive polyaniline is a

good candidate for the use in sensor fabrication. There are few reports on the use of polyaniline in the fabrication of fibre optic pH sensors [Ge, Z. F. e*t al.* 1993, Aizawa, M. 1991]. The sensor proposed in this project utilises polyaniline coating formed in chemical synthesis process on tapered section of an optical fibre in order to facilitate the redox sensing in solutions.

Polyaniline deposited tapers

The manufactured, characterized and cleaned tapers were subjected to the following studies of their potential use as redox sensors with a polyaniline (PANI) coating. In this research the standard procedure for PANI creation was used, see Fig. 4.13.

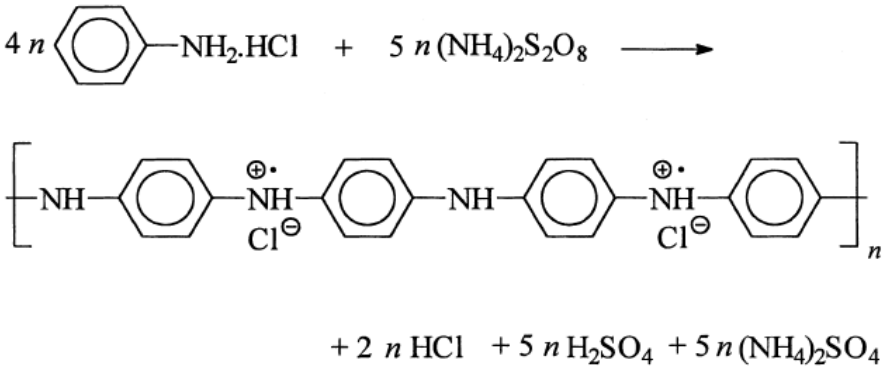

Fig. 4.13. Oxidation of aniline hydrochloride with ammonium peroxydisulphate yields polyaniline hydrochloride.

Tapered optical fibres were mounted on a holder and placed in glass dish. Both ends of a fibre were led outside the reaction dish to enable connection to the light source and CCD spectrum analyzer, see Fig. 4.14.

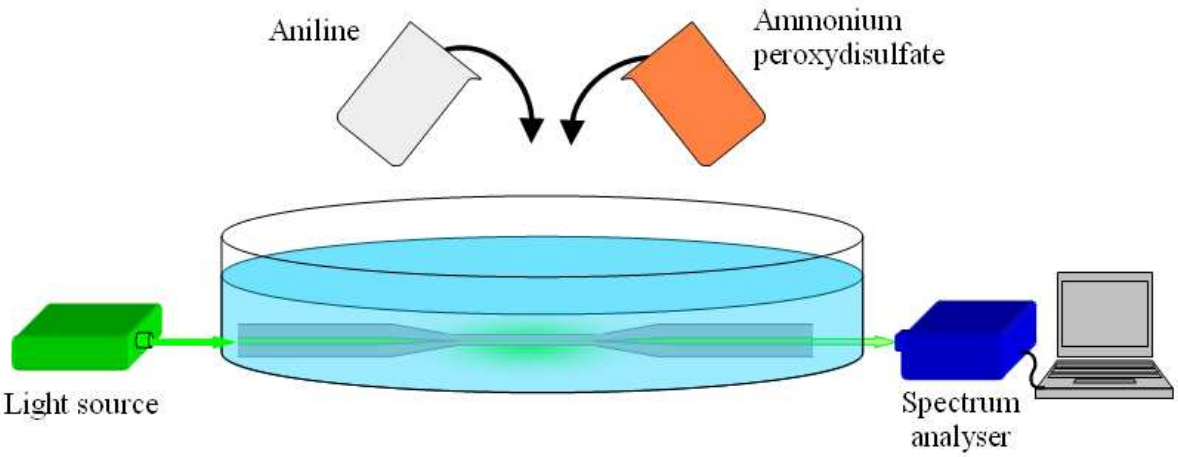

Fig. 4.14. Schematic diagram of the setup for polyaniline overlay deposition onto tapered optical fibre.

Then aniline hydrochloride was mixed with ammonium peroxydisulphate as an oxidizing-polymerizing agent. In order to maintain low temperature required for the polymerization process the experimental glass dish was immersed in a plastic cuvette 40 x 30 x 10cm filled with ice. The temperature was kept within the range (-10)-(-5)^{o}C by providing to an ice-bath a frozen salted ice. All chemicals were purchased from Aldrich. PANI molecules were formed in the polymerization process and precipitated onto immersed fibres, creating a thin film. For this purpose 50ml of 0.1M solution of aniline in 2M hydrochloric acid was placed in a glass dish and 50ml of solution of 0.1M ammonium peroxydisulfate in 2M hydrochloric acid was added.

A thin film formed in 10 min on the tapered fibre placed inside the experimental dish. The polymerization was stopped by taking out and washing a coated taper thoroughly with running distilled water. Subsequently, the coated tapered fibre was used for redox sensing experiments.

Just after the deposition of a functional layer on a taper, either chemically or by the LB technique, the tapers were used in reduction-oxidation experiments. In case the experiments were not carried out on the same day that the fibres were coated, then the fibres were stored at room temperature immersed in water. It has been reported

[Pringsheim, E. *et al.* 1997] that polyaniline films undergo irreversible change after few hours of the exposure to air, they are no longer sensitive.

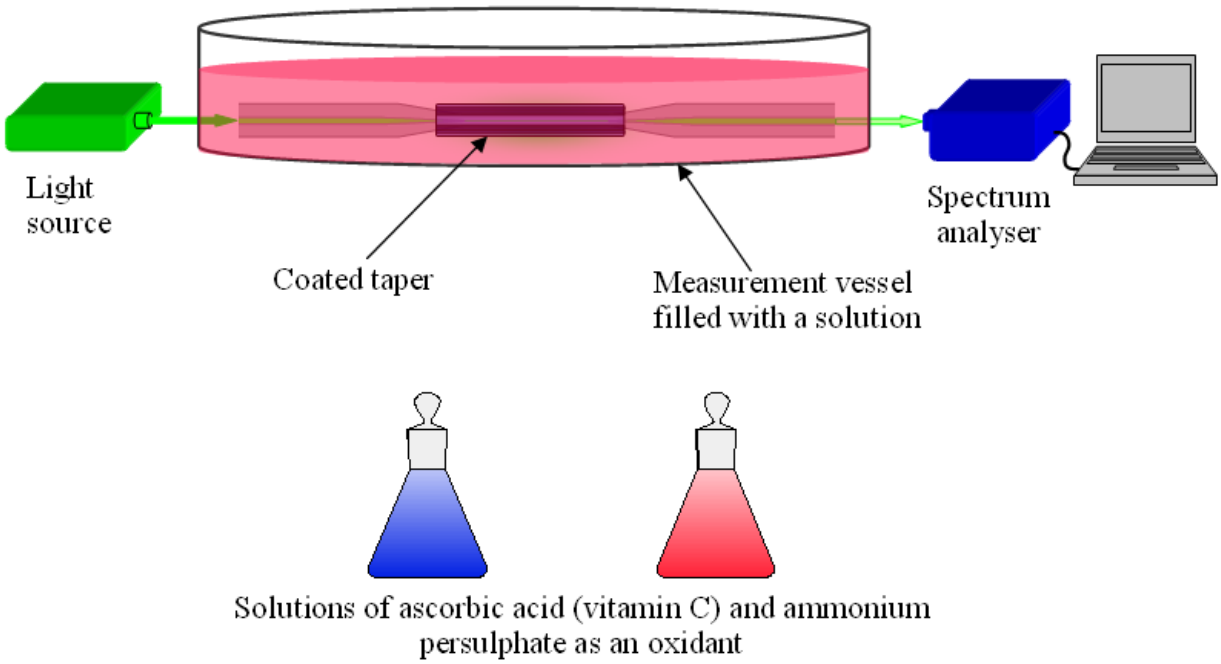

Fig. 4.15. Schematic diagram of the setup for red-ox experiments of the polyaniline-coated fibres.

Redo-ox experiments were carried in a water solution of ascorbic acid (vitamin C), which acted as a reductor, and ammonium persulphate, which acted as an oxidant, see Fig. 4.15. Freshly prepared water solutions of 0.5% ascorbic and 0.5% ammonium persulphate were alternately added to a vessel with taper coated with PANI film and the spectra were recorded over a period of 10 minutes. After each immersion a taper was thoroughly rinsed with distilled water. Measurements for each taper were repeated three times.

4.4. Electrostatic layer-by-layer (Lbl) self assembly deposition technique

The electrostatic layer-by-layer adsorption method was used for the deposition of thin nanostructured films onto tapered region of a fibre. Sequential Lbl assembly has proven to

be a competitive procedure for the thin film of well-defined organic films deposition [Schmitt, J. et al. 1993, Decher, G. *et al.* 1994]. The chosen target compound in our experiments was ammonia gas since its sensitive detection is desired in medical, environmental and chemical areas of human activity [Timmer, B. *et al.* 2005]. The sensing material composed of multilayer of cationic poly(allyamine hydrochloride) (PAH) and anionic tetrakis(4-sulfophenyl)porphine (TSPP) were deposited onto a taper, see Fig. 4.16.

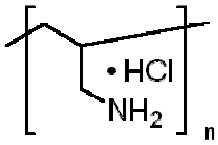

Fig. 4.16. (a) molecular structure of the poly(allyamine hydrochloride) – PAH

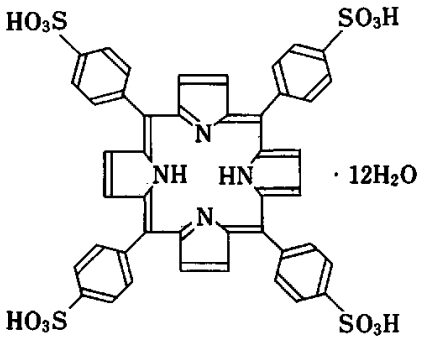

Fig. 4.16. (b) molecular structure of the tetrakis(4-sulfophenyl)porphine - TSPP.

A tapered fibre was mounted on the straight holder and placed in an experimental vessel made of Teflon, see Fig. 4.17. The tapered region of a fibre was placed in the solution gap (see Fig. 4.17) and the experimental vessel was filled subsequently with the reaction solutions.

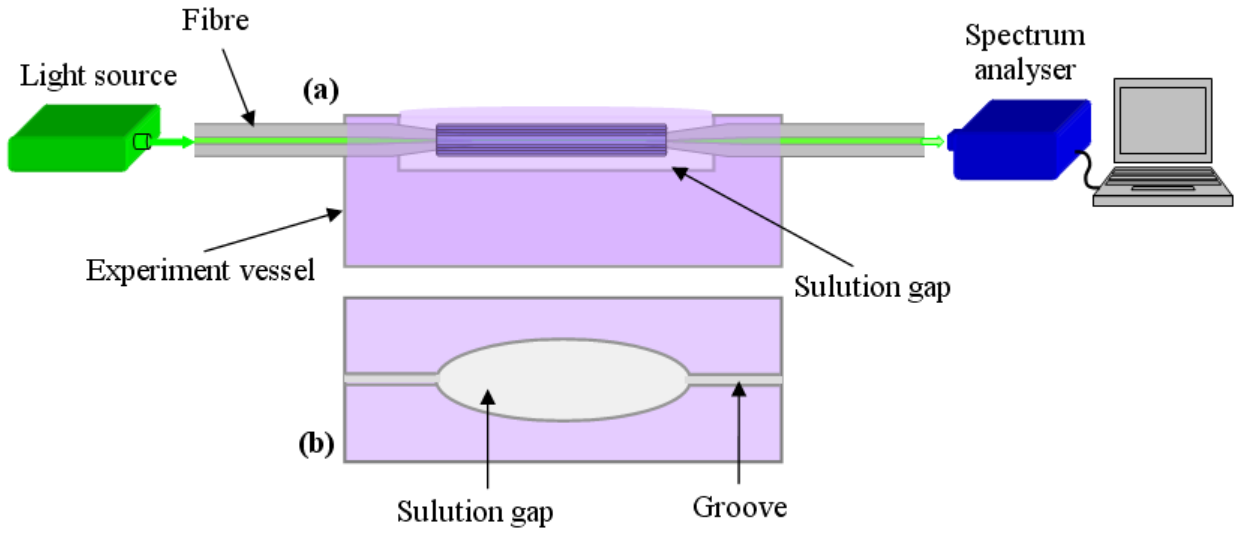

Fig. 4.17. Schematic diagram of the Lbl deposition setup; a) side view of the experiment vessel with a gap filled with solution and the tapered region of a fibre immersed in it; b) top view of the experiment vessel with the solution gap and fibre groove marked.

The tapered region of an optical fibre was fixed on holder, rinsed with deionized water and – prior to the deposition - immersed into 1% wt ethanol solution of KOH for 20min in order to negatively charge the fibre surface. Subsequently the fibre was immersed in a 5mg/ml water solution of positively charged polymer poly(allyamine hydrochloride) (PAH) for 20min. During this time a monolayer of PAH was deposited on the fibre surface. Next the fibre was rinsed thoroughly with distilled water and dried in a stream of nitrogen. The fibre was then immersed for 20min in a 1mM solution of a functional dye tetrakis(4-sulfophenyl)porphine (TSPP), which provides the specificity of the sensor. The fibre was then rinsed with distilled water and dried.

The deposition of a multilayered structure was achieved by the sequential dipping of the tapered fibre in PAH and TSPP solutions, as depicted in Fig. 4.18. Deposition was stopped after 5 cycles when the desired thickness of the multilayered film was achieved.

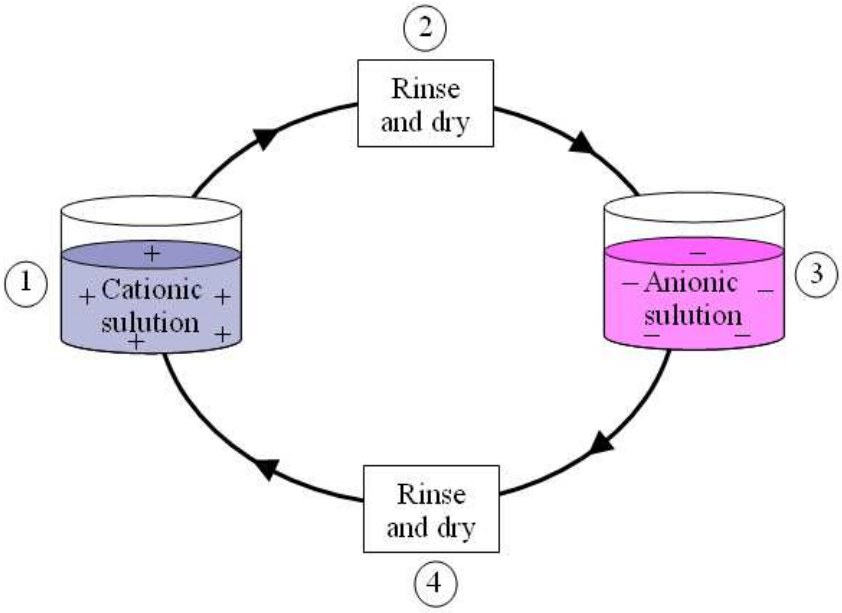

Fig. 4.18. Diagram of the layer-by-layer deposition process.

Experiments on this material were carried out in Japan in collaboration with the group of Environmental Materials of Graduate School of Environmental Engineering of the University of Kitakyushu. All chemicals were provided by Dr Sergiy Korposh from the University of Kitakyushu, Japan.

After the deposition of the multilayer coating film onto tapered fibres the ammonia sensitivity of the sensor was investigated. These experiments were carried out in gaseous environment. Figure 4.19 shows a schematic diagram of the experimental apparatus used for gas detection. The coated taper was placed in the measurement chamber where the desired gas concentration was set up. Compressed air was used as a carrier gas. The desired gas concentration was achieved by mixing the air with gas in a proper gas flow ratio.

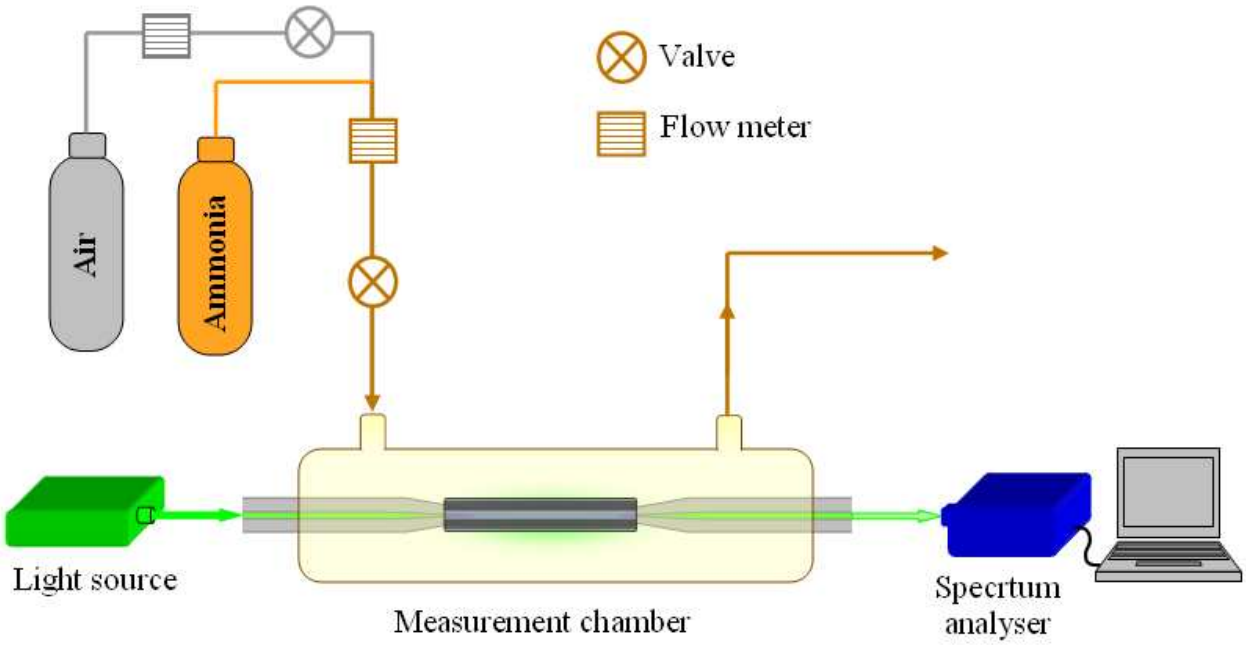

Fig. 4.19. Schematic diagram of experimental setup for ammonia sensing study of Lbl coated tapers.

Both ends of a fibre were led out of the experimental vessel and the light was coupled into the fibre. All spectra were recorded using CCD spectrometer.

In this chapter techniques and experimental setups utilized in realization of the project were described. The aim of the project was to create fibre optic sensors with an application potential in the solution and gaseous environments. It was carried out in the following steps: 1. manufacture of tapered optical fibres and their physical characterisation using microscopic techniques. 2. Deposition of functional nanocoatings onto the tapered region of optical fibres using one of the deposition techniques, it is Langmuir-Blodgett, or chemical deposition or electrostatic layer-by-layer self assembly technique. 3. Study of a coated tapered fibre as a potential sensors by exposure to a specific stimulus in water or in the gaseous environment.

4.5. Mathematical model

The planar multilayer model together with transformation of the optical properties of the cylindrical fibre to a planar geometry allows describing the tapered fibres operation in

terms of the spectral response to increasing overlay thickness. For the calculation of the transmission spectrum a structure depicted in Fig. 4.20 was analysed.

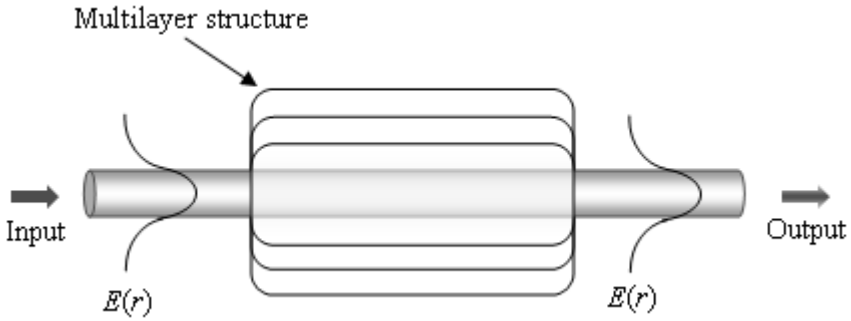

Fig. 4.20. Diagram of the structure used for the simulation of overlay device optical properties.

The complete theoretical formulation was coded in MATLAB7 (code access thanks to Dr Stephen W. James). A block diagram of calculation scheme is depicted in Fig. 4.21 and a program listing is shown in Appendix B.

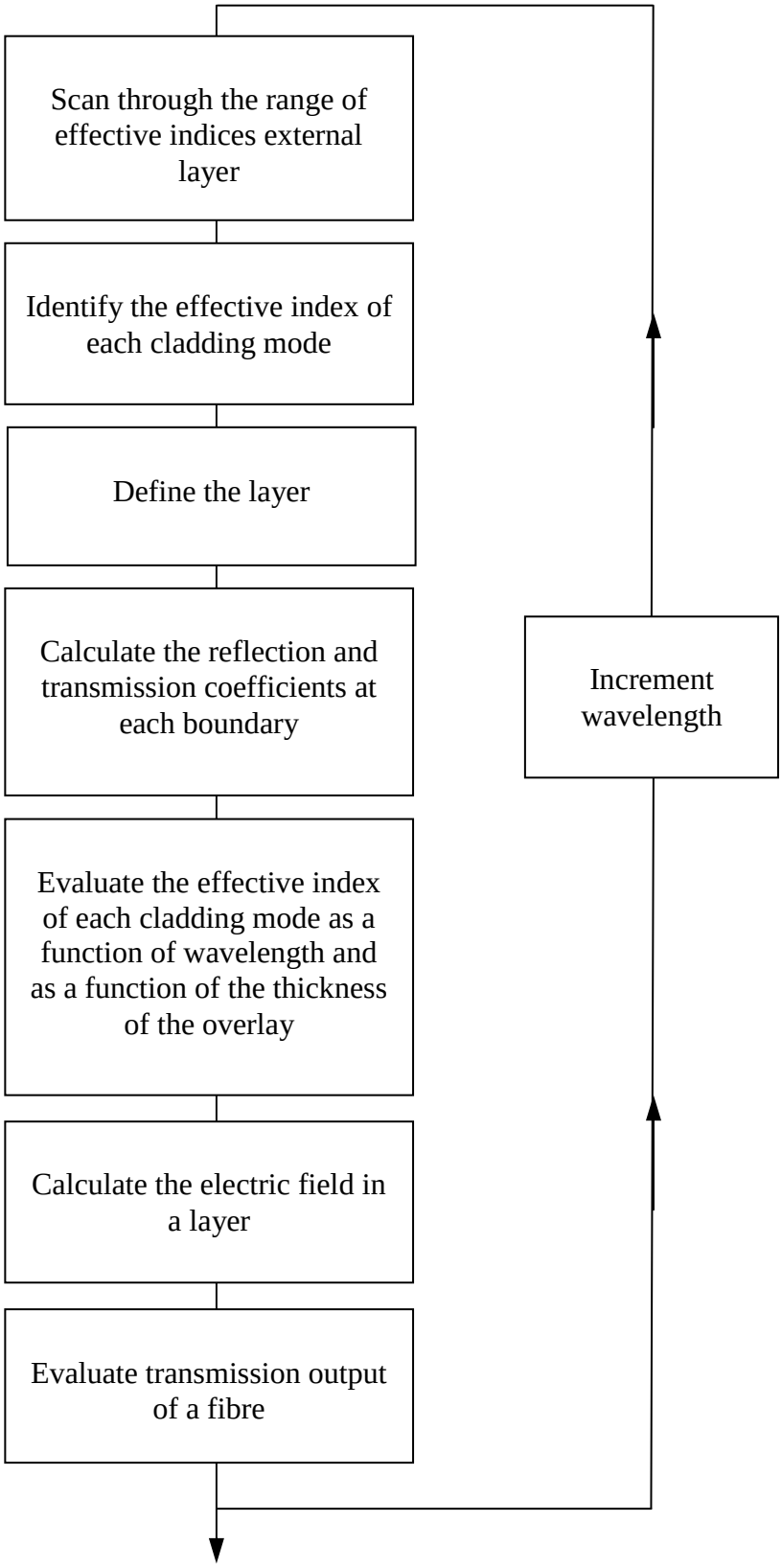

Fig. 4.21. Computational scheme for calculating tapered optical fibre transmission.

References

Aizawa, M., "Principles and applications of electrochemical and optical biosensors", *Analytica Chimica Acta*, Vol. 250, No. 1, pp. 249-256, 1991

Ashwell, G., Gandolfo, D. S., Hamilton, R., "Molecular rectification: characterization of a dye sandwiched between gold electrodes", *Journal of Materials Chemistry*, Vol. 12, No. 3, pp. 416-420, 2002

Ashwell, G., Jefferies, G., George, C. D., Ranjan, R., Charters, R. B., Tatam, R. P, "Z-type Langmuir-Blodgett film structures: surface plasmon resonance, second harmonic generation and fibre optic devices", *Journal of Materials Chemistry*, Vol. 6, No. 2, pp. 131-136, 1996

Blodgett, K.B., "Films built by depositing successive monomolecular layers on a solid surface", *Journal of American Chemical Society*, Vol. 57, pp. 1007-1002, 1935

Cao, Y., Andreatta, A., Heeger, A. J., Smith, P., "Influence of chemical polymerization conditions on the properties of polyaniline", *Polymer*, Vol. 30, No. 12, pp. 2305-2311, 1989

Decher, G., Lehr, B., Lowack, K., Lvov, Y., Schmitt, J., "New nanocomposite films for biosensors - layer-by-layer adsorbed films of polyelectrolytes, proteins or dna", *Biosensors & Bioelectronics*, Vol. 9, No. 9-10, pp. 677-684, 1994

Ge, Z. F., Brown, C. W., Sun, L. F., Yang, S. C., "Fiberoptic ph sensor-based on evanescent-wave absorption-spectroscopy", *Analytical Chemistry*, Vol. 65, No. 17, pp. 2335-2338, 1993

Genies, E. M., Syed, A. A., Tsintavis, C., "Electrochemical study of polyaniline in aqueous and organic medium - redox and kinetic-properties", *Molecular Crystals And Liquid Crystals*, Vol. 121, No. 1-4, pp. 181-186,1985

Hassan, A. K., Nabok, A. V., Ray, A. K., Lucke, A., Smith, K., Stirling, C. J. M., Davis, F., "Thin films of calix-4-resorcinarene deposited by spin coating and Langmuir-Blodgett techniques: determination of film parameters by surface plasmon resonance", *Materials Science & Engineering C-Biomimetic And Supramolecular Systems*, Vol. 8-9, Sp. Iss., pp. 251-255, 1999

James, S. W., Cheung, C. S., Tatam, R. P., "Experimental observations on the response of 1st and 2nd order fibre long period grating coupling bands to the deposition of nanostructured coatings", *Optics Express*, Vol. 15, No. 20, pp. 13096-13107, 2007

Lindfos, T., Ivaska, A., " Optical pH measurements with water dispersion of polyaniline nanoparticles and their redox sensitivity", *Analytical Chemistry*, Vol. 78, No. 9, pp. 3019-3026, 2006

Lindfors, T., Sandberg, H., Ivaska, A. "The influence of lipophilic additives on the: emeraldine base-emeraldine salt transition of polyaniline", *Synthetic Metals*, Vol. 142, No. 1-3, pp. 231-242, 2004

Peterson, I.R. "Langmuir-Blodgett films", *Journal of physics D: Applied Physics*, Vol. 23, pp. 379-395, 1990

Pietraszkiewicz, M., Pietraszkiewicz, O., Uzig, E., Prus, P., Brzozka, Z., Wozniak, K., Bilewicz, R., Borowiak, T., Maczynski, M., "Recent advances in calix[4]resorcinarene chemistry", *Chemistry and Computational Simulation. Butlerov Communications*, No. 3, pp. 55-65, 2000

Pringsheim, E., Terpatschnig, E., Wolfbeis, O. S., "Optical sensing of pH using thin films of substituted polyanilines", *Analytica Chimica Acta*, Vol. 357, No. 3, pp. 247-252, 1997

Rusanova, T. Y., Kalach, A. V., Rumyantseva, S. S., Shtykov, S. N., Ryzhkina, I. S., "Determination of volatile organic compounds using piezosensors modified with the Langmuir-Blodgett films of calix[4]resorcinarene", *Journal Of Analytical Chemistry*, Vol. 64, No. 12, pp. 1270-1274, 2009

Schmitt, J., Grunewald, T., Decher, G., Pershan, P. S., Kjaer, K., Losche, M., "Internal Structure Of Layer-By-Layer Adsorbed Polyelectrolyte Films - A Neutron And X-Ray Reflectivity Study", *Macromolecules*, Vol. 26, No. 25, pp. 7058-7063, 1993

Stokes, D. J., "Principles and Practice of Variable Pressure: Environmental Scanning Electron Microscopy (VP-ESEM)", John Wiley & Sons Ltd., 2008

Stone, M. M., Franz, A. H., Lebrilla, C. B., "Non-covalent calixarene-amino acid complexes formed by MALDI-MS", *Journal Of The American Society For Mass Spectrometry*, Vol. 13, No. 8, pp. 964-974, 2002

Sugden, M. W., Richardson, T. H., Davis, F., Higson, S. P. J., Faul, C. F. J., "Langmuir and LB properties of two calix[4]resorcinarenes: Interactions with various analytes", *Colloids And Surfaces A-Physicochemical And Engineering Aspects*, Vol. 321, No. 1-3, Sp. Iss., pp. 43-46, 2008

Timmer, B., Olthuis, W., van den Berg, A., "Ammonia sensors and their applications - a review", *Sensors And Actuators B-Chemical*, Vol. 107, No. 2, pp. 666-677, 2005

Topliss, S. M., James, S. W., Davis, F., Higson, S. P. J., tatam, R. P., "Optical fibre long periog grating based selective vapour of volatile organic compounds", *Sensors and Actuators B: Chemical*, Vol. 143, pp. 629-634, 2010

Turshatov, A. A, Melnikova, N. B., Semchikov, Yu. D., Ryzhkina, I. S., Pashirova, T. N., Mobius, D., Zaitsev, S. Yu., "Interaction of monolayers of calix[4]resorcinarene derivatives with copper ions in the aqueous subphase", *Colloids and Surfaces A*, Vol. 240, No. 1-3, pp. 101-106, 2004

Wallace, G. G., Spinks, G. M., Kane-Maguire, L. A., Teasdale, P. R., "Conductive Electroactive Polymers: Intelligent materials systems", 2nd edition, CRC press, Boca Raton, Florida, pp. 121-177, 2003

Yao, N., "Focused Ion Beam Systems: Basis and Applications", Cambridge University Press, 2007

RESULTS 5

In this section the characteristics of the fabricated tapers the response of their transmission spectra to the deposition of nanostructured coatings, and a study of the use of coated tapers for chemical sensing are presented.

5.1 Fabrication and characterisation of tapers

The waist diameters of the optical fibre tapers fabricated over the course of the research described in this thesis were within the range 3 – 40μm. The uniform section of the taper was observed using an optical microscope and an ESEM. Typically the section of the taper with uniform diameter was found be of length of order hundreds of micrometers, the exact length being dependent on the taper waist diameter. The smaller the taper diameter, the longer the duration of the pulling process and the longer the uniform waist region. The diameter of each taper was measured at 10 locations along it length.

Figure 5.1 shows two typical ESEM (Environmental Scanning Electron Microscope) images of typical tapered fibres fabricated using the process described in section 4.1.

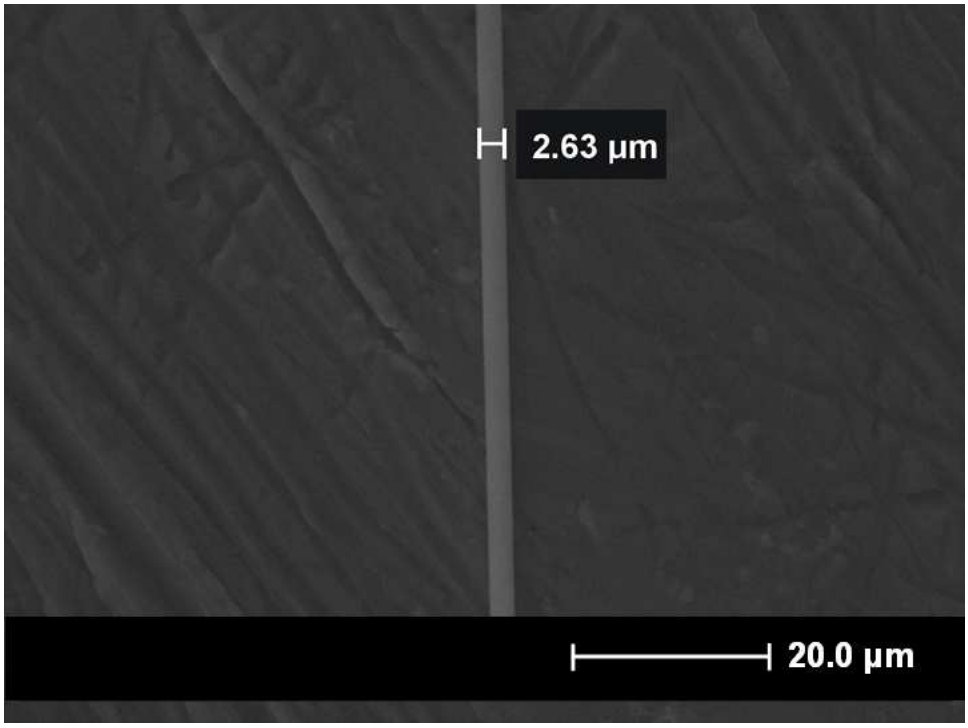

(a)

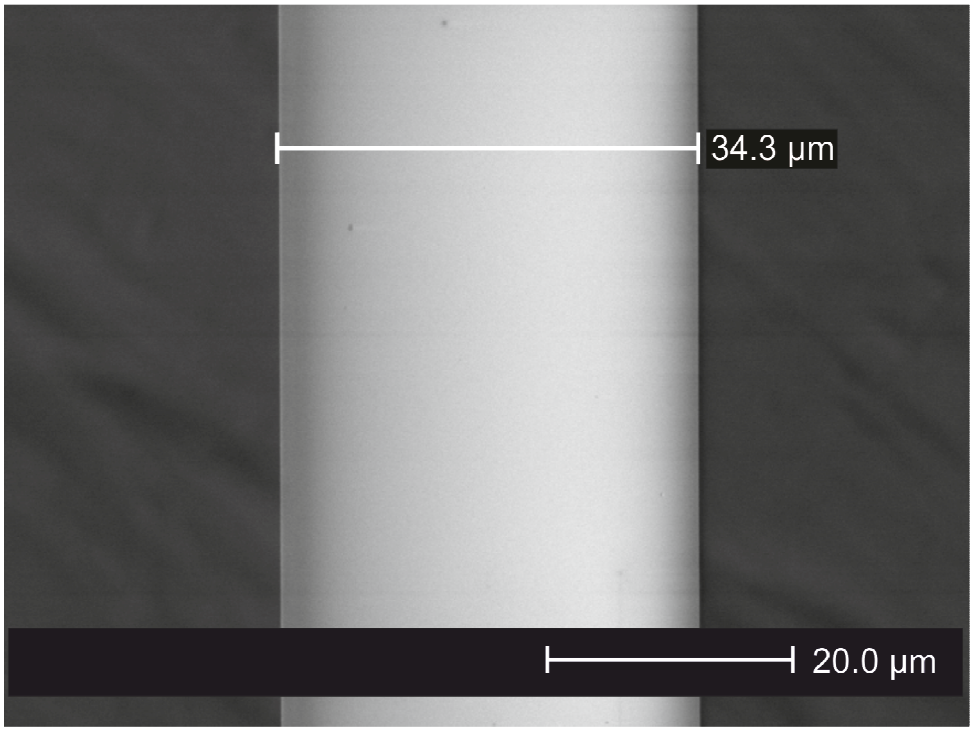

(b)

Fig. 5.1. ESEM images of examples of tapered fibres. (a) ~3µm taper; (b) ~37µm taper.

The visual inspection of ESEM images shows very good side–wall smoothness, which is required for low loss operation [Love, J. D. *et al*. 1991]. The cross-section of a tapered fibre was also studied; using the Focus Ion Beam (FIB) technique to cut a waist and subsequently using ESEM to scan its surface (see Fig. 5.2).

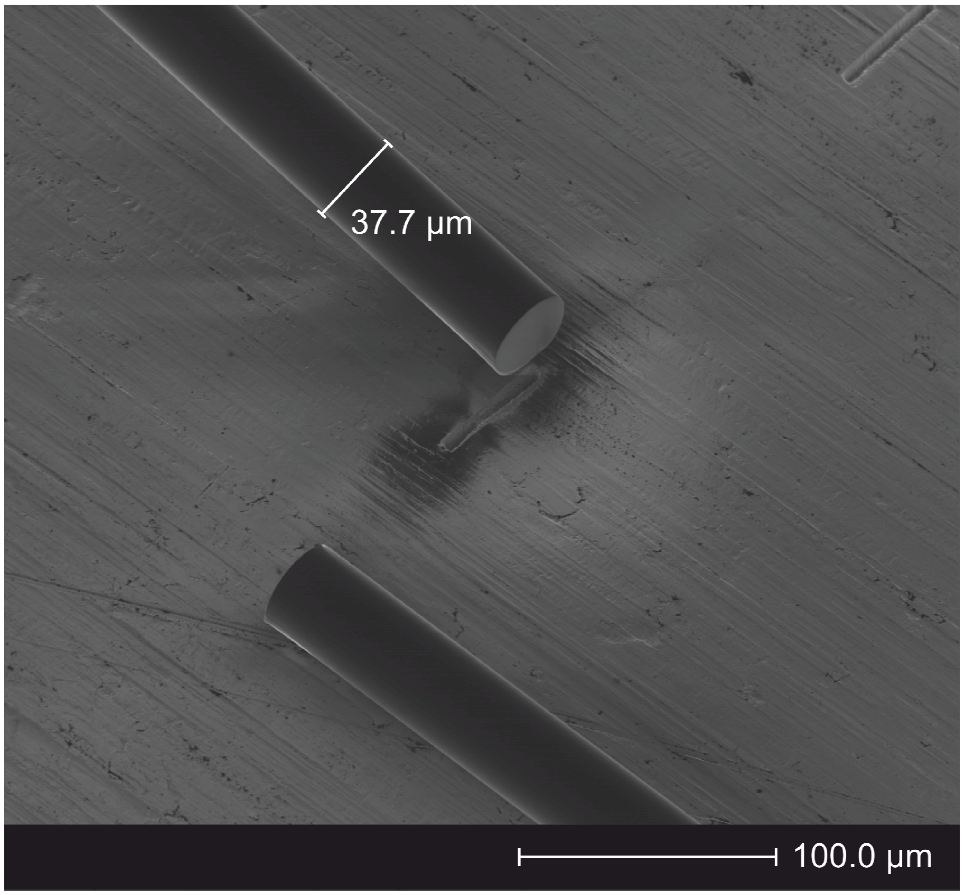

(a)

Fig. 5.2. Fibres cleaved using FIB. (a) 37.7µm diameter taper imaged using the SEM built into the FIB device.

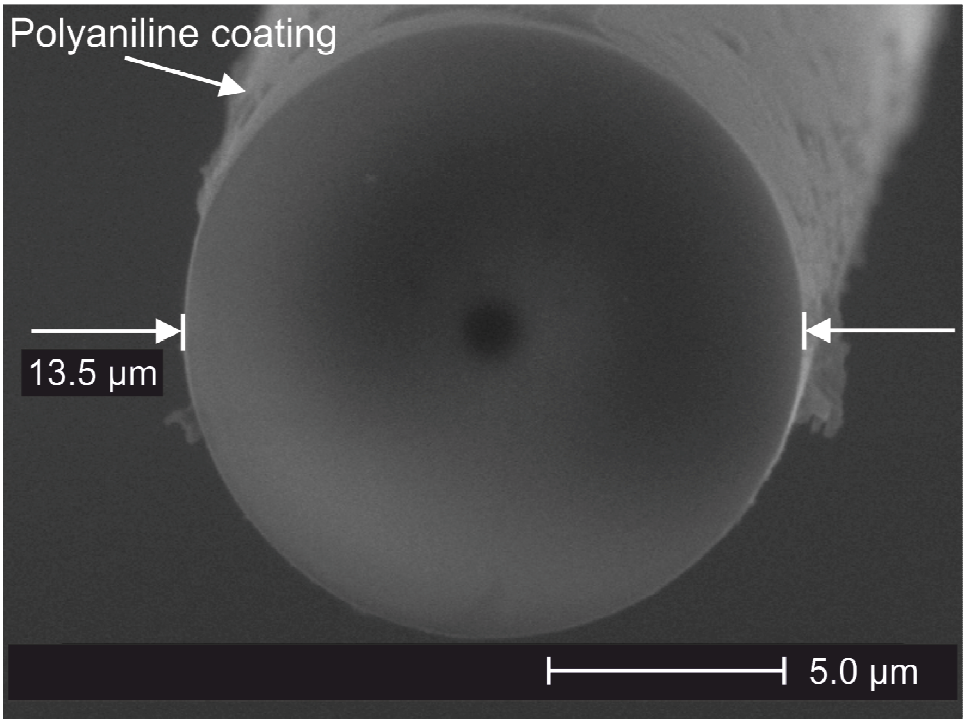

(b)

Fig. 5.2. Fibres cleaved using FIB. (b) cross-section of a 13.5µm taper waist cut with FIB and scanned using an ESEM. Both fibres were single mode Fibrecore SM750.

Figure 5.2(b) suggests the presence of the fibre core within the tapered fibre waist, which in this case has ~1.3µm diameter, and that the circular symmetry of a fibre has not been disturbed. Prior to FIB cutting and recording the ESEM image, the taper shown had been coated with an overlay material (polyaniline) for a separate, unrelated experiment, which explains the rough side-wall surface.

The transmission spectrum of each fibre was recorded before and after tapering. The spectral analysis showed that the form and intensity of the spectrum of tapers with waist diameters greater than 20µm was not changed, whilst it showed substantial change for tapers with waist diameters smaller than 20µm (see Fig. 5.3(a)-(f)).

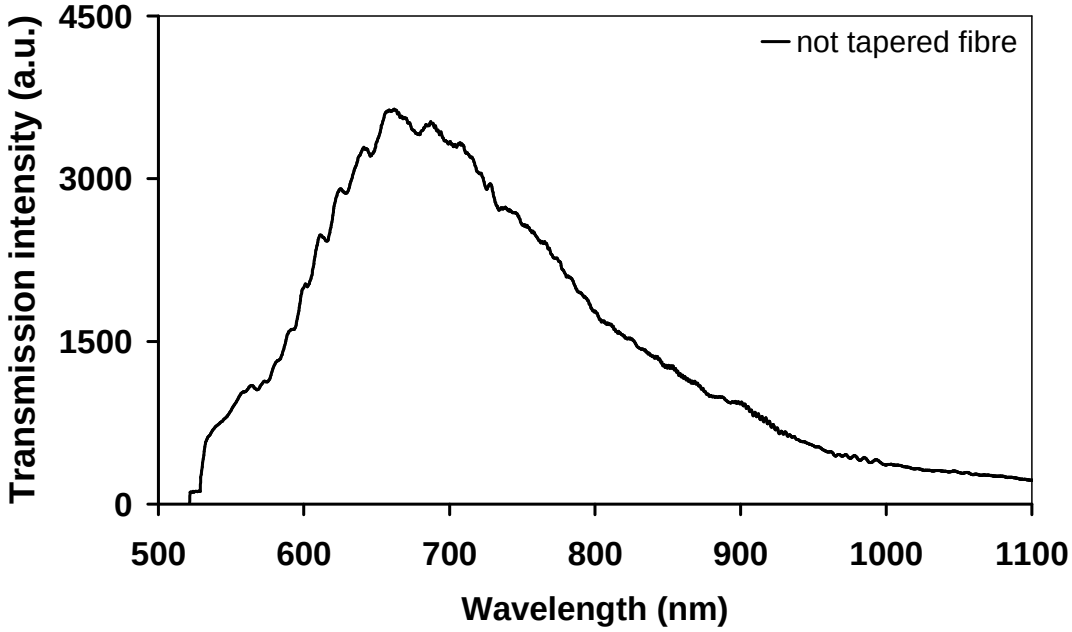

(a)

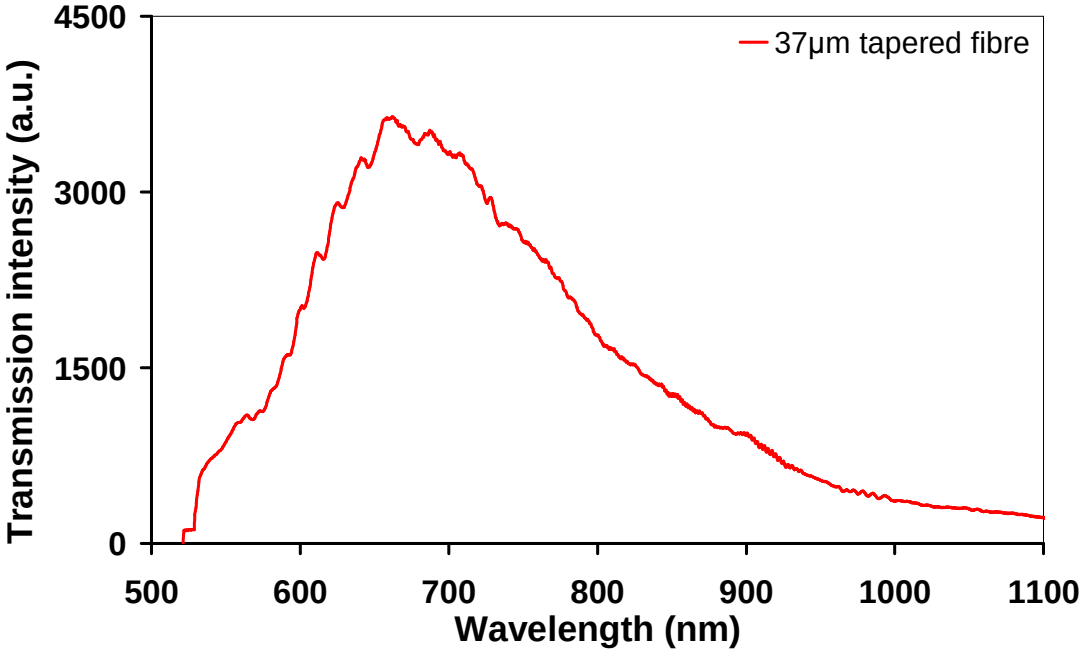

(b)

Fig. 5.3 (a)(b). The transmission spectra of fibre before the tapering (a) and after the process and their difference due to the taper waist diameter; (b) transmission spectrum of a 37µm fibre taper.

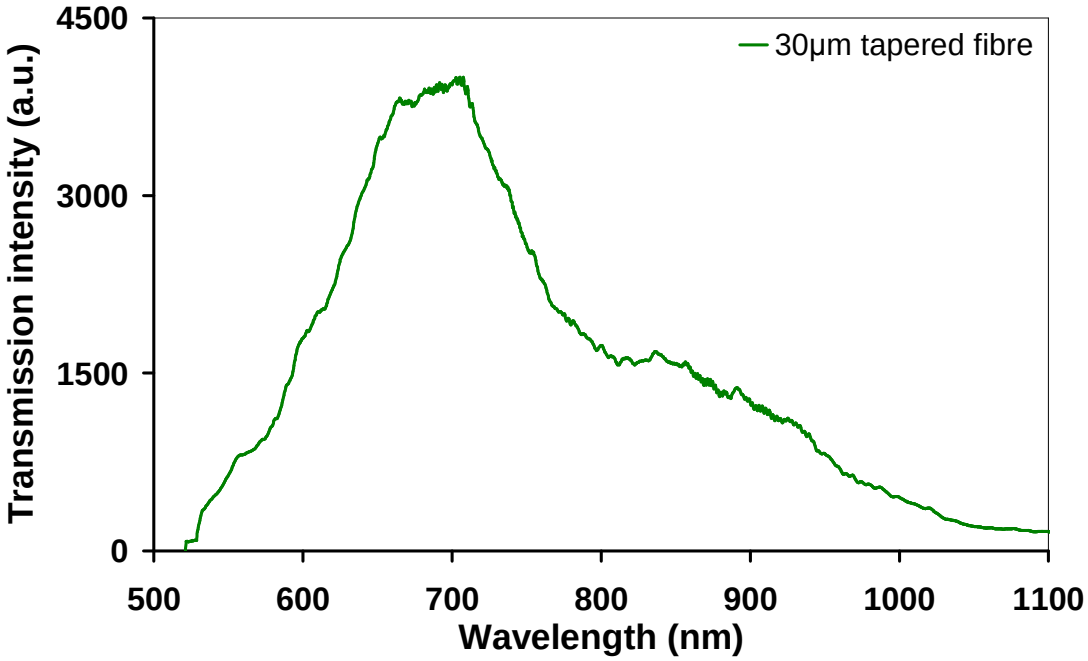

(c)

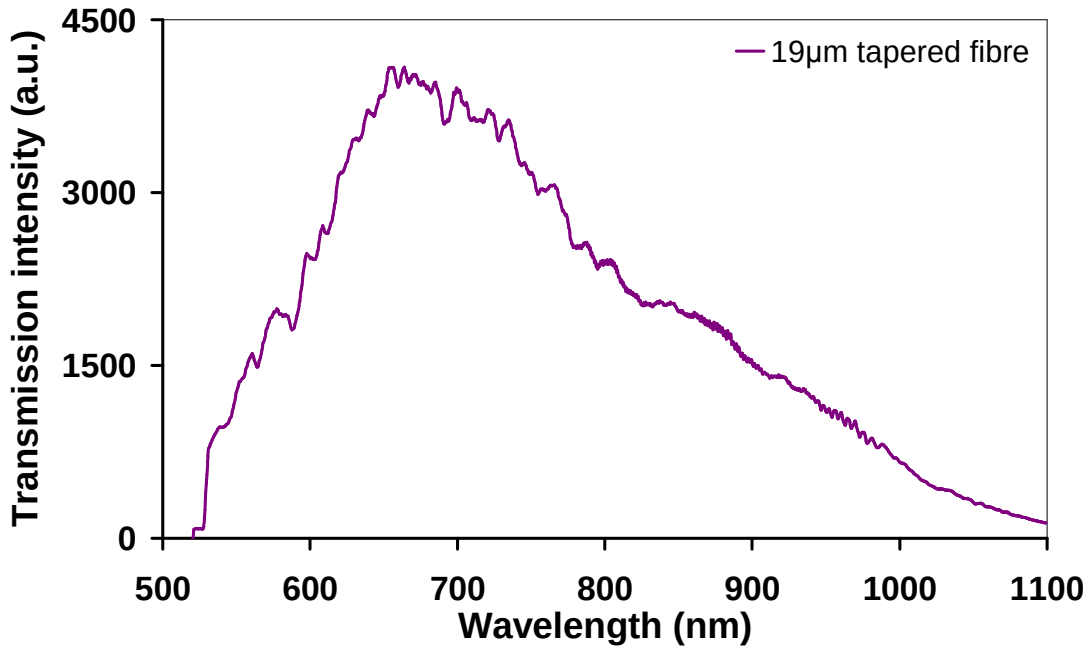

(d)

Fig.5.3(c)(d). Transmission spectrum of a 30μm fibre taper (c) and 19μm taper (d).

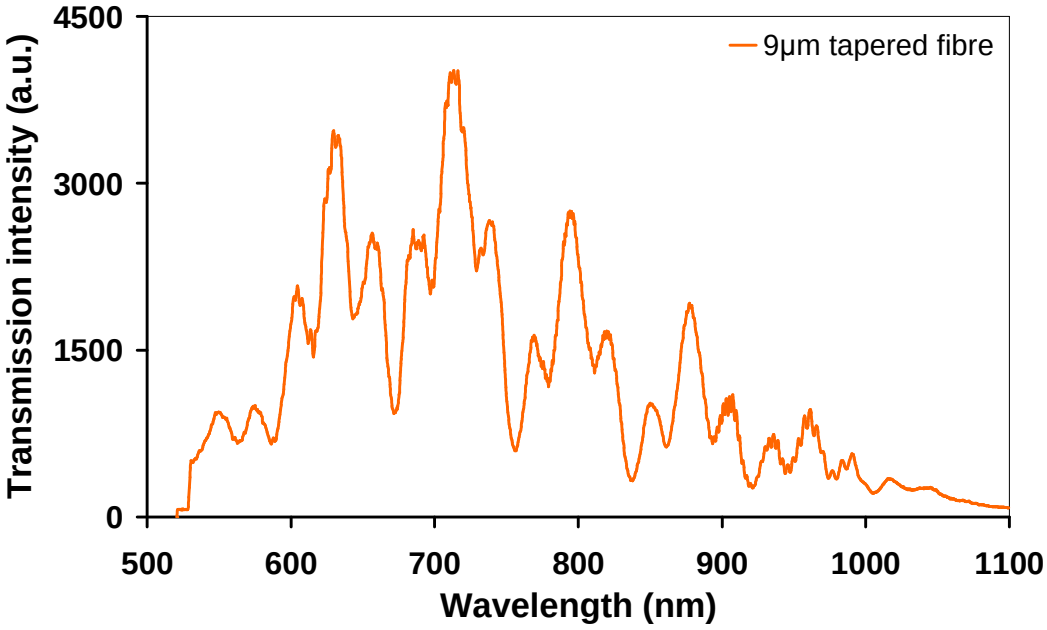

(e)

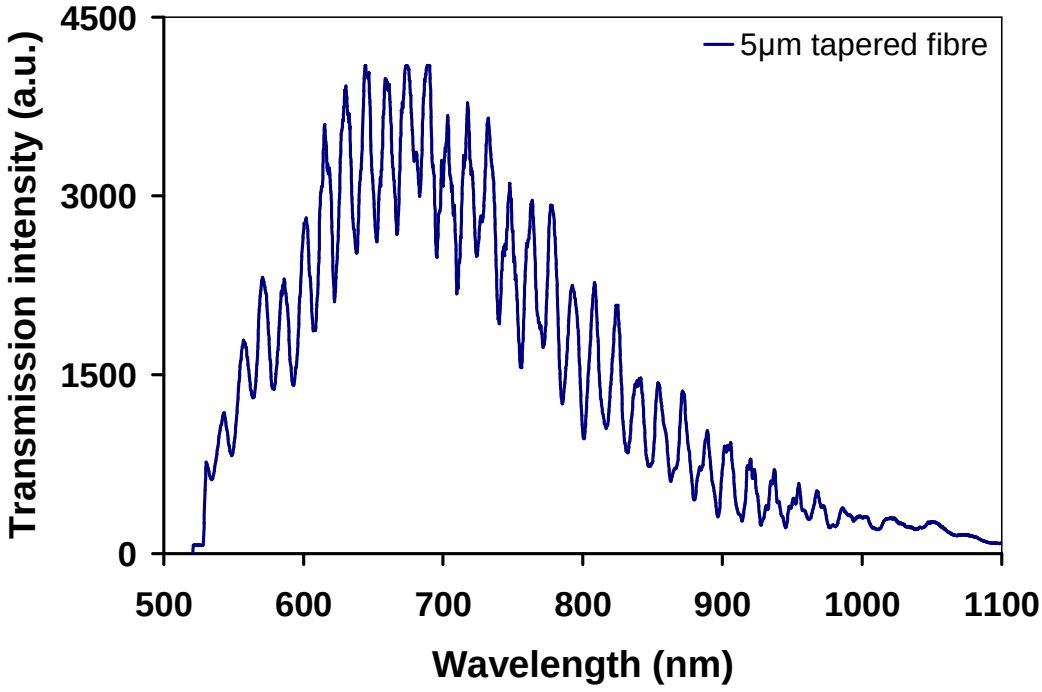

(f)

Fig. 5.3(e)(f). transmission spectrum of a 9µm fibre taper (e) showing a spectrum response containing interference effects; (f) transmission spectrum of a 5µm taper showing channelled spectrum response due to interference effects.

Tapers with diameters in the range 5 – 20μm develop features within the transmission spectrum. These features taking on a sinusoidal form for tapers of 5μm diameter, which, as has already been described in chapter 3.1, corresponds to a channeled spectrum arising from the interference between two modes of the fibre taper, and effect characteristic of a nonadiabatic taper.

5.2. Langmuir – Blodgett (LB) film deposition onto tapered optical fibres

In this section the observation of the influence of the nanostructured coating, deposited onto the taper utilizing the LB deposition technique, on the transmission spectrum of the tapered fibres is shown. The deposition of nanostructured coatings of materials change the optical properties of the modes of fibres as has been described in Chapter 3.3. In non-adiabatic tapers, the LP_{01} mode of the single mode fibre may couple to the numerous modes of the tapered section of the fibre because of the high refractive index contrast between the silica and surrounding medium. In general the coupling occurs only to HE_{11} and HE_{12} modes of the tapered waist. These two modes propagate along the tapered region and couple back to the LP_{01} mode at the output of the taper. The form of the observed transmission spectrum, and its response to changes in the surrounding environment, are dependent upon the effective refractive indices of the modes, which in turn are related to the taper diameter. Initial experiments revealed two distinct modes of operation and the tapers that are described here with diameters for 5μm and 37μm were fabricated to allow investigation of these two operating regimes.

During the L-B deposition process, the taper was alternately raised and lowered through a floating monolayer of the coating material at the air-water interface. Transmission spectra were recorded when the tapered region of the fibre was above the interface - when a fibre was in the air, as well when the tapered region was beneath the interface - when a fibre was immersed in water. The intensity of the transmission spectra of uncoated tapers immersed in water was slightly lower than that recorded when surrounded by air. The difference originates from different refractive indices of those environments (refractive index of water

is 1.3330 at λ=589.29nm and t=20˚C; refractive index of air equals 1.000293 at 589.29nm and t=20˚C, p=1atm). The efficiency of propagation through the optical fibre core is proportional to the difference between the refractive index of the optical fibre core and the refractive index of the cladding. Accordingly, the efficiency of propagation increases as the difference between the refractive index of the core and the refractive index of the cladding increases. In the case of a tapered fibre the surrounding medium acts as a cladding. The refractive index difference between air and fibre is larger than between water and fibre. Thus the transmission intensity of a tapered fibre immersed in water is smaller than of a taper surrounded by the air. The evolution of the transmission spectra of tapers during the deposition of overlay coating was similar with the taper in air and in water, but it was found that the effects observed would occur earlier in the spectra recorded under the water. This was is a result of the smaller difference in the refractive indices of the overlay material and water, so that to observe a given change in the transmission spectrum of the tapered fibre when surrounded by air a thicker overlay had to be deposited onto the tapered region. This fact must be taken into account in designing the sensor for use for sensing in gaseous or liquid environment.

Prior to the deposition of the 4-[2-(4-dimethylamino-naphtalen-1-yl)-vinyl]-1-octadecyl-quinolinium iodide and calix[4]resorcinarene material onto the tapered fibres, chloroform/methanol (1:1) solutions of both chemicals were submitted to spectroscopic analysis. The aim of this is to examine whether or not absorption in the deposited material contributes to the spectral response of tapers to the overlay deposition. The absorption spectra of quinolinium salts in base and acidic environments show a change. In the vicinity of absorption peaks a refractive index of a material is governed by the Kramers-Kronig relationship, which allows determining changes in the material dispersion of the overlay waveguide, and thus a complex refractive index to be estimated [Flannery, D. *et al.* 1999].

Two materials suitable for LB deposition were investigated: 4-[2-(4-dimethylamino-naphtalen-1-yl)-vinyl]-1-octadecyl-quinolinium iodide (merocyanine dye) for pH sensing and calix[4]resorcinarene for ammonia gas sensing, which were described in section 4.2.1. Prior to their deposition both chemicals were submitted to the spectroscopic analysis, as mentioned in the previous paragraph, see Fig. 5.4.

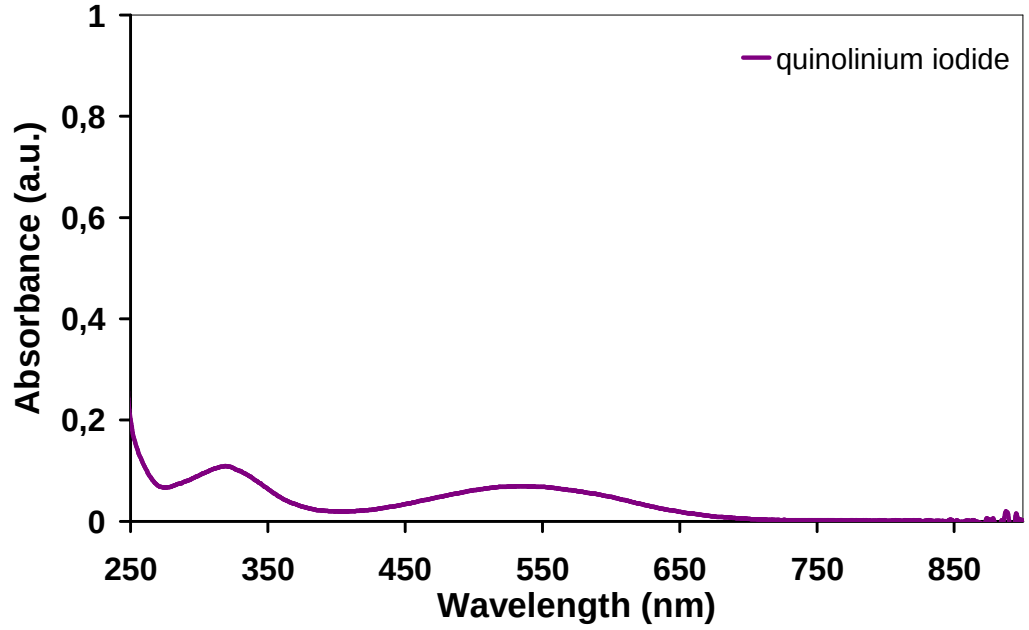

(a)

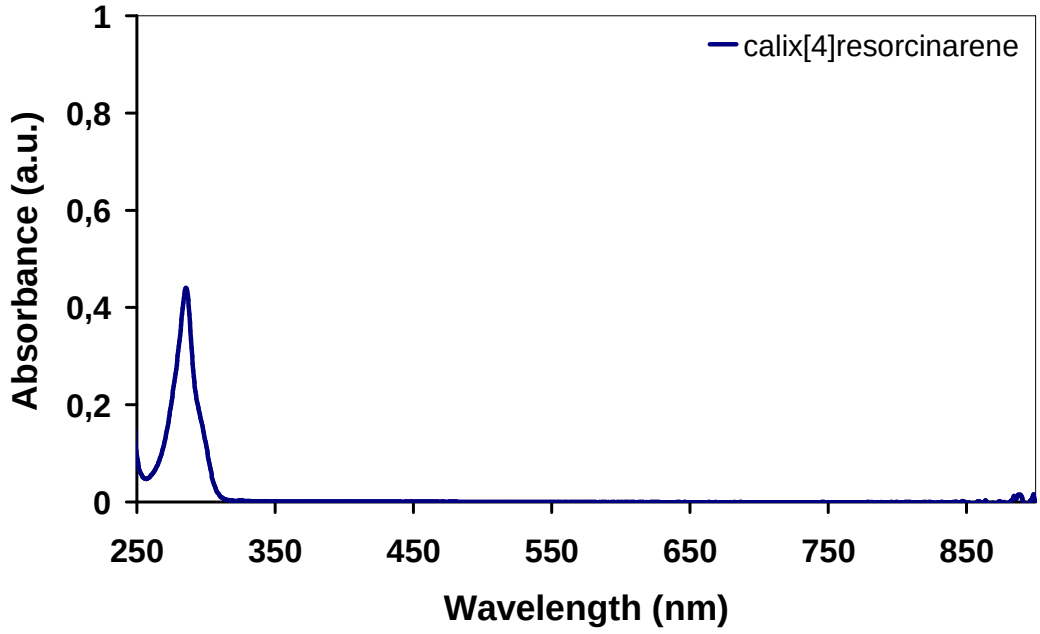

(b)

Fig. 5.4. Absorbance spectra of materials used for an overlay deposition; (a) quinolinium iodide spectrum (initial concentration 0.03mg/ml, subsequently diluted so that the absorbance level is below 0.5; optical path 10mm), (b) calix[4]resorcinarene spectrum (initial concentration 0.08mg/ml, subsequently diluted so that the absorbance level is below 0.5; optical path 10mm).

Within the spectral range of 250 nm – 900 nm the quinolinium salt is observed to contain two broad absorption peaks, one in the UV region at 315nm and one in visible light region at 530nm. This indicates the possible contribution of the material to the optical response of the coated fibre to the refractive index change in the fibre environment. The calix[4]resorcinarene molecule shows a strong absorption in the UV region at 285nm while it is transparent in the visible light region. Therefore it is anticipated that the optical properties of the material, in the range of wavelengths within visible region, do not contribute to the optical response of the coated taper to refractive index change in the surrounding medium.

The materials were deposited on tapers of different diameters using the deposition parameters discussed in section 4.2.1. In both cases a change in the transmission spectrum in response to an increasing number of layers and for any fibre taper with the waist diameter from the range 4 – 40μm was studied. It is of great interest that the optical response of a fibre taper due to increasing number of layers of an overlay material shows periodic change in the transmission spectrum (see Fig. 5.5(b)). It has been observed that the transmission spectrum of tapers with ~5μm waist diameter show different behaviour from the 20μm and larger tapers in response to the deposition of an overlay. However, within the waist diameter range 0f 20-40μm, they show the same optical response to the deposition of different materials. Therefore the results for one of the deposited materials are depicted in this section. Detailed analysis of all overlay materials used is discussed in sections 5.2.1. and 5.2.2.

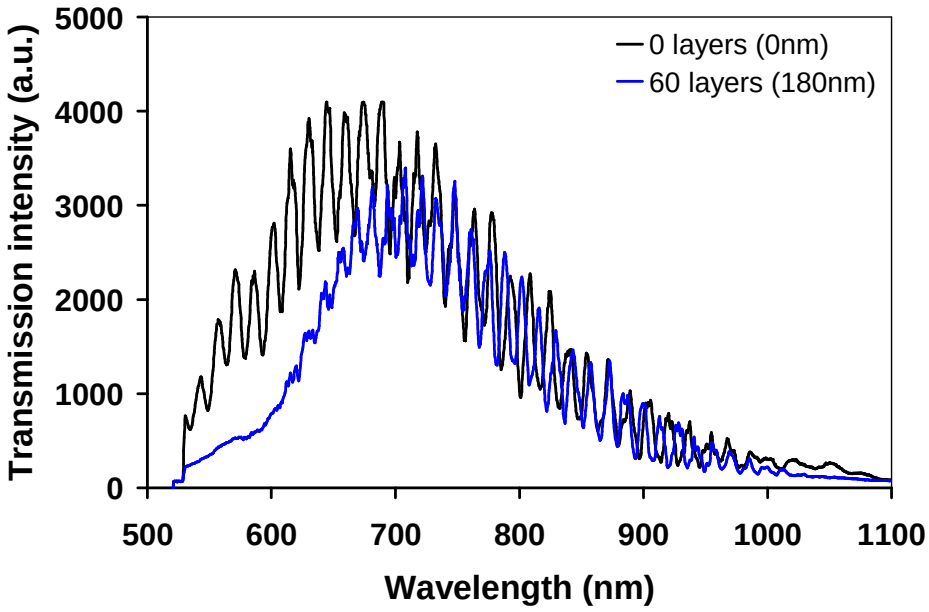

(a)

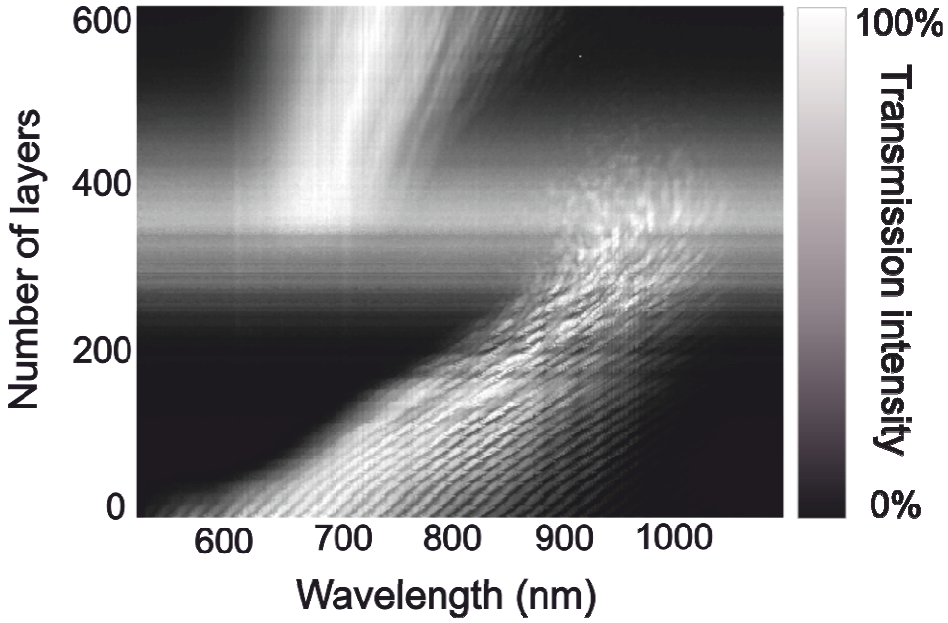

(b)

Fig. 5.5(a),(b). Optical response of tapered fibres due to the increase of number of layers deposited onto tapered region. Upper graphs show transmission spectra for chosen numbers of layers, lower pictures show transmission spectra recorded during whole deposition processes. (a) transmission spectrum of a 5μm taper coated with 180nm of material, (b) gray-scale image of the spectrum recorded during deposition of 180nm of material.

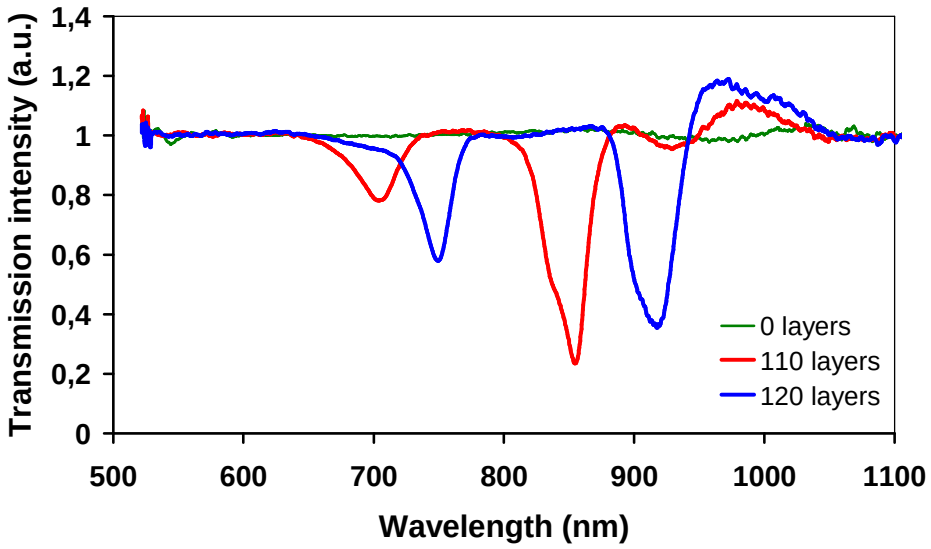

(c)

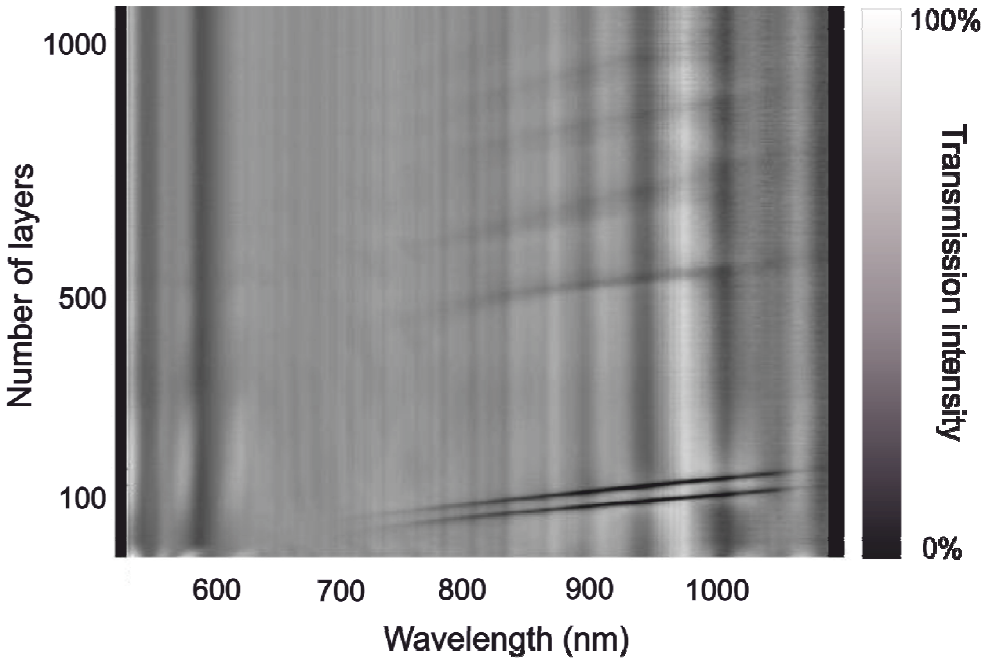

(d)

Fig. 5.5(c),(d). Optical response of tapered fibres due to the increase of number of layers deposited onto tapered region. Upper graphs show transmission spectra for chosen numbers of layers, lower pictures show transmission spectra recorded during whole deposition processes. (c) Transmission spectrum (with baseline correction applied) of a 37µm taper coated with 330nm (red line) and 360nm (blue line) of material, (d) gray-scale image of the transmission spectrum (with baseline correction applied) recorded during deposition of 1100nm layers of material.

The characterization of the response of the tapered fibres to the deposition of nanoscale coatings has revealed that there are two distinct modes of operation that are dependent on the diameter of the taper.

In case of the 37μm taper, the transmission spectra have been normalized in order to emphasize the spectral changes occurring during an overlay deposition, see graph (c) and (d) in Fig. 5.5. The grey-scale image shown in Figure 5.5(d) has been created from transmission spectra with the baseline correction applied. Results for the 37μm taper show the appearance of two dropout bands in the spectrum which shift towards long wavelengths with increasing coating thickness. The two features appear periodically with further increases in thickness, but with smaller strength. The decrease of the dropouts' depth may be caused by larger scattering of the overlay, which contains more structural imperfections as the number of layers increases. The phase matching wavelength is dependent on the dimensions of both waveguides – a substrate and an overlay – and their refractive indices. Therefore when the overlay is thick enough cladding modes are guided by the overlay. The film deposited onto a substrate that is an optical waveguide acts as a waveguide itself. Attenuation bands of the transmission spectrum corresponding to energy being coupled out of the taper into the overlay at wavelengths at which the taper and overlay modes are phase matched – they are attenuated in the cladding and are not coupled back to the fibre at the end of the taper. The increase of the overlay thickness causes the variation of effective indices of cladding modes. The consequence of the variation of effective indices is a displacement of the attenuation bands. The presence of two features indicates the two-step transition of refractive indices in which two modes of the taper are contributing to the effect - as predicted by the scalar analysis covered in section 3.3. Changes in the spectrum offer the ability to develop sensor with high sensitivity – the minimum magnitude of a measurand for used setup arrangement, and the response time of 20 seconds.

The spectral response of the 5μm taper indicates two phenomena occurring during the overlay deposition: one is a red shift of the channeled spectrum, and the second is a periodic attenuation of the spectrum, see Fig. 5.5(b). The progressive shift of the channeled spectrum towards long wavelengths is caused differential change of the propagation

constants of the modes guided within the tapered region. This results in a change in the phase of the interference between the modes when they couple back to the LP_{01} mode of the fibre at the end of the tapered region. The signal intensity of the spectrum was observed to decrease and the attenuation of the spectrum increase for coating thickness of ~1000nm. It has been confirmed that 5μm tapers' spectrum rebuilds periodically with the increasing coating thickness. This indicates that the absorption of the material does not contribute to this phenomenon. The overlay acts as a waveguide and allows modes to propagate within it. The change of the intensity of the transmission spectrum is due to one of the taper modes being phase matched to a mode of an overlay waveguide and thus being coupled out of the taper. In case of the 5μm taper the width of the spectral feature caused by the phase matching phenomenon is broader than that produced in the thicker tapers. The broadening of the width of the phase matching wavelength range is the dispersion of the taper modes. With the overlay thickness increase the spectrum reappears, but with lower transmission intensity. Changes in the spectrum may be detected from the deposition of the first few monolayers, offering the ability to develop sensor with the sensitivity of 0.31-0.38 within the wavelength range: 750-950nm and the response time less than 0.5s.

5.2.1. Demonstration of a pH sensor based on quinolinium iodide coated optical fibre tapers

Prior to the deposition of the 4-[2-(4-dimethylamino-naphtalen-1-yl)-vinyl]-1-octadecyl-quinolinium iodide onto tapered fibres the chloroform/methanol solution of the quinolinium material was submitted to the spectroscopic analysis. The absorbance of the quinolinium in base and acidic environment is shown in Fig. 5.6.

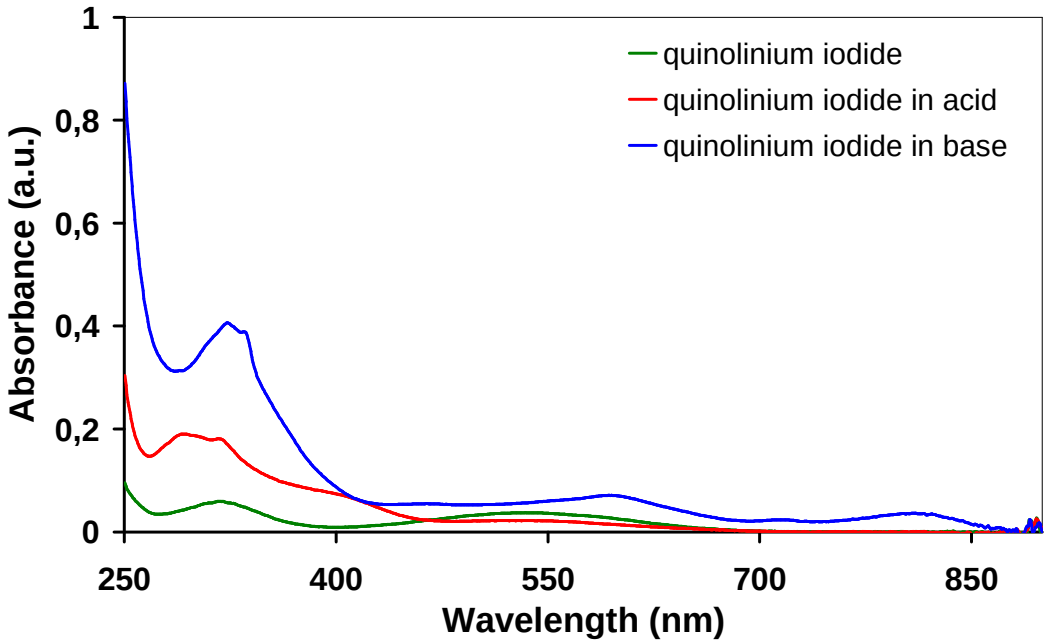

Fig. 5.6. Absorbance spectra (with baseline correction applied) of the quinolinium dye in neutral, base and acidic environments.

It can be observed in Fig. 5.6 that the spectrum of the quinolinium solution changes due to change of pH environment. In the vicinity of absorption peaks the refractive index of a material is governed by the Kramers-Kronig relationship, which allows a complex refractive index to be estimated. The change of the absorption spectra of the used materials due to change of the pH of environment indicates change of the refractive index of the material. The modification of the optical properties of the film contributes to the coupling wavelength of the overlay modes, which is presented in the following paragraph.

pH sensitivity of the 37μm taper coated with quinolinium iodide salt

4-[2-(4-dimethylamino-naphtalen-1-yl)-vinyl]-1-octadecyl-quinolinium iodide was deposited onto the 37μm diameter taper. The optimal coating thickness is that when the two dropout bands are present in the transmission spectrum and the drop of the signal intensity of one of them is at the highest magnitude (it is the lowest signal intensity at the dropout that is desired). To establish the optimum coating thickness, a thick film in excess

of 1μm was deposited. This allows the gray scale plot to be generated, see Fig. 5.5(d). The picture highlights the response of the transmission spectrum to the coating deposition. Next the film was removed by wiping thoroughly the taper with clean soaked in acetone, and subsequently in isopropanol, optical lens cleaning tissue. The taper was then coated with 133 layers of quinolinium iodide, corresponding to a calculated coating thickness of 397nm. The evolution of the transmission spectrum of the fibre in response to the deposition of the coating is depicted in Fig. 5.7.

The normalized transmission spectra of the taper with no coating and with a coating of thickness 400 nm are shown in the Figure 5.7(b), and the grey-scale image – in the Fig. 5.7(a), where the transmission was normalized before plotting. In the Fig. 5.7(a) two transmission dropouts appear and scan across the spectrum as the coating thickness increases.

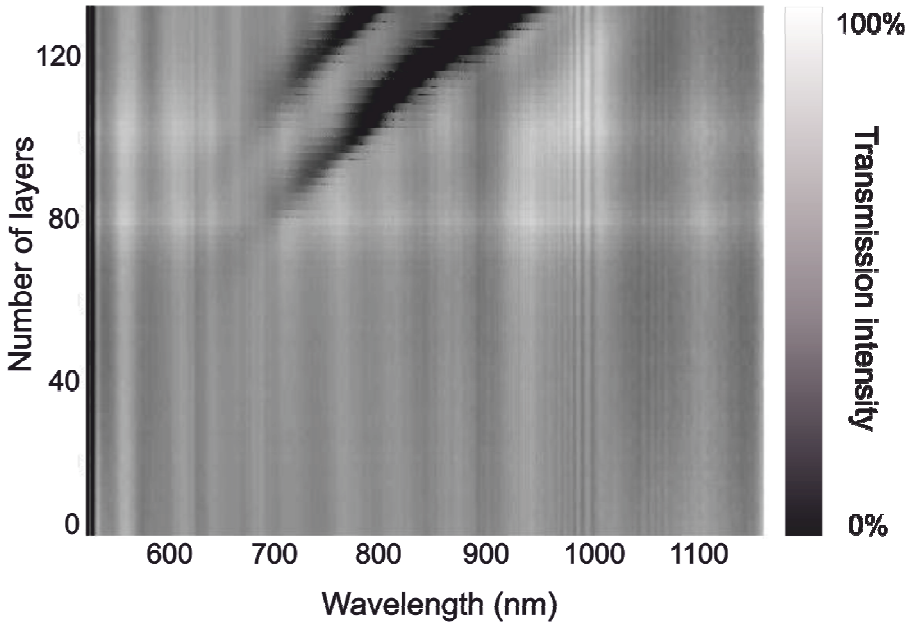

(a)

Fig. 5.7(a). Evolution of the transmission spectrum (with baseline correction applied) of the 37μm taper during deposition of a multilayer coating of 4-[2-(4-dimethylamino-naphtalen-1-yl)-vinyl]-1-octadecyl-quinolinium iodide; gray-scale image of the transmission spectrum (with baseline correction applied) recorded during deposition of 133nm layers of material.

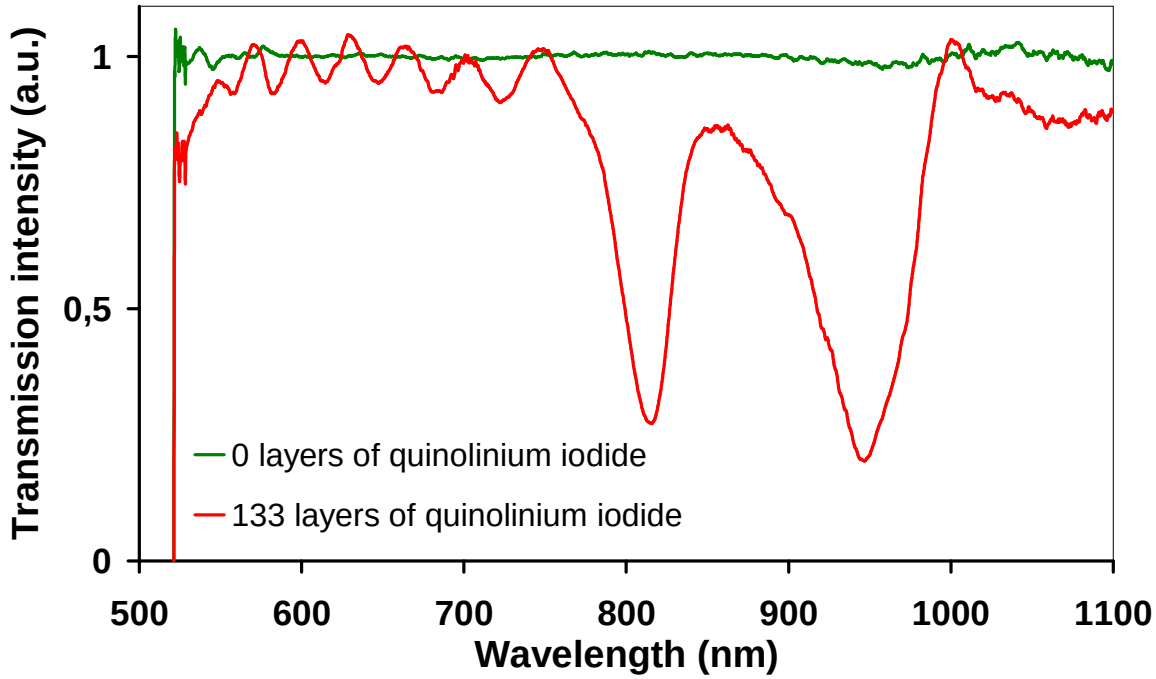

(b)

Fig. 5.7(b). Evolution of the transmission spectrum (with baseline correction applied) of the 37μm taper during deposition of a multilayer coating of 4-[2-(4-dimethylamino-naphtalen-1-yl)-vinyl]-1-octadecyl-quinolinium iodide; the black line represents the initial spectrum (with baseline correction applied), the red line shows the spectrum of the taper when the coating was of thickness 397nm.

The sensitivity of the coated tapered fibre to immersion in solutions of different pH was characterized. The coated tapered fibre was mounted on a holder (see Fig. 4.4) to keep the fibre taut during the subsequent experiments. The tapered and coated section was immersed in solutions of different pH, as shown in Fig. 4.10. Experiments were carried in the room temperature of 21°C. Each immersion lasted 15 minutes. During this time the spectrum was recorded in order to establish the response time and the magnitude of the response. After immersion in a given pH solution, the fibre was thoroughly rinsed with distilled water before immersion in the next solution. The transmission spectrum always returned to its initial form. The results are shown in Fig. 5.8. The spectral features show a blue-shift with increasing pH, with the longer wavelength band exhibiting the largest sensitivity.

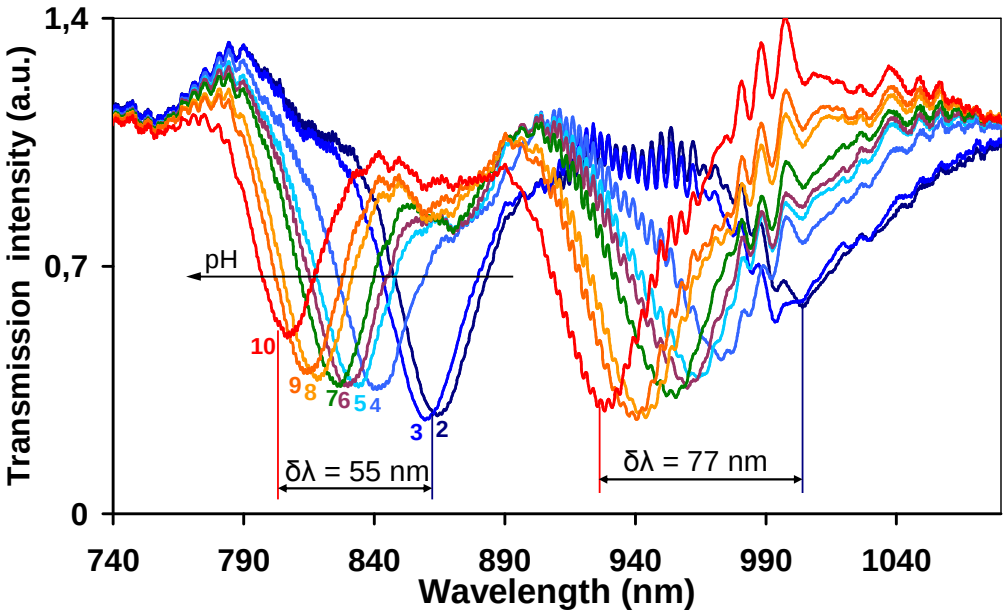

(a)

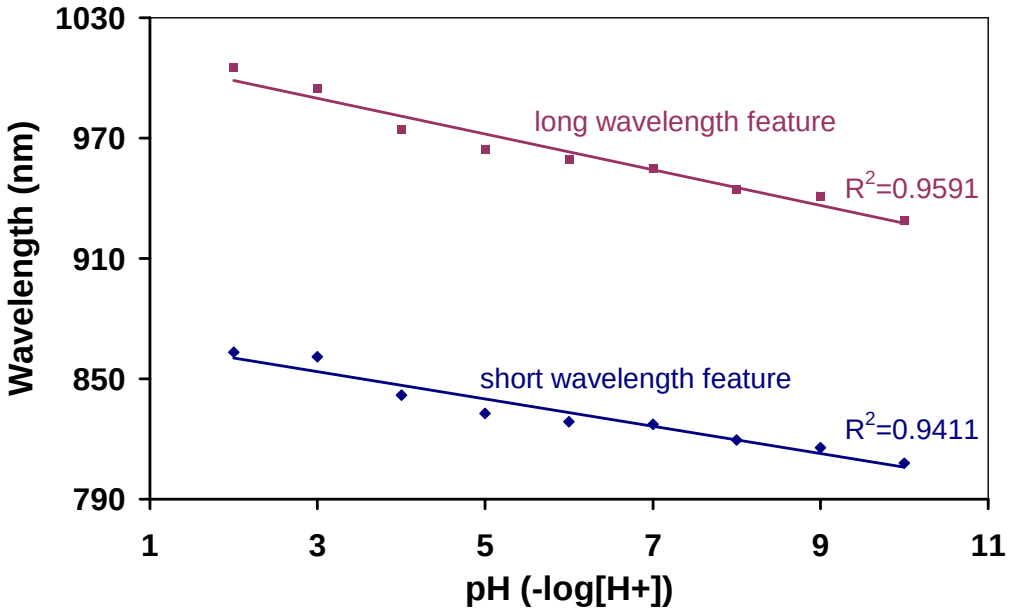

(b)

Fig. 5.8. (a) Changes in the transmission spectrum (with baseline correction applied) of the 37µm diameter taper with a coating with of the quinolinium dye of thickness 397nm in response to pH change in the environment of the taper; (b) wavelength shift of the spectral features as a function of pH.

The wavelength shifts, for a pH range of 2-10 for both features, were measured to be 55nm for the shorter wavelength feature and 77nm for the longer wavelength feature (Fig. 5.8(a)). Given the 0.3nm spectral resolution of the spectrometer, the pH sensitivity of this taper is $\Delta pH \sim 3 \times 10^{-2}$ for the long wavelength feature and $\Delta pH \sim 5 \times 10^{-2}$ for the short wavelength feature. The comparison with commercially available sensors is shown in paragraph 6.3. The response time was found to be dependent on the pH value. The response time ($1/e$) was measured to be 20 seconds. The dependence of wavelength on pH was approximately linear for both spectral features, with the longer wavelength feature having the higher sensitivity, as depicted in Fig. 5.8(b).

pH sensitivity of the 5μm taper coated with quinolinium iodide salt

To establish the optimum coating thickness for the 5μm taper a thick film in excess of 1μm was deposited. Then the gray scale plot was generated, see Fig. 5.5(b). The picture highlights the response of the transmission spectrum to the coating deposition. The taper was then coated with 60 layers of quinolinium iodide, corresponding to a calculated coating thickness of 180nm. The response of the transmission spectrum, in the water, to increasing coating thickness is shown in Fig. 5.9.

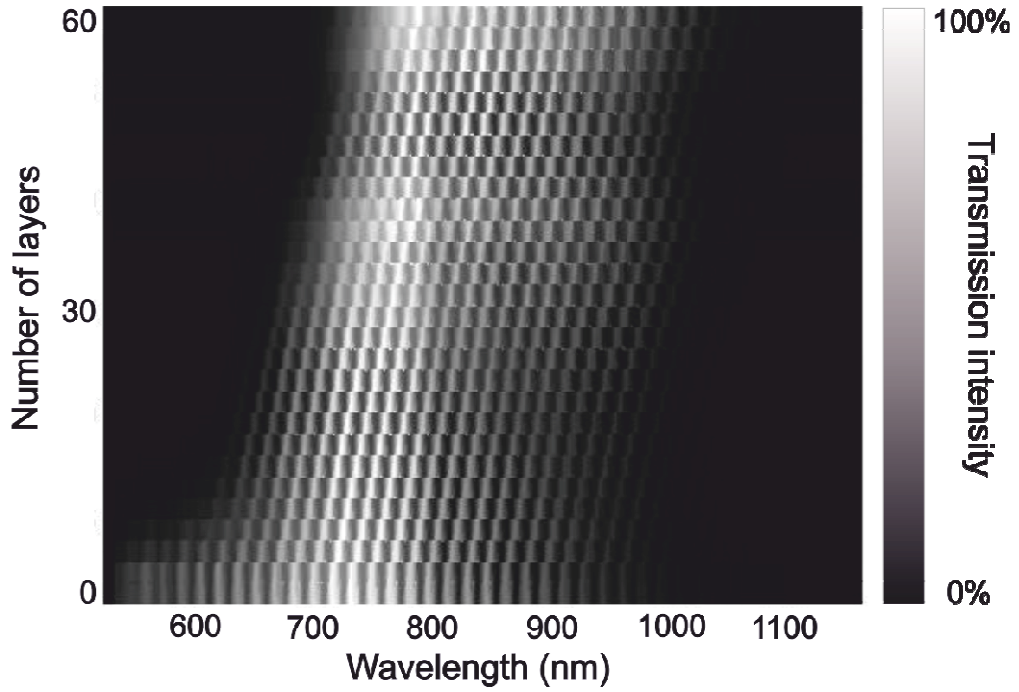

(a)

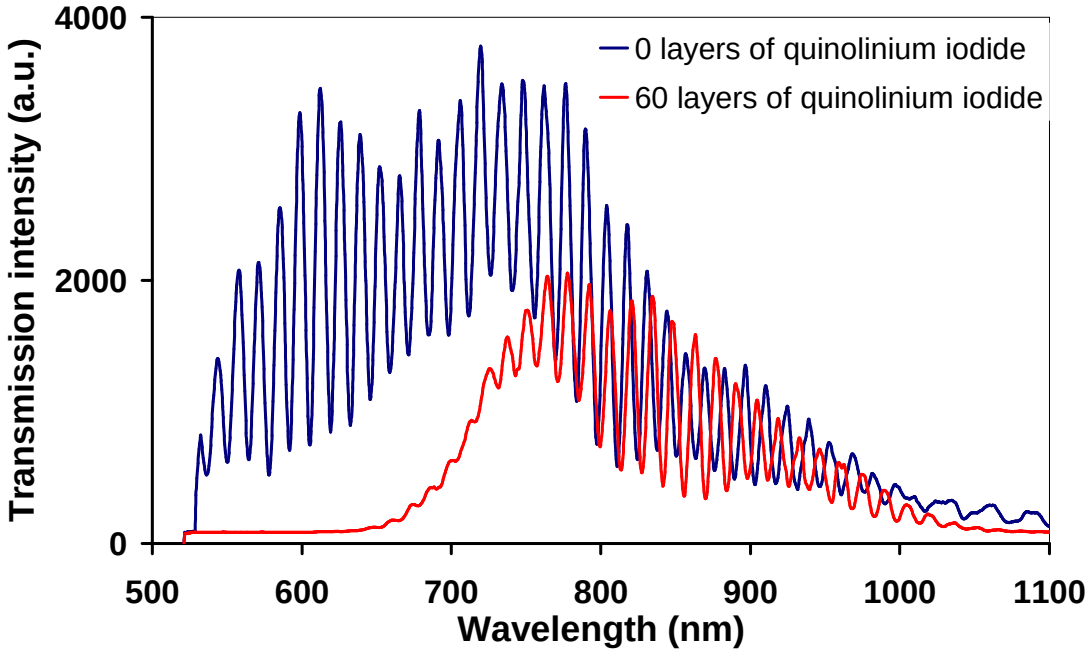

(b)

Fig. 5.9. (a) Evolution of the transmission spectrum of the 5μm coated taper in response to the deposition of the quinolinium dye taken under water; (b) transmission spectrum of the taper before the deposition - blue line and after deposition of a coating of thickness 180 nm - red line.

The grey-scale image (Fig. 5.9(a)) shows the transmission spectrum. It has been observed that there is no spectral response of a taper until ~3 layers of an overlay have been deposited onto. This effect results from the too small refractive index change in the taper environment to influence a detectable shift of the channeled transmission spectrum. This has been observed for all 5μm tapers. The spectrum of the 5μm taper shifts towards long wavelengths with increasing coating thickness and is accompanied with the decrease of the transmission intensity. The change in wavelength of the channeled spectrum is a result of a differential change of the propagation constants of the two modes propagating within the tapered region. The reduction in intensity of the spectrum is a result of increased attenuation of one of the modes, which occurs when one mode is phase matched to a mode of the overlay waveguide. The width of the spectral feature caused by the phase matching phenomenon is broad so it overlaps with the transmission spectrum range.

Subsequently the coated taper immersed in solutions of different pH and the transmission spectrum was recorded. The experiments were carried out in the same way as for the 37μm fibre taper, discussed in section 5.2.1.1. The shift of the spectrum in response to pH change from the range 4-10 is depicted in Fig. 5.10.

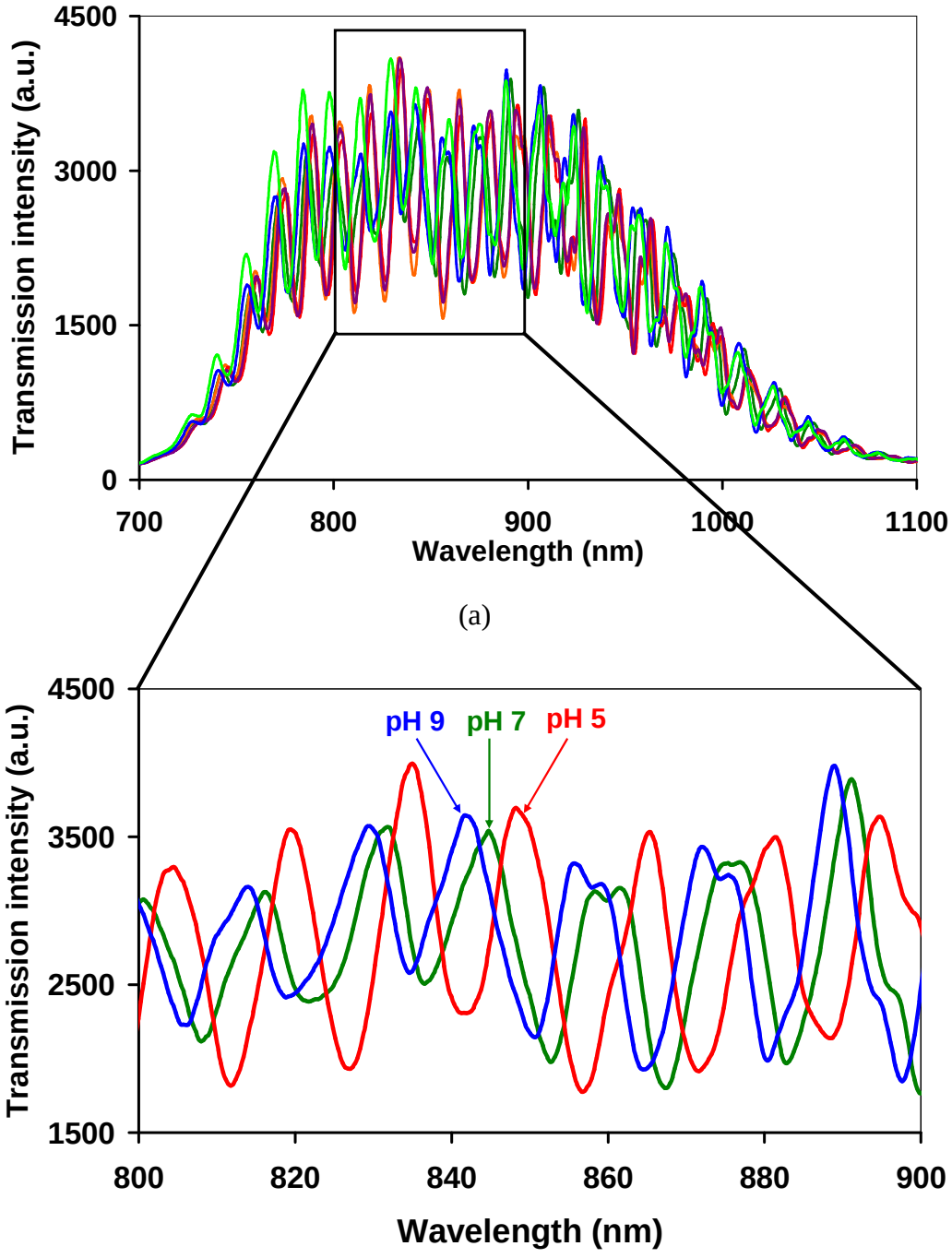

Fig. 5.10(a)(b). (a) Changes in the transmission spectrum of the 5μm diameter taper coated with (60 layers) 180nm of the quinolinium dye in response to pH change in the environment of the taper; (b) changes in the transmission spectrum of the spectral range (800-900nm) marked in the Fig. 5.10(a) in response to pH change in the environment of the taper, for clarity reasons limited to three pH solutions.

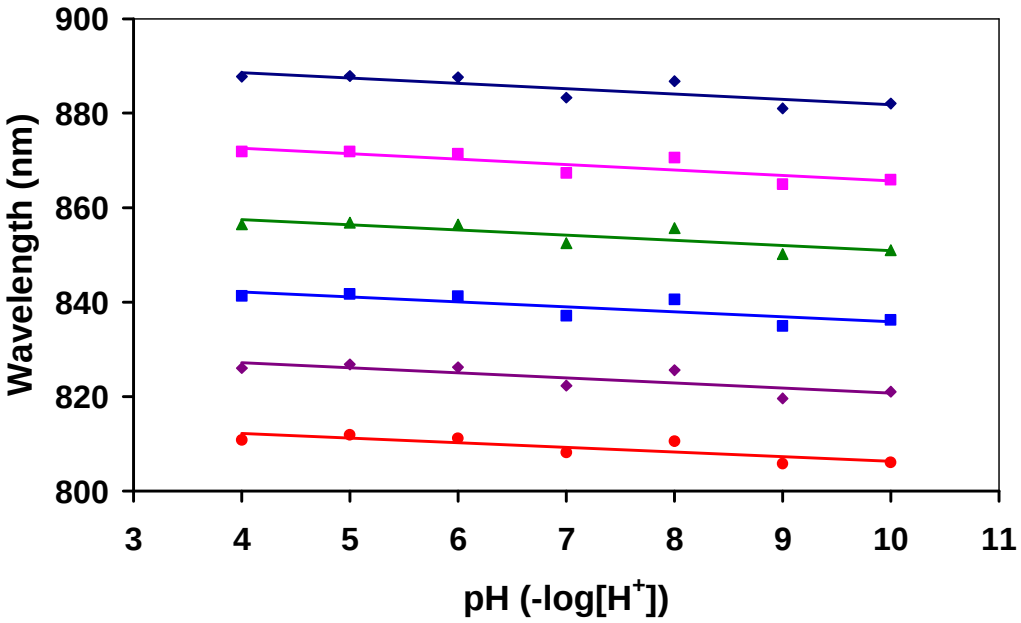

(c)

Fig. 5.10. (a) Changes in the transmission spectrum of the 5μm diameter taper coated with (60 layers) 180nm of the quinolinium dye in response to pH change in the environment of the taper; (b) changes in the transmission spectrum of the spectral range (800-900nm) marked in the Fig. 5.10(a) in response to pH change in the environment of the taper, for clarity reasons limited to three pH solutions; (c) wavelength shift of the spectral features as a function of pH.

Figure 5.10(a) shows the dependence of the wavelength of the spectral features within the spectral region 700-1100nm on the pH of the environment. For clarity reasons, the transmission spectra within the spectral region 800-900nm obtained when the coated taper was immersed in pH solutions of 5, 7 and 9 are shown in Fig. 5.10(b). Using a spectrum analyser with a resolution of 0.3 nm, the pH sensitivity of this taper is ΔpH~0.38 for the wavelength range 750-850nm and ΔpH~0.31 for the wavelength range 850-950nm. The sensitivity of features in the spectrum varies for different wavelength. The response time was less than 0.5 s. The measurement of which was limited by the integration time of the CCD spectrometer used.

5.2.2. Demonstration of a gas sensor based on calix[4]resorcinarene coated optical fibre tapers

During the calix[4]resorcinarene deposition the transmission spectra were recorded when the tapered fibre was above the water/air interface, since the sensor was to be used for vapour detection.

Ammonia sensitivity of the 37μm taper coated with calix[4]resorcinarene film

The taper with the 37μm waist diameter was submitted to the L-B deposition of the calix[4]resorcinarene film using the L-B technique. The deposition parameters were as detailed in section 4.2.1. A thick film in excess of 1μm was deposited in order to establish the optimum coating thickness. This allows the grey scale plot to be generated, see Fig. 5.5(d). The deposited film was removed by wiping the taper thoroughly with optical lens cleaning tissue soaked in acetone and subsequently in isopropanol. The taper was then coated with 498 layers of calix[4]resorcinarene, corresponding to a calculated coating thickness of 585nm. The optical response of the fibre to the increase of the overlay is shown in Fig. 5.11.

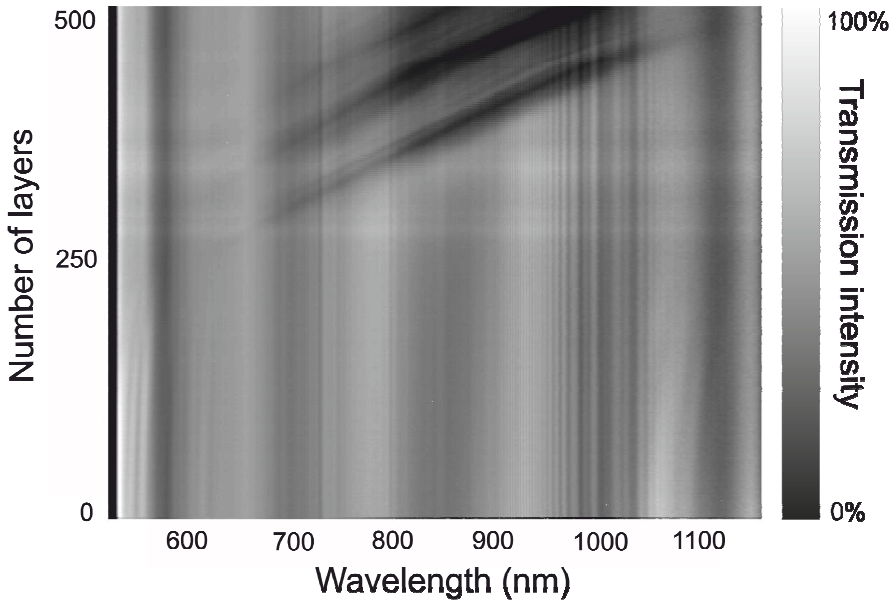

(a)

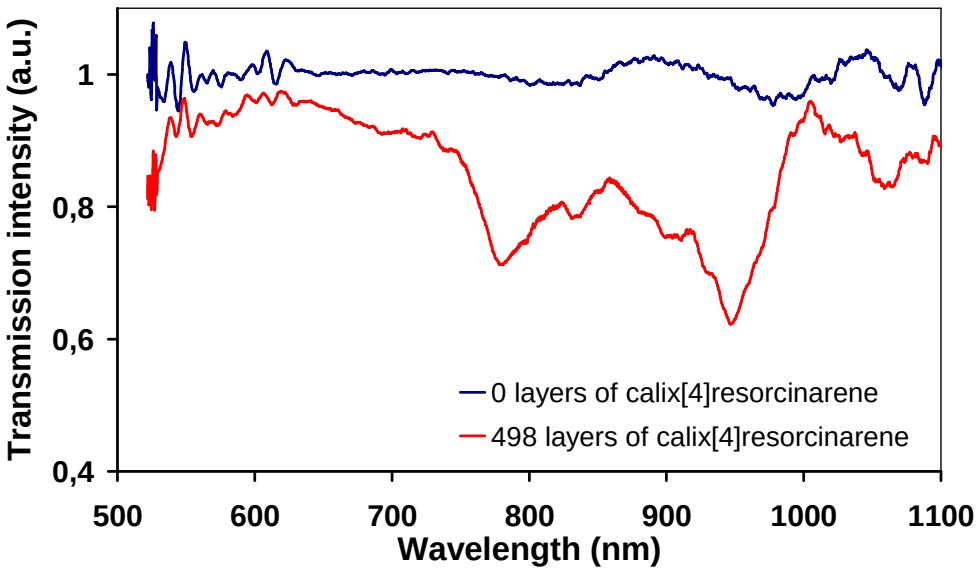

(b)

Fig. 5.11. Evolution of the transmission spectrum (with baseline correction applied) of the 37µm taper coated with 1165nm calix[4]resorcinarene film; spectra taken in the air environment; (a) gray-scale image of the transmission spectrum during the deposition, (b) spectrum graph - black line represents the initial spectrum, red line represents spectrum after the 1165nm film deposition.

After deposition of the functional film onto the tapered region, the fibre was subsequently exposed to ammonia using the setup depicted in Fig. 4.11. Experiments were performed in a gaseous environment at room temperature. The fibre was mounted on the cross-holder and placed in the experimental chamber. The volume of the chamber was 3 litres. The concentration of ammonia vapour was controlled by the number of micro-drops injected into the chamber. The volume of each drop was 20µl. The ammonia concentration in the gas vessel was presented in ppmv units and calculated according to the formula [Beychok, M. R. 2005]:

$$\text{ppmv} = \frac{C_g\left(273.15 + T\right)}{12.187 \cdot \text{M}_\text{W}} \tag{5.1}$$

where ppmv stands for parts per million volume, C_g is the ammonia vapour concentration in 3l vessel in $\frac{\text{mg}}{\text{m}^3}$, T is the temperature of the environment in ^{o}C, M_W is the molecular weight of a molecule. After each droplet injection the response of a taper was recorded over 20 minutes. The optical response of the coated taper to change in the ammonia concentration within the range: 8.4 – 42.0kppmv is shown in Fig. 5.12.

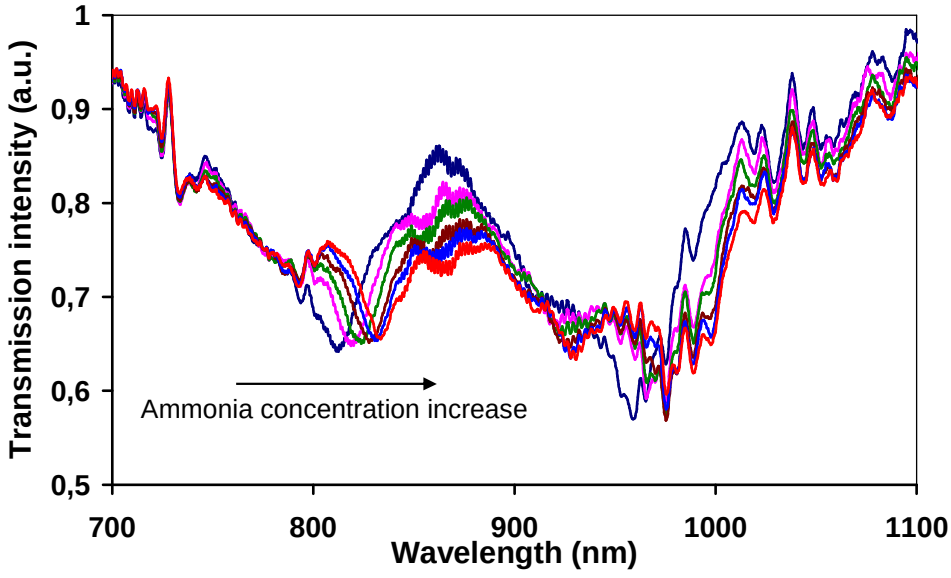

(a)

Fig. 5.12(a). Transmission spectrum (with baseline correction applied) of the 37µm diameter taper coated with 1165nm of the calix[4]resorcinarene in response to ammonia vapour concentration change in the environment of the taper.

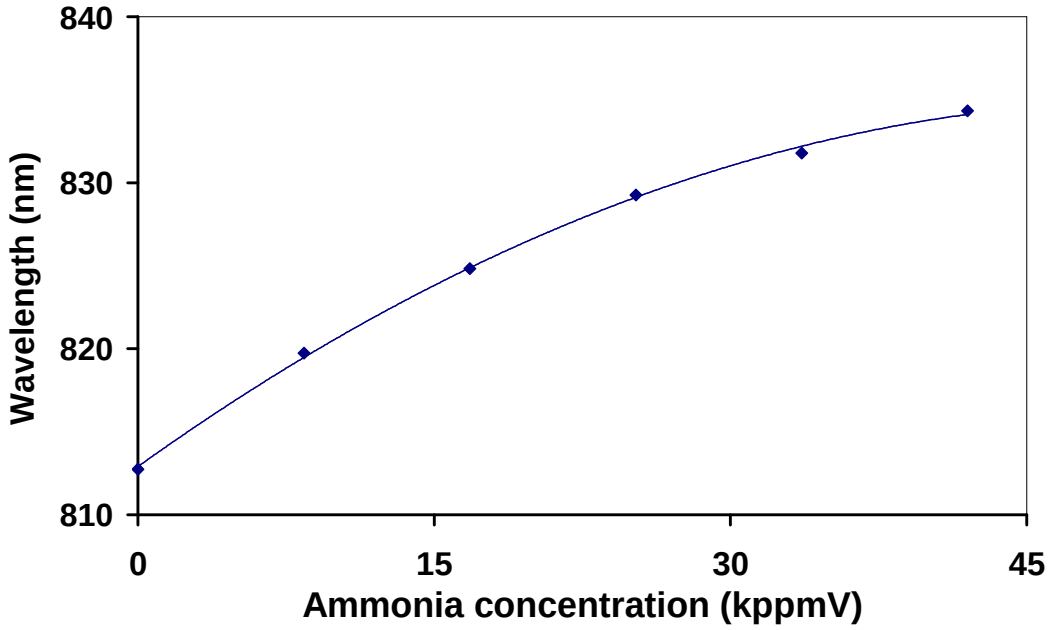

(b)

Fig. 5.12.(b) Wavelength shift of the spectral feature as a function of concentration.

The wavelength shift for the short wavelength features was measured to be 21nm. With a resolution of 0.3nm for the wavelength shift detection, the resolution of this taper is ΔC_g~1.97 kppmv. The relationship between the concentration and resonance feature position show non-linear dependence, as depicted in Fig. 5.12(b). The response time for the wavelength to shift on immersion into ammonia vapour was found to be dependent on the concentration value. The response to immersion in low gas concentration takes less than 60 seconds while for higher concentration values longer response times – longer than 20 minutes - were observed. This indicates the saturation of the calix[4]resorcinarene coating.

Ammonia sensitivity of the 6μm taper coated with calix[4]resorcinarene film

The 6μm diameter taper was coated with 98 layers of the calix[4]resorcinarene film, corresponding to the calculated coating thickness of 114.7nm. The optical response to the increasing coating thickness is shown in Fig. 5.13. The gray-scale image presents transmission intensity plotted as a function of overlay thickness and wavelength. The

spectrum of the 6μm taper shifts towards long wavelengths and is accompanied with the decrease of the transmission intensity in response to the deposition of a material. It has been observed that there is no spectral response of a taper until ~3 layers of an overlay have been deposited. This effect results from the refractive index change in the taper environment being too small to influence a detectable shift of the channelled transmission spectrum. The spectrum of the 6μm taper shifts towards long wavelengths with increasing coating thickness and is accompanied with the decrease of the transmission intensity. The change in wavelength of the channelled spectrum is a result of a differential change of the propagation constants of the two modes propagating within the tapered region. The reduction in intensity of the spectrum is result of increased attenuation of one of the modes, which occurs when one mode is phase matched to a mode of the overlay waveguide. The width of the spectral feature caused by the phase matching phenomenon is broad so it overlaps with the transmission spectrum range.

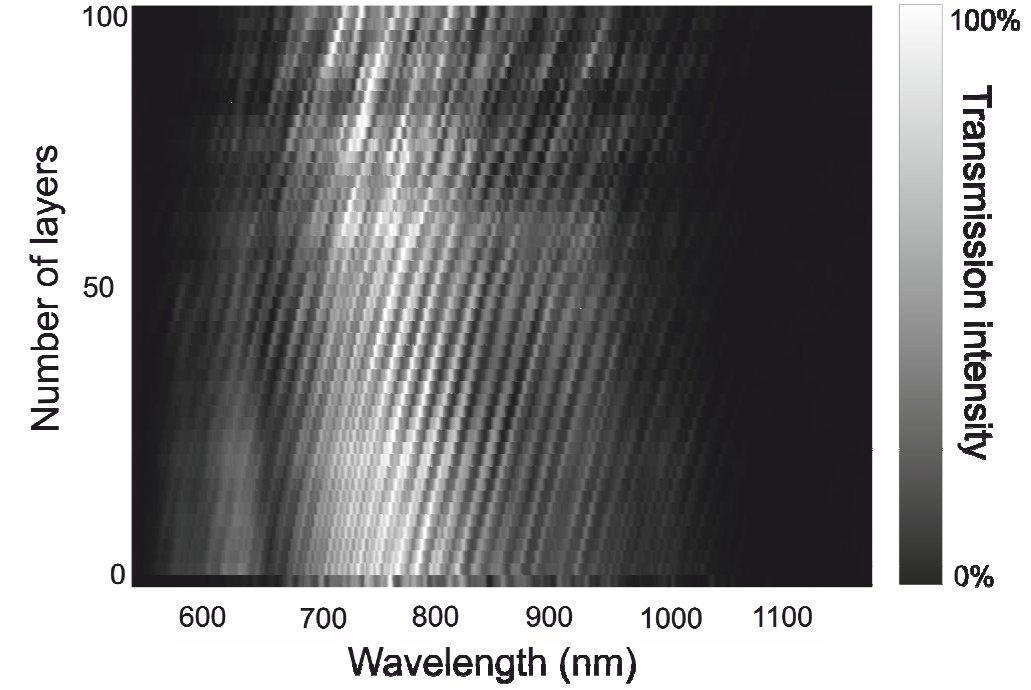

(a)

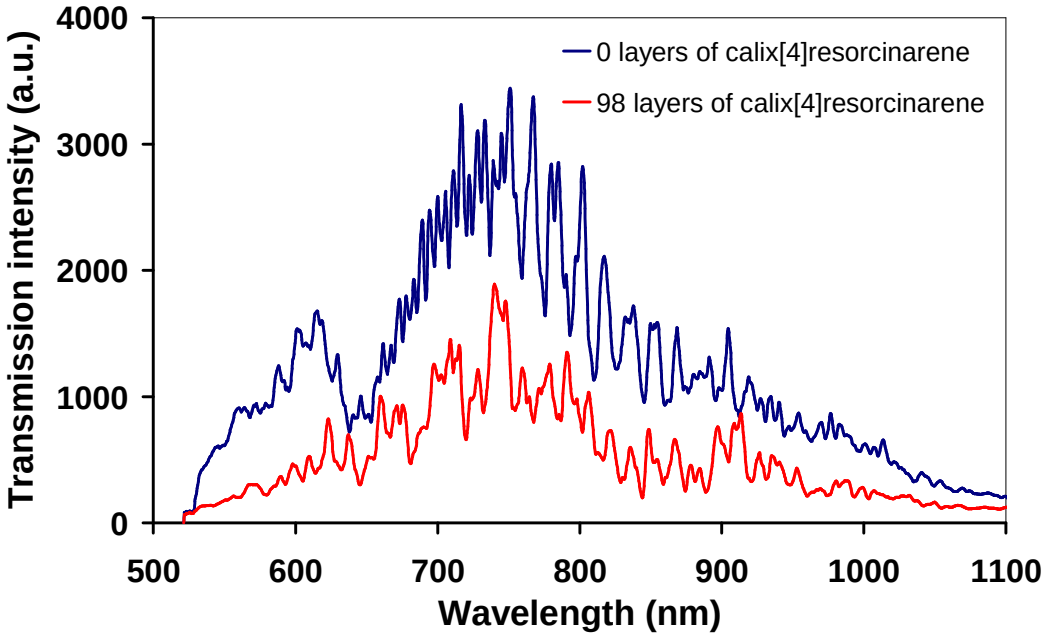

(b)

Fig. 5.13. (a) Evolution of the transmission spectrum of the 6μm taper coated with 98 layers of calix[4]resorcinarene film; (b) transmission spectrum of the taper before the deposition - blue line and after deposition - red line.

Subsequently the coated taper was exposed to different concentrations of ammonia gas within the range 0 – 42kppmv and the transmission spectra were recorded. Experiments were carried out in the same way as for the 37μm taper described in paragraph 5.2.2.1. The shift of the spectrum in response to pH change is depicted in Fig. 5.14.

Figure 5.14 shows the dependence of the wavelength of spectral features located within 740-840nm wavelength range on the ammonia concentration. For clarity reasons transmission spectra obtained for the coated taper immersed in two ammonia concentrations, 16.8kppmv and 42.0ppmv, are shown in Fig. 5.14(a). The wavelength shift for chosen feature of the transmission spectrum in whole studied concentration range is shown in the inset of Fig. 5.14(a). The relationship between concentration change and wavelength shift shows linear dependence, with R^2 values above 0.94, as depicted in Fig. 5.14(c). The ammonia sensitivity of this taper is $\Delta C \sim 2.8$kppmv.

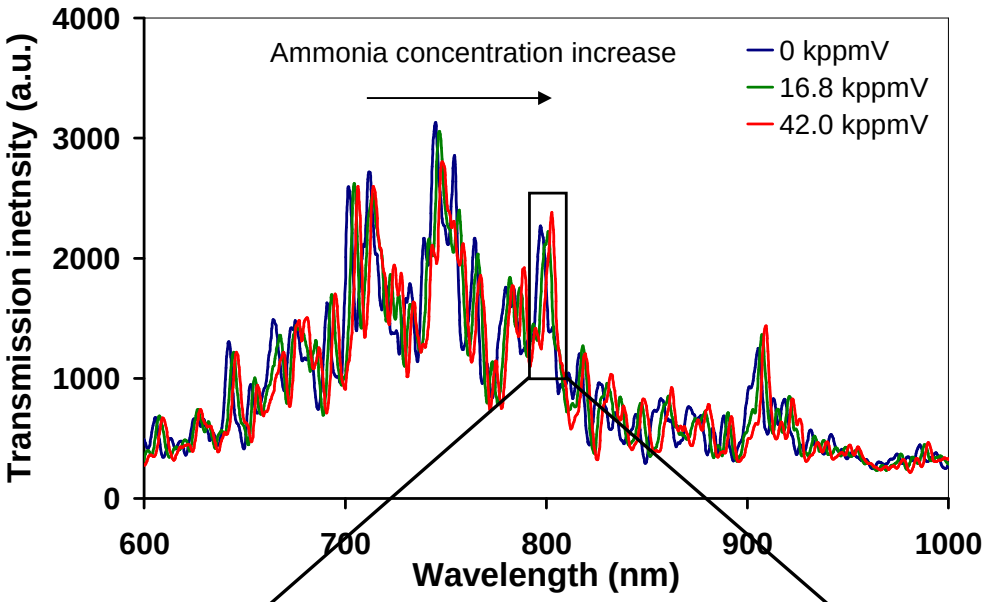

(a)

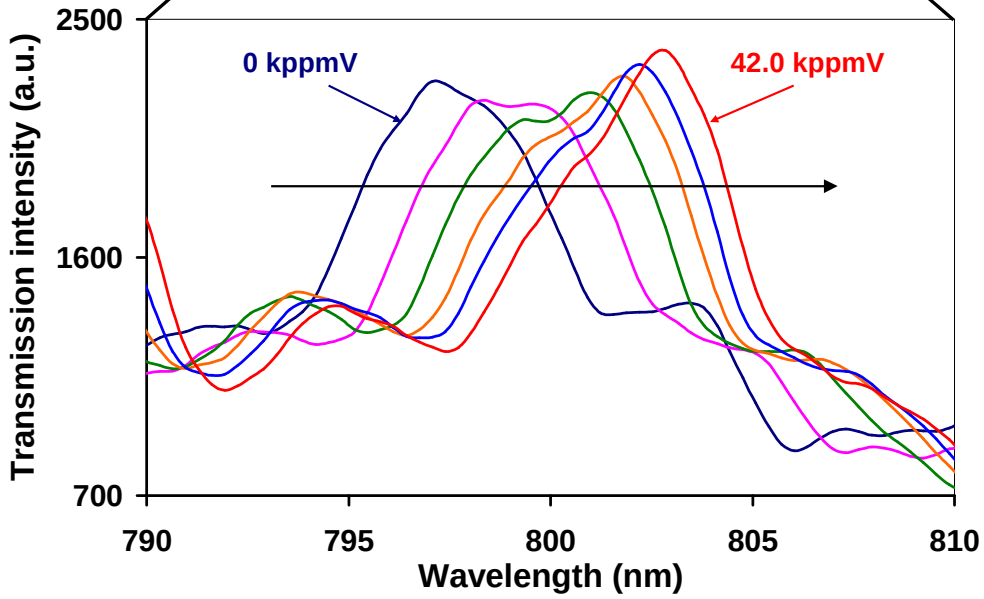

(b)

Fig. 5.14. (a) Transmission spectrum of the 6μm diameter taper coated with 98 layers of the calix[4]resorcinarene in response to ammonia concentration change in the environment of coated taper, for clarity reasons limited to three spectra corresponding to three ammonia concentrations; (b) changes in the transmission spectrum in the spectral range (790-810nm) marked in the Fig. 5.14(a), in response to ammonia concentration change for six values of concentration from the range 0.0 - 42.0kppmV.

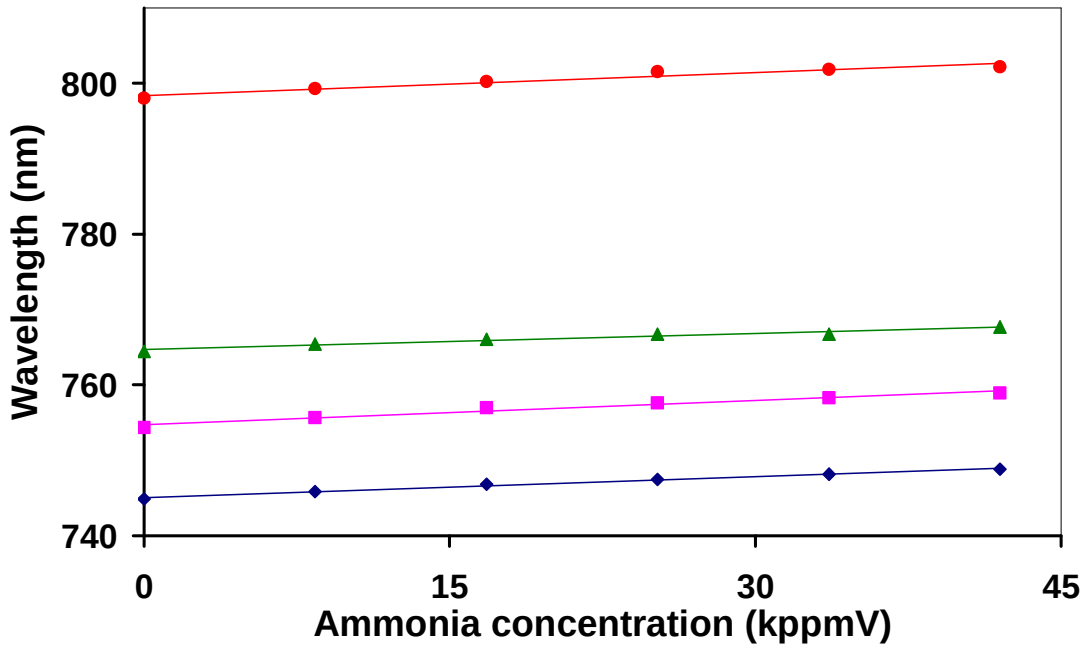

(c)

Fig. 5.14. (c) Wavelength shift of the spectral features as a function of ammonia concentration, R^2 for all data was above 0.94.

5.3. Chemical deposition of a polyaniline (PANI) film onto tapered fibres

Tapered and characterised fibres were subsequently submitted to the chemical deposition of the polyaniline overlay using the technique described in section 4.3 and the setup shown in Fig. 4.14.

5.3.1. Demonstration of a redox sensor based on polyaniline (PANI) coated optical fibre tapers

To establish the optimum taper waist diameter, PANI film was deposited onto tapers with the waist from the range of 5 - 40μm. It has been observed that any transmission change occurs for tapers with diameters bigger than 20μm, while a rapid transmission intensity decrease occurs for tapers smaller than 10μm. Therefore results for two diameters of optical fibre tapers, namely 21μm and 12μm, are presented in this work. During the PANI

deposition the transmission spectra were recorded when the tapered fibre was immersed in the water solution.

21 μm diameter taper

A taper with the waist diameter of 21μm was coated with a PANI film. The deposition process lasted 10 minutes. During the deposition process a fibre was immersed in the glass dish where reaction solutions of 1.5M aniline hydrochloride and 1.5M ammonium persulphate were poured. Both solutions were kept at -10^{o}C in an ice-bath for about 30min before reaction. The polymerization process starts immediately after the mixing of the agents. While the polymerization proceeded the created polymer chains precipitated and cover the immersed fibre. The chemical reaction temperature was found to be crucial for the overlay film. Decreasing the temperature down to -10^{o}C ensured better optical quality of the deposited coating. In terms of application it is important to minimize the attenuation of the taper. For thinner tapers it was observed that during coatings deposition drop of transmission intensity was larger. It has been also observed here that, created using this technique, the overlay film does not support the guidance of cladding modes so the transmission spectrum does not show dropout features in the spectrum with the thickness increase like it was observed for LB coated tapers. The coating thickness of a PANI overlay deposited in 10min-process was found to measure ~215nm as depicted in Fig. 5.15.

(a)

(b)

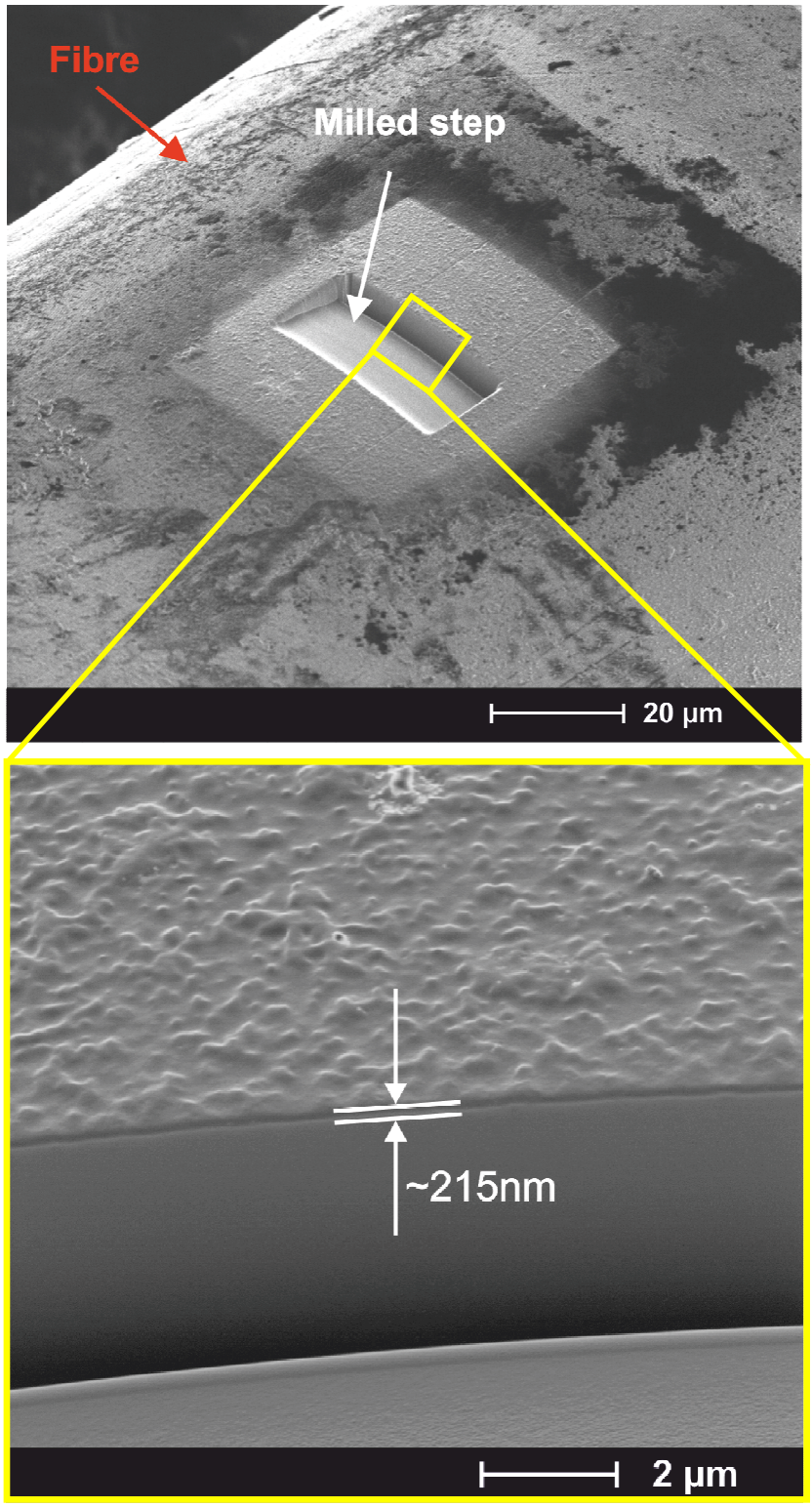

Fig. 5.15. Side wall images of a PANI coated fibre milled using the FIB technique; (a) hollowed out step viewed at an angle, (b) enlarged section of milled step with the coating thickness measured.

During the deposition an additional fibre was coated with PANI for the overlay thickness measurement purpose. The thickness was measured using the focus ion beam technique. Measuring procedure followed after a milling process of small area on side wall of a coated fibre (Fig. 5.15(a)). The hollowed out step in a fibre revealed (in Fig. 5.15(b)) the texture difference between silica and polyaniline material thus enabled the thickness estimation. The change in the transmission spectrum of a 21μm diameter taper recorded during the deposition process is depicted in Fig. 5.16.

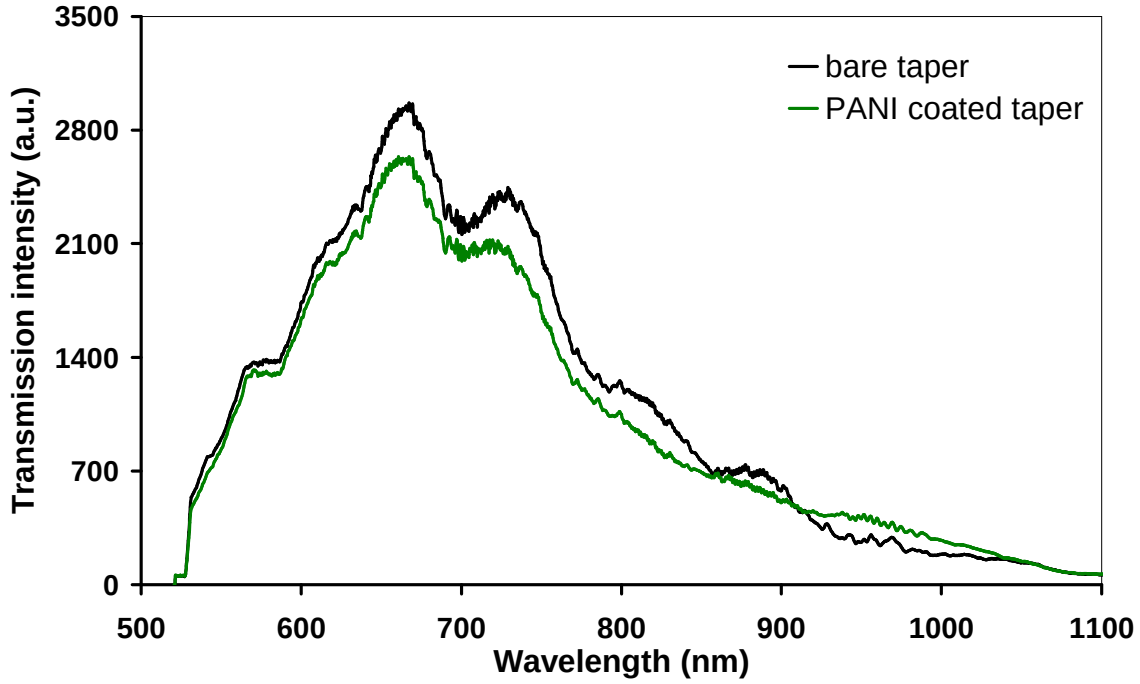

Fig. 5.16. Optical response of 21μm diameter taper to the PANI film deposition; transmission spectrum recorded before– black line and after 10min deposition – green line.

The UV-vis spectra of all forms of polyaniline are well known to the polymeric metals community and are frequently presented. Therefore the absorption spectrum of PANI forms is referred after [Neudeck, A. *et al.* 1999] in Fig. 5.17.

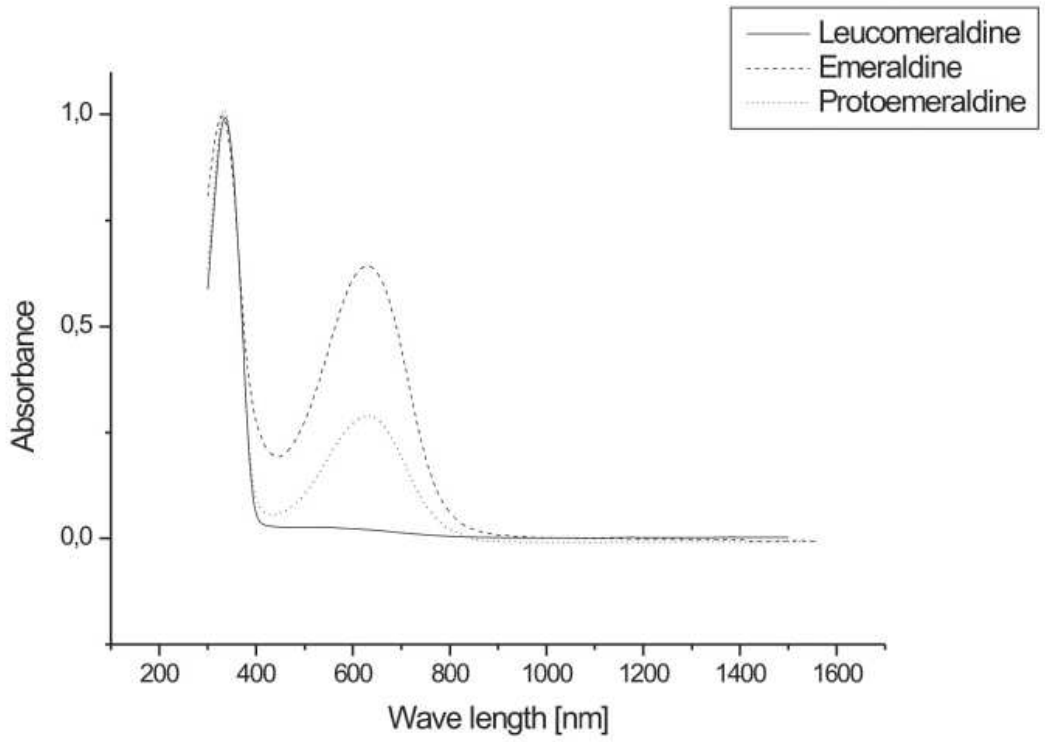

Fig. 5.17. UV-vis spectra of leucoemeraldine form, emeraldine form, and protoemeraldine form of PANI (insert after Neudeck, A. *et al.* 1999).

Two forms of PANI, i. e. emeraldine and protoemeraldine, show absorption in the 500-800nm wavelength range. Optical response of the 21μm taper to the PANI film deposition show the change in transmission spectrum in the 500-800nm wavelength range. This indicates that the film was formed of one of the PANI forms: emeraldine or protoemeraldine.

After the deposition the taper was submitted to red-ox experiments. The results are plotted in Fig. 5.18.

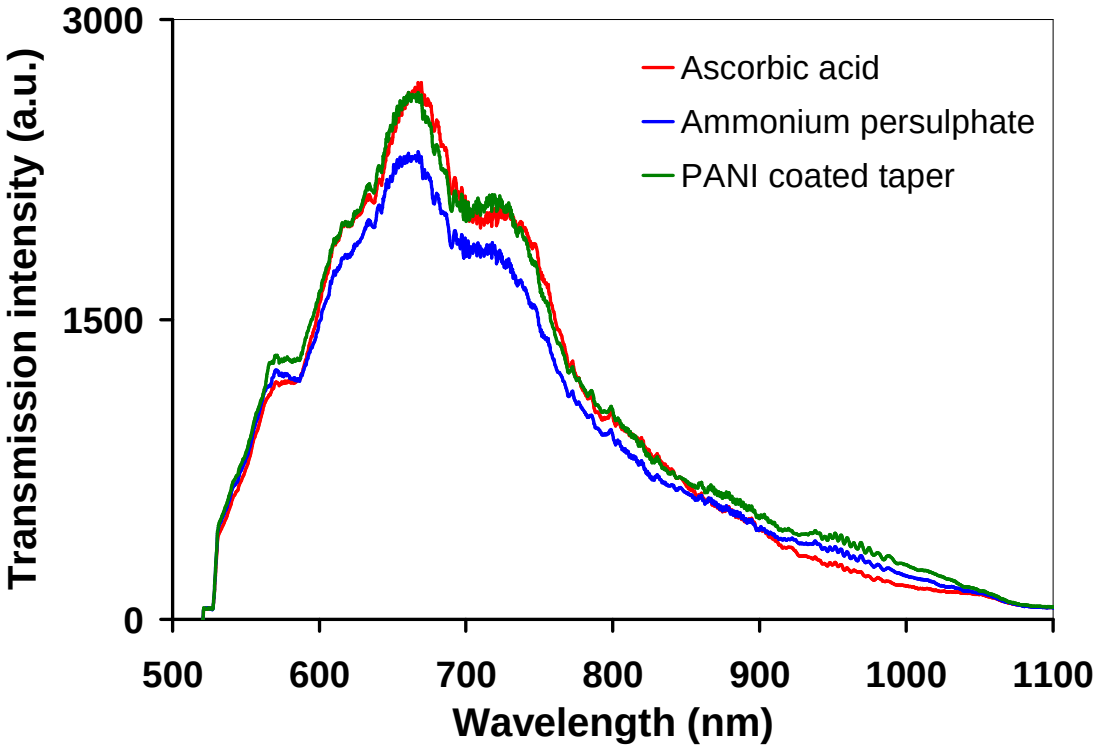

Fig. 5.18. Transmission spectra of the 21μm diameter taper coated with the PANI overlay. The absorption spectra were measure in 0.1M ammonium persulphate (blue line) and 0.06M ascorbic acid (red line).

The results were repeated three times for each red-ox reaction and showed good repeatability. A change in transmission spectrum of the PANI coated taper, due immersion in different oxidizing agent, was expected - as reported by [Jin, Z *et al*. 2000; Cao, Y. *et al.* 1989], (see Fig. 5.19). However it was not observable for this taper diameter.

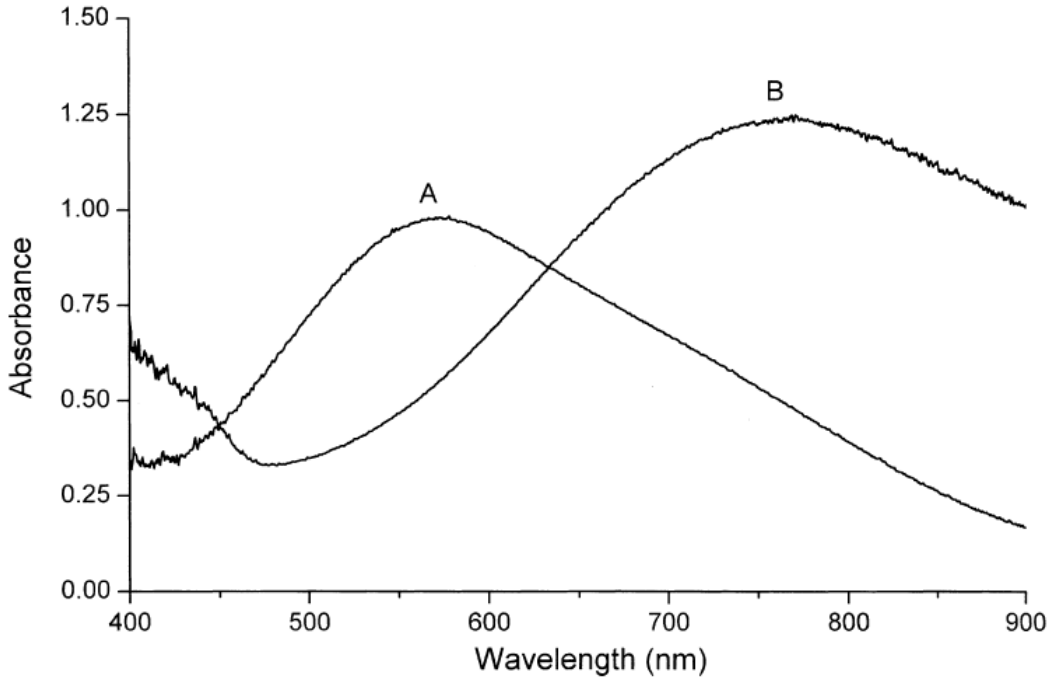

Fig. 5.19. Absorption spectra of polyaniline films measured in (A) sodium hydroxide and (B) hydrochloric acid solutions (insert after Jin, Y. *et al*. 2000).

The depicted in Fig. 5.19 results show that the wavelength maximal absorption shifts to a long wavelength following polyaniline reduction – when immersed in acid solutions.
The undetectable response and immeasurable change in transmission spectrum do not indicate a potential of the PANI coated tapers as a pH sensors. In order to improve the coated taper sensor performance, under the same conditions and the same experimental setup used, a smaller diameter taper was submitted the PANI deposition.

5.3.1.2. 12 µm diameter taper

The change in transmission spectrum of a 12µm diameter taper, recorded during the deposition process is depicted in Figure 5.20.

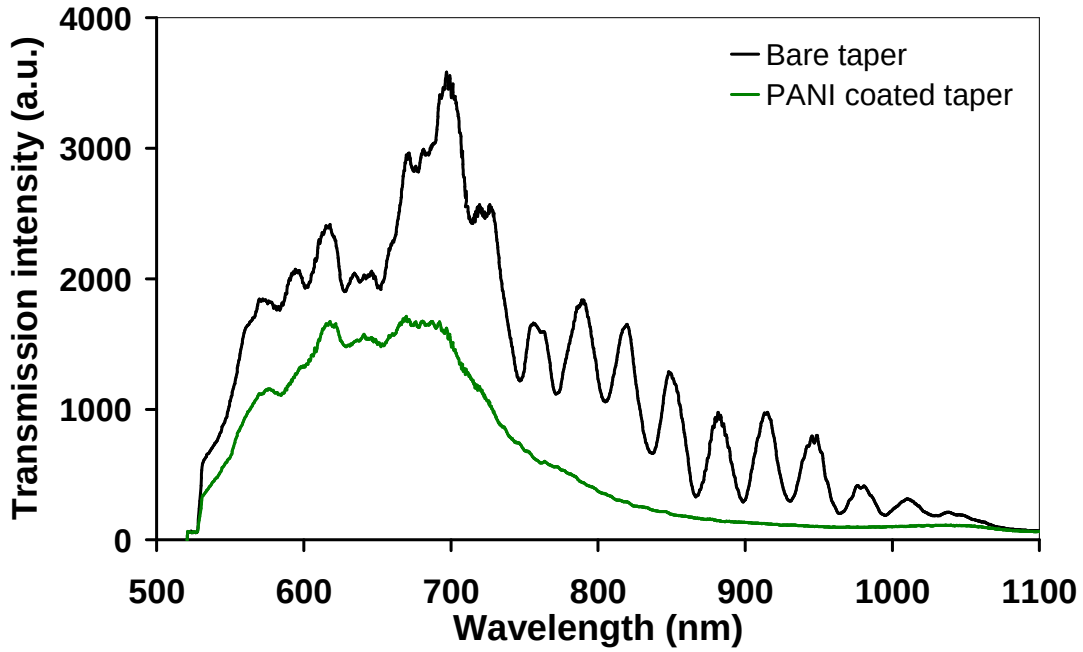

Fig. 5.20. The change in transmission spectrum of the 12μm diameter fibre taper before the polyaniline film deposition (black line) and after 10min deposition (green line).

The transmission spectrum of the 12μm taper (black line) show features which, as has already been described in chapter 3.1, corresponds to a channeled spectrum arising from the interference between modes of the fibre taper, and effect characteristic of a nonadiabatic taper.

Optical response of the 12μm taper to the PANI film deposition show the change in transmission spectrum in the 500-800nm wavelength range, see Fig. 5.20. The deposition process was carried in identical way as for taper 21μm described in section 5.3.1.1. Following the analysis presented in section 5.3.1.1 we believe to obtain the emeraldine form of the PANI deposited onto the taper.

After the deposition the taper was submitted to redox experiments. The results are depicted in Fig. 5.21.

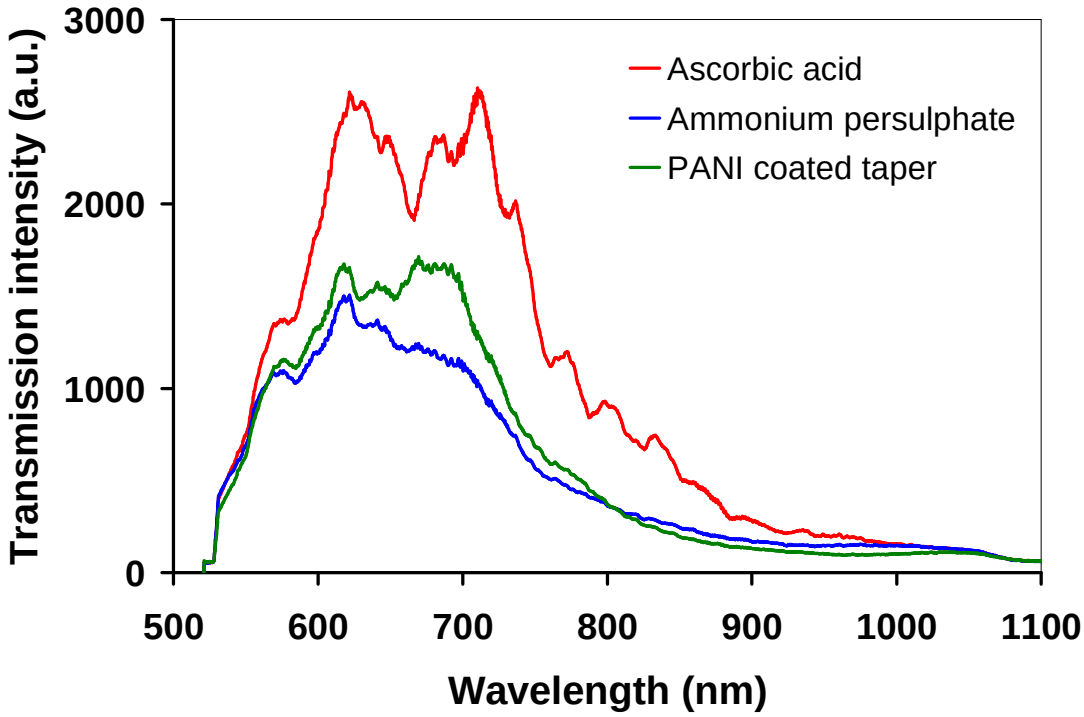

Fig. 5.21. The change in transmission spectrum of the 12μm diameter fibre taper after the reduction of the PANI film by immersion in ascorbic acid (red line) and after the oxidation by immersion in ammonium persulphate (blue line).

The change in transmission spectra show the distinct intensity increase when the fibre was immersed in ascorbic acid solution and intensity decrease when immersed in ammonium persulphate solution. The change of the transmission spectrum of polyaniline due immersion in different oxidizing agent has been reported by [Jin, Z *et al.* 2000; Cao, Y. *et al.* 1989], see Fig. 5.19. Depicted in Fig. 5.19 results show that the wavelength maximal absorption shifts to a long wavelength following polyaniline reduction – when immersed in acid solutions. The intensity increase and broadening of the transmission spectrum in response to immersion of the coated taper in acidic solution indicates reduction of the film, whilst the intensity decrease in response to immersion in the ammonium persulphate solution indicates oxidation of the film. Both effects occur immediately with the exposure of a fibre to the stimulus.

The depicted results do not show a spectrum shift occurring in the channelled spectrum of the uncoated fibre. Thus one can infer that there in no mode developing in the coating layer

and that the coating does not act as a waveguide. The observed change is due to the absorption of the polyaniline in different oxidation states. However the fast response and measurable change in transmission spectrum show a potential of the PANI coated tapers as a pH sensors.

5.4. Layer-by-layer electrostatic self assembly of PAH/TSPP film onto tapered fibres

The schematic diagram and experimental setup for the electrostatic layer-by-layer adsorption method used for the deposition of an alternate layer film onto tapered fibres was shown in Fig. 4.17 and 4.18. A series of experiments employing different coating materials was performed on tapered fibres with different waists diameters. In order to characterize sensors' performance a tapered sections of fibres were coated with functional layers composed of three different pairs of materials: 1) PAH and TSPP, 2) TiO_2 nanoparticles imprinted with NPAN ((1-(4-Nitrophenylazo)-2-naphthol (NPAN) compound), 3) PAH and cyclodextrine. The first pair of compounds showed measurable response of the transmission spectrum of a taper to the increase of number of layers. Therefore the biggest interest was devoted for this type of coating and for further ammonia sensing potential study of tapers PAH /TSPP coated.

Results for three different waist diameter tapers: 9, 10 and 12μm are presented here.
Optical response of the three tapers coated with 5 bilayers of PAH/ TSPP to the overlay thickness increase is shown in Fig. 5.22.

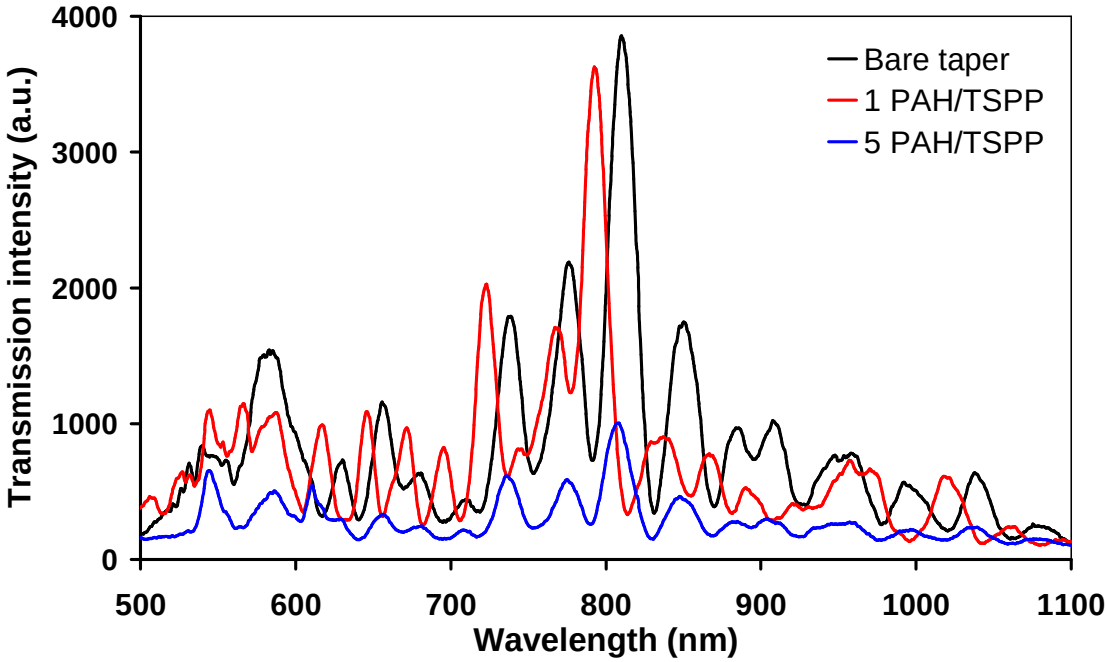

(a)

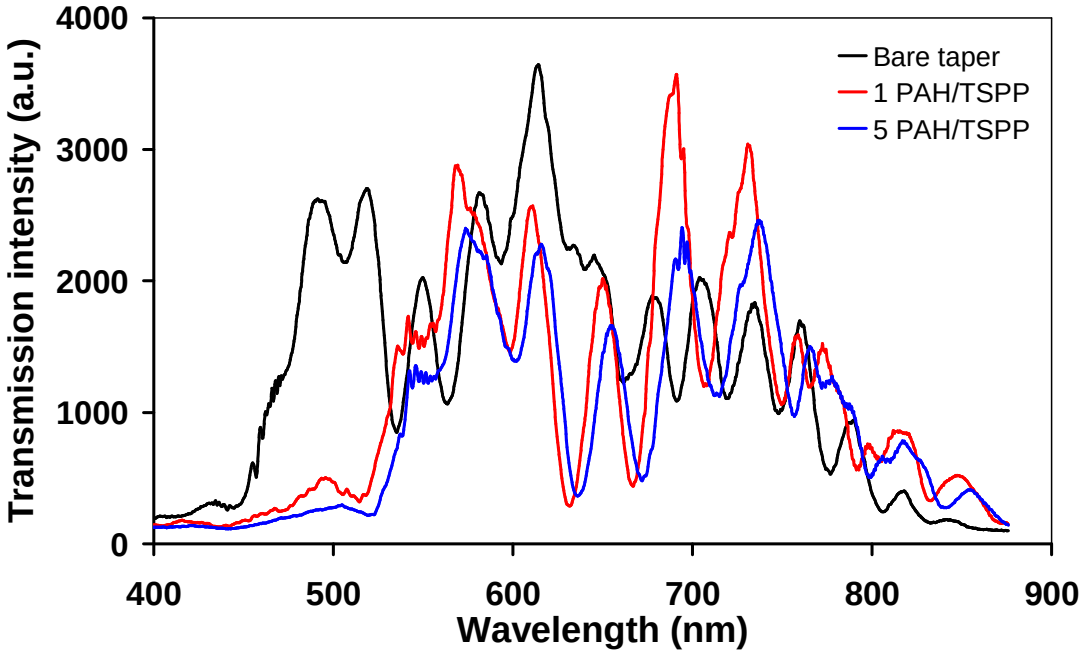

(b)

Fig. 5.22 (a),(b). Evolution of the transmission spectra of the 9 (a), 10 (b) tapered optical fibre in response to deposition of five bilayers of PAH/TSPP film measured in the air.

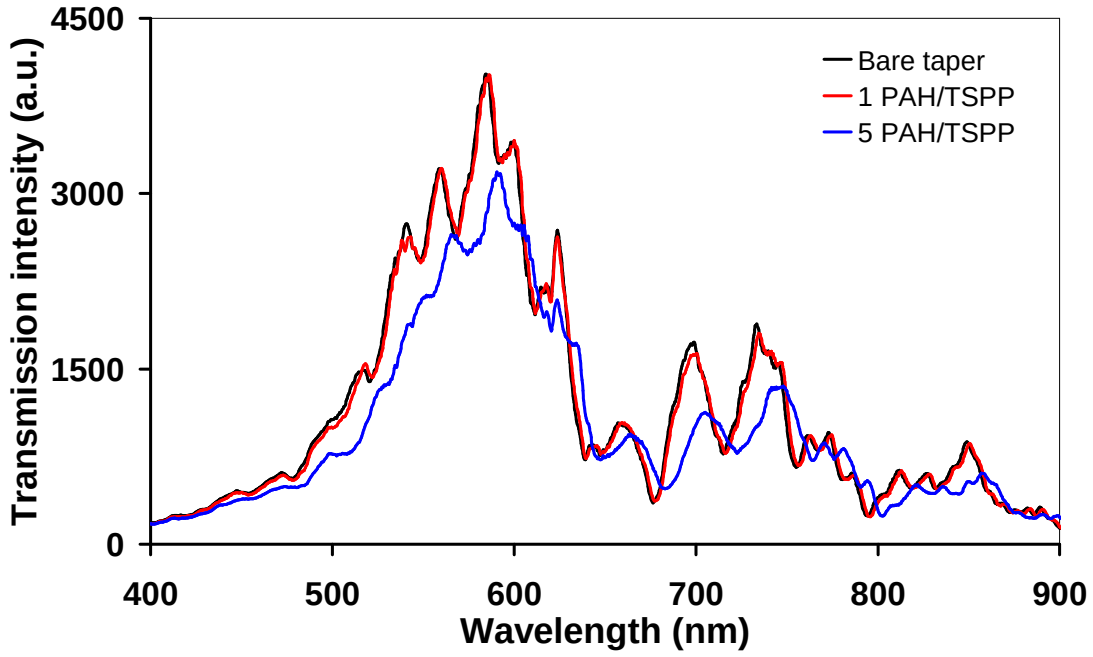

(c)

Fig. 5.22(c). Evolution of the transmission spectra of the 12μm tapered optical fibre in response to deposition of five bilayers of PAH/TSPP film measured in the air.

After the deposition of the functional layer onto the tapered region, the response of the coated taper to exposure to ammonia was characterised using the setup depicted in Fig. 4.19. For this purpose the fibre was placed in a special chamber and connected to the light source and spectrum analyser. The desired gas concentration was achieved using a two arm flow system (see Fig. 4.19). Ammonia gas of concentration of 104.3ppmv passed through one arm of the flow system and was combined in the measurement chamber with compressed air that passed through the other arm. The concentration of ammonia was controlled by adjusting the flow rate of both gases. The spectral responses to different ammonia concentration of three tapered fibres of different waist diameters are shown in Fig 5.23. The most pronounced response of a PAH/TSPP coated fibre was for the 10μm waist diameter taper which is shown in Fig. 5.23(c)-(d). The normalised transmission (the baseline transmission spectrum was subtracted) is presented in order to emphasize the absorbance change.

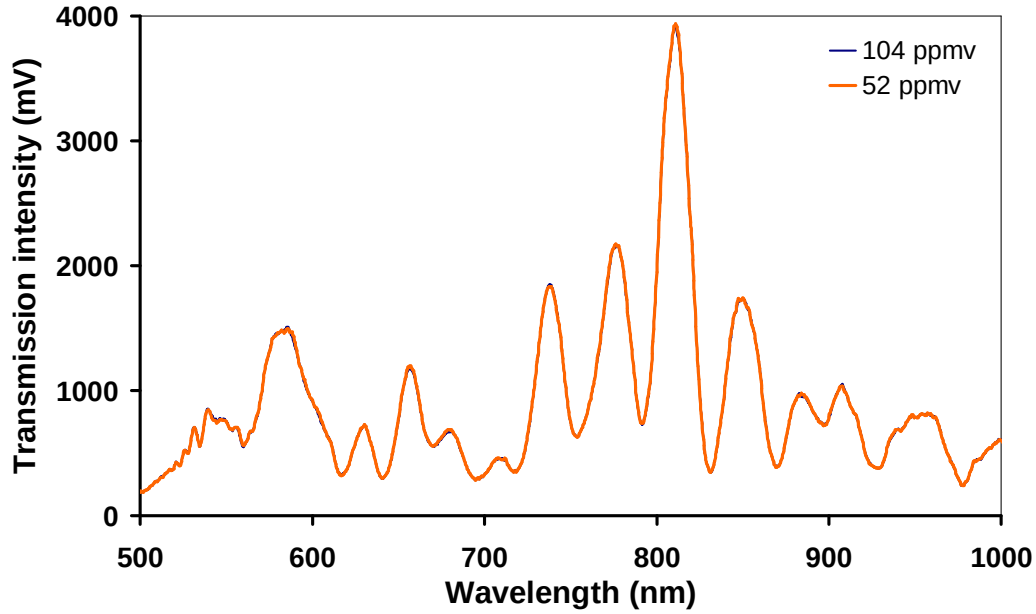

(a)

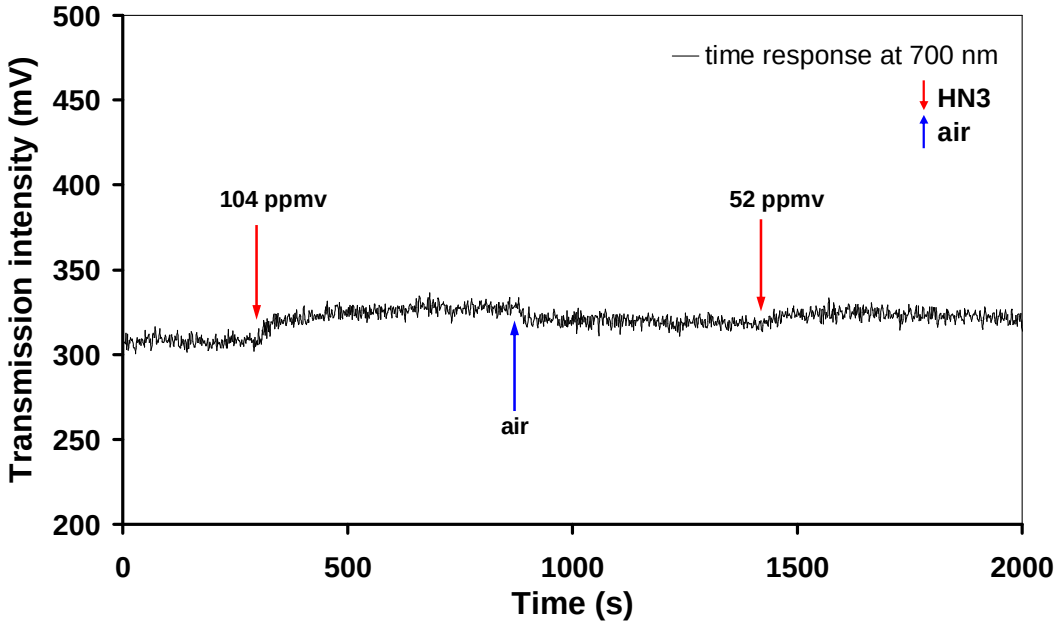

(b)

Fig. 5.23(a)(b). Spectral response of 9μm taper coated with 5 bilayers of the PAH/TSPP film to different ammonia gas concentration and the dynamic response at 700nm.

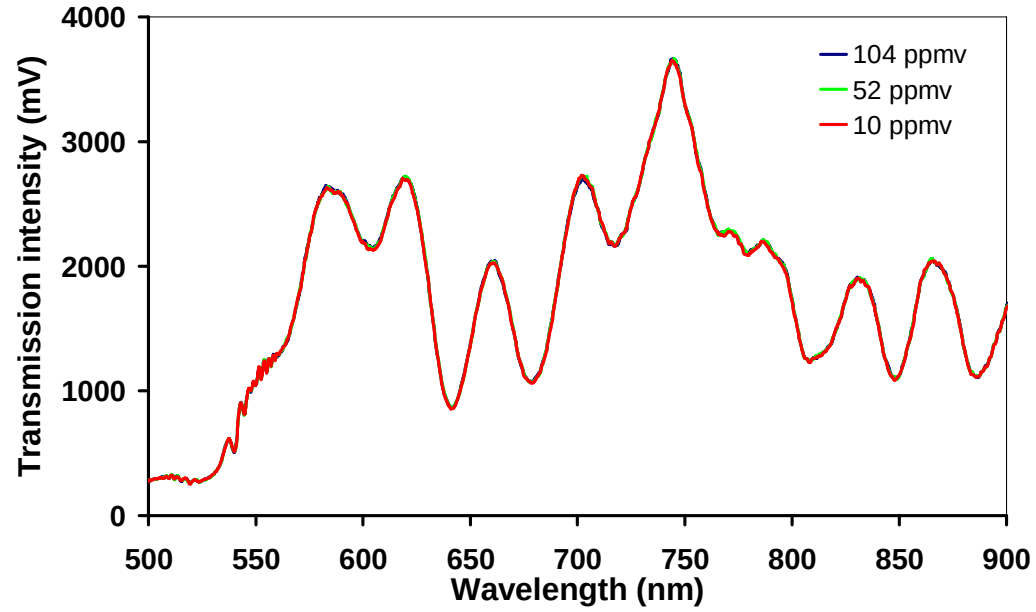

(c)

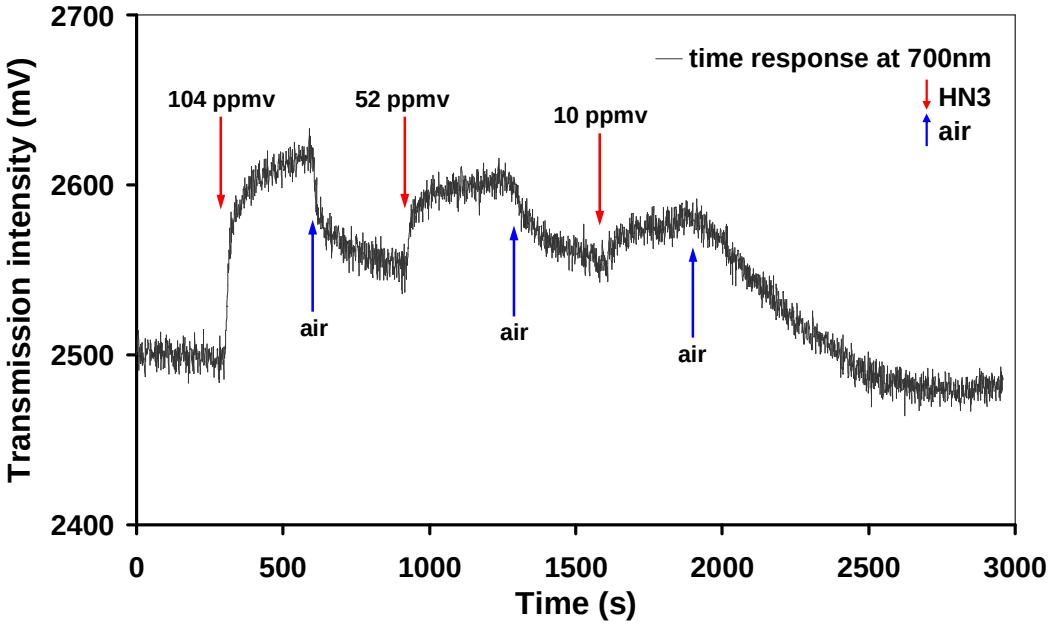

(d)

Fig. 5.23(c)(d). Spectral response of 10μm taper coated with 5 bilayers of the PAH/TSPP film to different ammonia gas concentration and the dynamic response at 700nm.

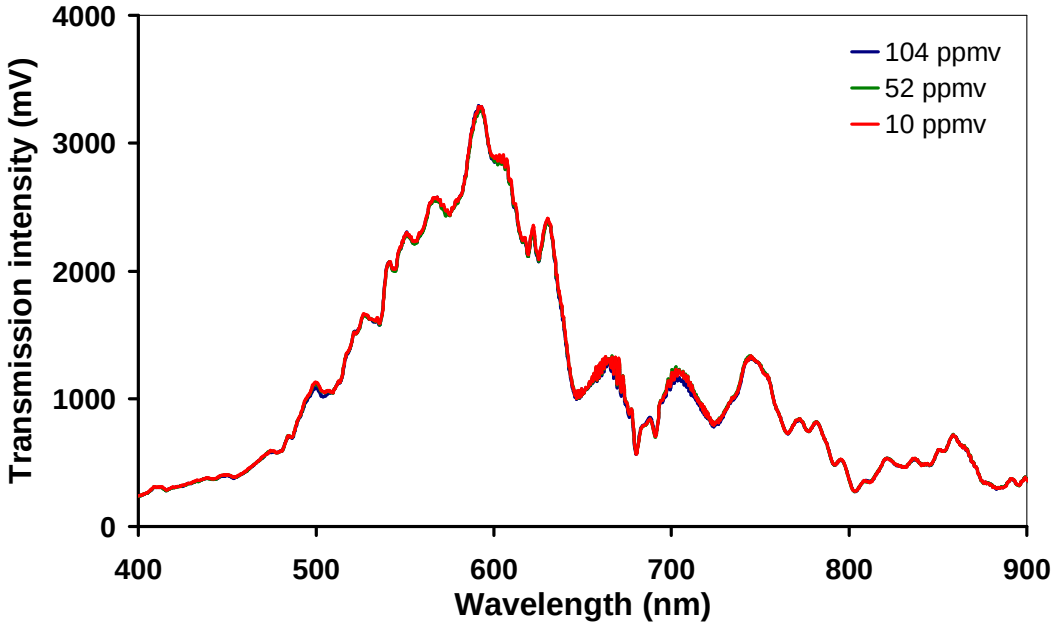

(e)

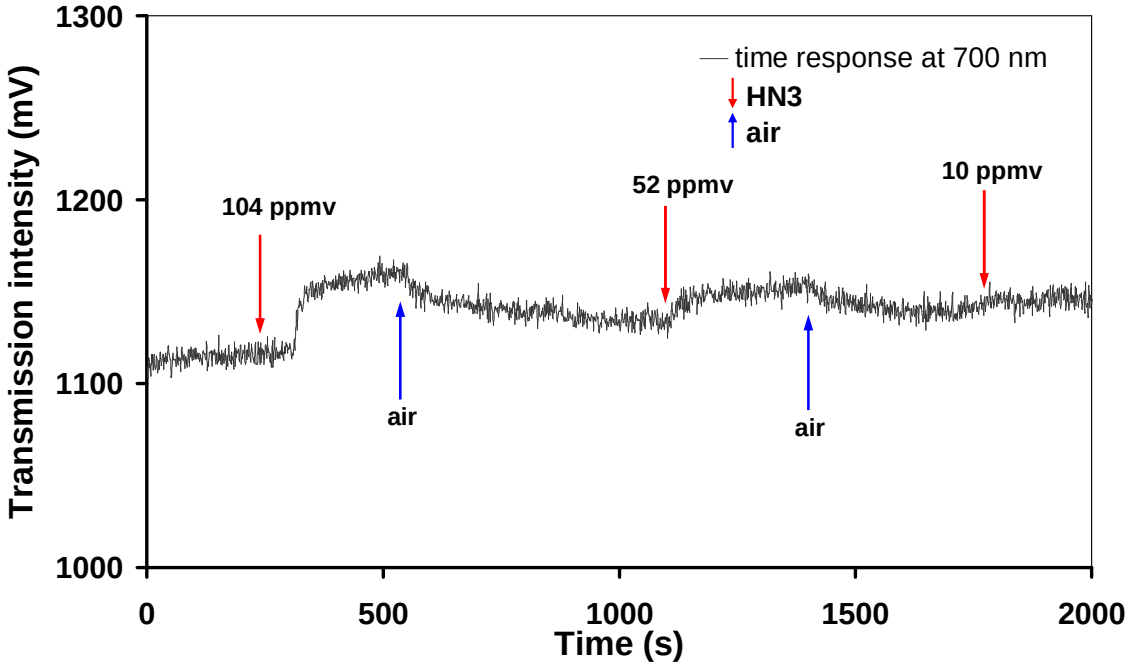

(f)

Fig. 5.23(e)(f). Spectral response of 12μm fibre taper coated with 5 bilayers of the PAH/TSPP film to different ammonia gas concentration and the dynamic response at 700nm.

The biggest change in absorbance is observed at 700nm (Q band) which is attributed to the ammonia-induced changes in the electrostatic interaction between TSPP and PAH layers. The dynamic response of the coated taper to the varying ammonia concentration from 10ppmv to 104ppmv recorded at 700nm is shown in Fig. 5.23(b). Arrows indicate the time at which the ammonia and air were admitted into the experimental chamber. The response time – 10-90% - to different ammonia concentrations was 100 seconds and recovery time was 240 seconds.

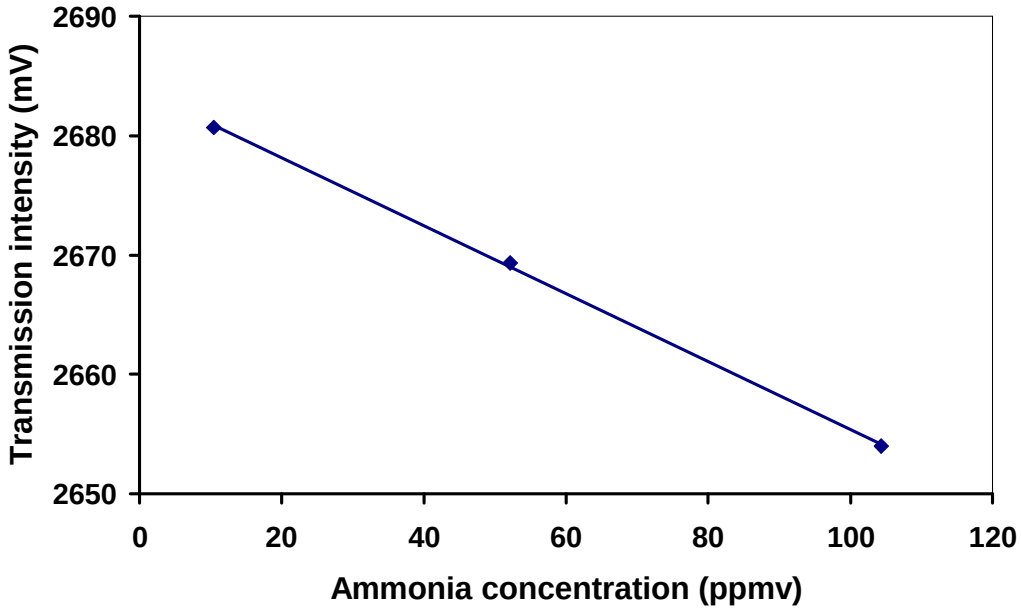

Fig. 5.24. Calibration curve of the sensor plotted for the data of normalized transmission spectrum measured at 700nm (R^2=0.98, slope= (0.28320±0.002) mV/ ppmv).

The sensitivity of the 10μm taper coated with five PAH/TSPP layers was calculated from the slope of the curve in Fig. 5.24 to be (0.2800±0.002) ppmv/mV.

Although it has been observed that dynamic response of the coated tapers to ammonia concentration is the biggest for the 10μm taper it is worth of noticing that transmission intensity around 700nm is the most pronounced for this taper. Spectra of all three tapers show irregular structure that is due to the tapering. Transmission spectrum of the 9μm taper shows an intensity drop in the vicinity of 700nm, which may handicap the sensitivity of the sensor. Similarly the transmission of the 12μm taper shows smaller intensity around

700nm that can affect its response to different ammonia concentrations. Therefore it is believed by author that it is justified to ascertain all above tapers' diameters to have similar sensitivity.

Tapered fibres coated using different deposition techniques and their performance as sensors are gathered in summary tables below.

Langmuir-Blodgett deposition technique				
	Quinolinium iodide pH sensor		Calix[4]resorcinarene Ammonia sensor	
	Sensitivity	Response time	Sensitivity	Response time
37μm taper	$\Delta pH=(3\text{-}5)10^{-2}$	20s	ΔC_g~1.97kppmv	1-20min
5μm taper	ΔpH=0.31-0.38	<0.5s	ΔC_g~2.8kppmv	<1min

Table 5.1. Summary of the performance of examined tapered fibres coated using Langmuir-Blodgett technique.

Chemical grafting technique of PANI deposition		
	Sensitivity Red-ox sensor	Response time (s)
21μm taper	no sensing observed	—
12μm taper	Sensitivity observed (*)	<0.5

Table 5.2. Summary of the performance of examined tapered fibres coated using chemical grafting technique. (*) Sensitivity of PANI coated tapers was observed as whole transmission spectrum intensity change in response to different red-ox agent. No systematic study of transmission intensity vs red-ox agent concentration has been done.

Electrostatic self-assembly technique (ESA) PAH/TSPP Ammonia sensor		
	Sensitivity	Response time
9μm taper	0.28 (**)mV/ppmv	~100s
10μm taper		~100s
12μm taper		~100s

Table 5.3. Summary of the performance of examined tapered fibres coated using electrostatic self-assembly technique. (**) All tapers appear to have approximately the same sensitivity.

5.5. Tapered optical fibres imprinted with fibre Bragg gratings (FBGs)

The experiments presented in this section were undertaken as a preliminary study of the potential for the use of fibre Bragg gratings written in tapered optical fibre as sensors. These experiments were carried in the cooperation with Dr Edmon Chehura from Engineering Photonics Group of School of Engineering of the Cranfield University, UK. Since the research presented below is beyond the scope of this thesis therefore detailed theoretical discussion is sacrificed for the sake of brief introduction.

5.5.1. FBG theory and operation

A fibre Bragg grating (FBG) consists of a periodic perturbation of the refractive index of the core of an optical fibre. Typically, for FBGs operating in the visible near infra red regions of the spectrum the grating period Λ is of the order of 500nm, see Fig. 5.25.

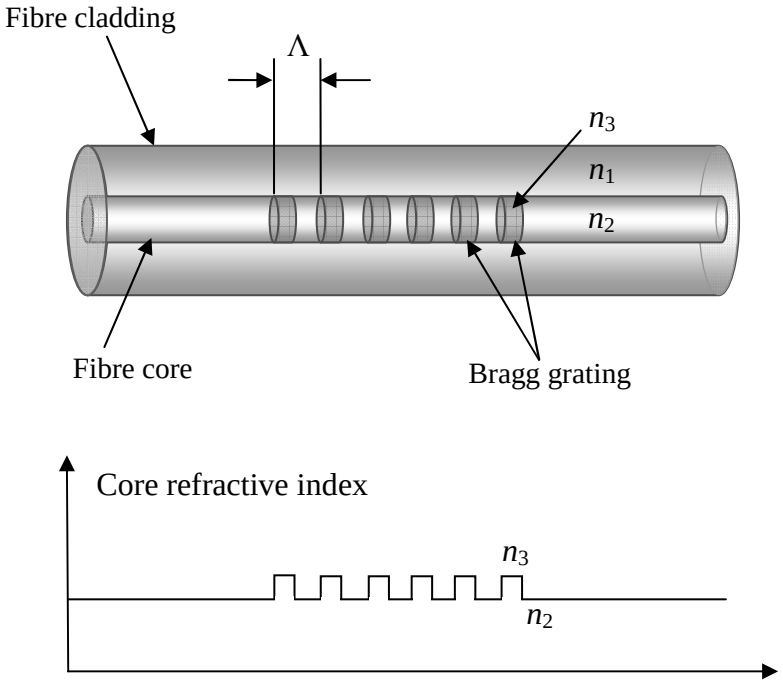

Fig. 5.25. Schematic of a fibre Bragg grating structure showing the refractive index profile.

The principle underlying the Bragg grating operation is the coupling of the fundamental forward propagating mode to the contra propagating core mode at a wavelength λ_B (Bragg wavelength) that satisfies the phase matching condition:

$$\lambda_B = 2n_{eff}\Lambda \tag{25}$$

where Λ is grating period, n_{eff} is the effective refractive index of the core mode of a fibre. For a FBG the coupling occurs between a forward-propagating guided mode and a backward-propagating guided mode. Their transmitted spectrum is characterized by a narrow resonance dip at the Bragg wavelength corresponding to the core mode coupling.

The use of fibre tapers imprinted with FBGs as a sensor elements for dynamic strain and vibration monitoring have been proposed by [Gonzalez-Segura, A. *et al*. 2007; Mora, J. *et*

al. 2001]. In these devices the constant period grating was written within the untapered region and within the transition zone of a tapered fibre. An effective spectral chirp is thus produced due to the change of the mode refractive index along the transition zone of a taper.

5.5.2. TFBG theory and operation

The properties of the FBG can be modified by varying the orientation of the refractive index modulation with respect to the optical axis of a fibre. When the orientation of the refractive index modulation is at an angle Θ to the optical axis a tilted FBG is created (TFBG), see Fig. 5.26.

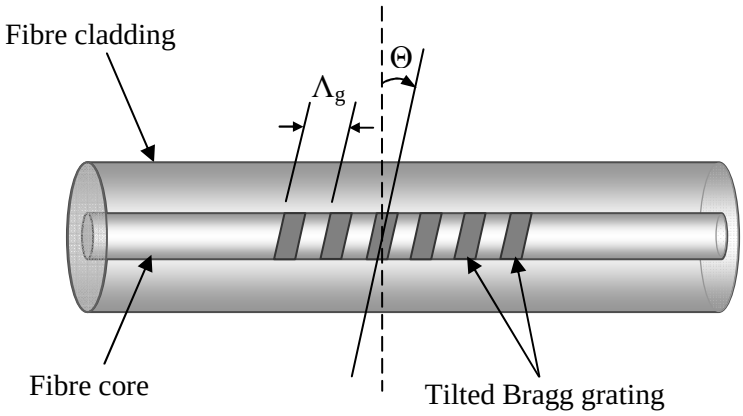

Fig. 5.26. Schematic of a tilted fibre Bragg grating structure.

Weakly TFBGs, with planes tilted at small angles – 0-2° - with respect to the fibre axis, couple light from forward-guided core mode to both backward-guided core and cladding modes [Huy, M. Ch. P. *et al.* 2006, Chehura, E. *et al.* 2007], see Fig. 5.27.

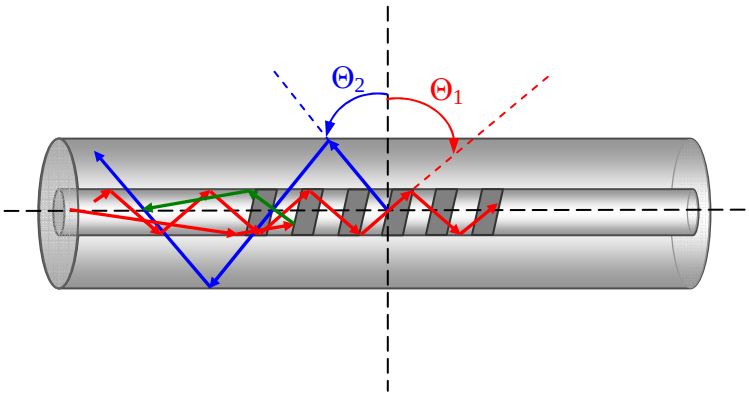

Fig. 5.27. Diagram showing fundamental forward-guided core mode (red line) coupled to a backward-propagating core (green line) and cladding (blue line) mode induced by TFBG.

The principle underlying the Bragg grating operation is the coupling of the fundamental forward propagating mode to the contra propagating core mode at a wavelength that satisfies the phase matching condition. The spectral response of the TFBG is governed by the phase matching condition:

$$\lambda_i = \left(n_{\text{eff}}^{\text{co}} + n_i^{\text{clad}}\right) \cdot \frac{\Lambda_{\text{B}}}{\cos\Theta} \tag{5.2}$$

where λ_i is the *i*th cladding mode resonance wavelength, $n_{\text{eff}}^{\text{co}}$ is the effective refractive index of the core, n_i^{clad} - effective index of the *i*th cladding mode, θ – tilt angle.

While the core mode resonance (at Bragg wavelength) is sensitive to axial strain and temperature, cladding mode resonances are sensitive to external perturbations (strain, temperature, external refractive index). TFBGs photowritten in single-mode fibres are used for refractive index measurement [Laffont, G. *et al*. 2001; Huy, M. C. P. *et al*. 2006], strain sensing [Caucheteur, C. *et al*. 2006] as well as for simultaneous strain and temperature sensing [Chehura, E. *et al*. 2007; Rahimim S. *et al*. 2009].

In TFBG, two kinds of coupling take place. One corresponds to the coupling between self contra-propagating coupling of core mode at Bragg wavelength given by [Lee, K. S. *et al*. 2000]:

$$\lambda_B = 2n_{eff,core}\frac{\Lambda_g}{\cos\Theta} \tag{5.3}$$

where Θ is tilt angle of a grating (Fig. 5.27), Λ_g is nominal grating period. The second type of coupling occurs at resonant wavelengths of core modes and contra-propagating cladding modes, and is given by [Lee, K. S. *et al*. 2000]:

$$\lambda_B = \left(n_{eff,clad,i} + n_{eff,core}\right)\frac{\Lambda_g}{\cos\Theta} \tag{5.4}$$

where $n_{eff,clad,i}$ is effective refractive index of i-th cladding mode, i=1,…,m, m is the total number of cladding modes.

Figure 5.28 presents the typical transmission spectrum of TFBG with cladding mode resonances situated below the Bragg wavelength. An important feature of a weakly tilted FBG is the presence of the strong resonance immediately to the left of the Bragg resonance, called “ghost mode”. The ghost mode is made up of several low order cladding modes.

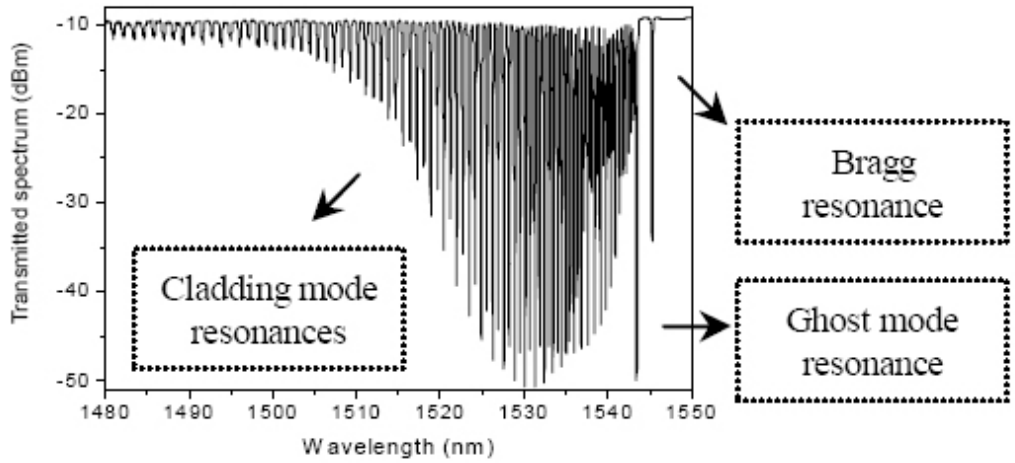

Fig. 5.28. Transmission spectrum of a 3° TFBG written in the core of a standard single mode fibre using a pulsed lacer (KrF – 248nm) and phasemask (insert after Caucheteur, C. *et al.* 2006)

The idea that we have developed is to write constant period tilted fibre Bragg grating (TFBG) in the center of the narrowed waist of a taper rather than in the transition regions as it has been done by [Gonzalez-Segura, A. *et al.* 2007]. TFBGs fabricated in the tapered region of the fibre can be anticipated to provide improved sensibility to external refractive index for both the cladding and Bragg resonances as they are more exposed to the external environment. Since the cladding modes resonances are proved to be sensitive to external perturbations, it is anticipated that the tapered region of a fibre will improve their sensitivity in comparison to the untapered TFBG written fibres. The experimental results presented below were obtained on TFBGs written into photosensitive single mode tapered fibres using a pulse laser and a phase mask. The response of the transmission spectra of five tapered optical fibres, with taper diameters within the range of 33-53μm, to the TFBG imprinting is investigated and their potential applications as sensors is reported.

5.5.3. FBG and TFBG fabrication procedures

There are two methods commonly used in FBG fabrication, namely the two beam interference and the phase mask technique. The first method involves the exposure of the

optical fibre, with it protective buffer coating removed to an interference pattern formed between two intersecting UV laser beams that are mutually coherent [Meltz, G. *et al.* 1989]. The second technique involves the fabrication of a FBG in the core of a fibre placed in the near field of a phase mask when illuminated by an UV laser beam [Hill, K. O. *et al.* 1993; Anderson, D. Z. *et al.* 1993]. In order to achieve high Bragg reflectivity, the photosensitivity of the fibre is enhanced either by doping the core with elements such as Ge, Eu or Sn, or by hydrogen loading via immersion of a fibre in hydrogen at high pressure for up to two weeks typically [Kashyap, R. 1999]. Hydrogen loading is commonly used to allow FBG fabrication in telecommunication optical fibres [Guan, B.-O. *et al.* 2000].

5.5.4. Results

For the experiments a single mode fibre (Fibercore, SM750) was used, with cladding-core diameters of 125/5μm and cut-off wavelength λ =669nm. Prior to grating imprinting, the fibres were tapered using the setup presented in Fig. 4.2 using the procedure which was described in chapter 4.1. Five tapers were prepared with waist diameters as follows: 33, 44, 48, 50 and 53μm and TFBG written is the center of the taper waist.

Fabrication of TFBGs in tapered fibres

Tapered fibres were hydrogen loaded in a steel chamber filled with hydrogen at a pressure of 120 bar at room temperature for four weeks. After that time fibres were taken out of the chamber and Bragg gratings were imprinted. The fabrication of TFBGs was carried by exposing the tapered section of each fibre to a UV beam with the phase mask placed between the fibre and the light source, see Fig. 5.29.

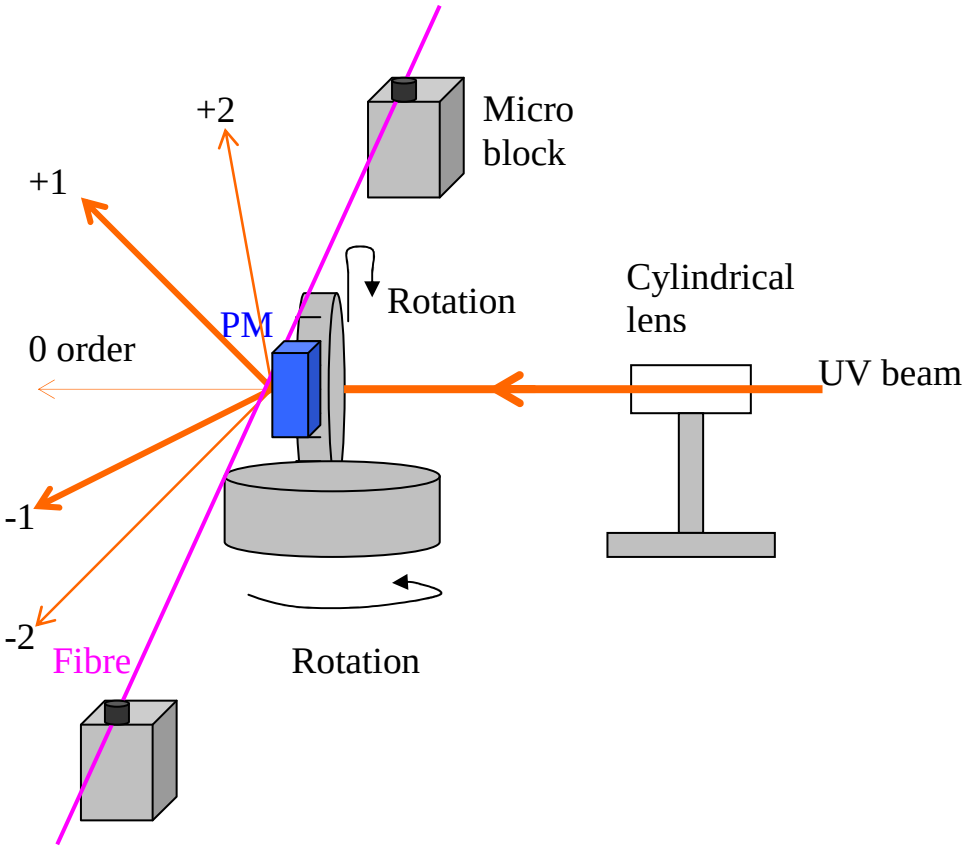

Fig. 5.29. Schematic diagram of the TFBG fabrication system, PM is a phase mask.

The source of a UV light was the output from a wavelength tunable pulsed laser operating at 248nm with pulse duration of 10ns, 25Hz repetition rate and an average power of 30mW. The TFBGs were fabricated with the phase mask of period 896nm, the tilt angle was 1.5°, and the resonance Bragg wavelength was 793nm. The exposure time for each fibre was 5 min. The presented results show the grating transmission (or reflectivity) dependence on the waist diameter of the taper. The reflectivity was estimated from the resonance dips occurring in the transmission spectra of fibres. During the TFBG fabrication process the transmission spectra were recorded by coupling the output from super luminescent diode (SLD) broadband source (Exalos, EXS8001) into a fibre, and analyzing the transmitted light by using an optical spectrum analyzer (Ando, AQ-6310B) within the wavelength range 770-820nm.

Figure 5.30 presents transmission spectra with the baseline correction applied of tapered fibres imprinted with TFBGs. The normalization was performed in order to provide the reference for interpreting the transmission change in the spectrum.

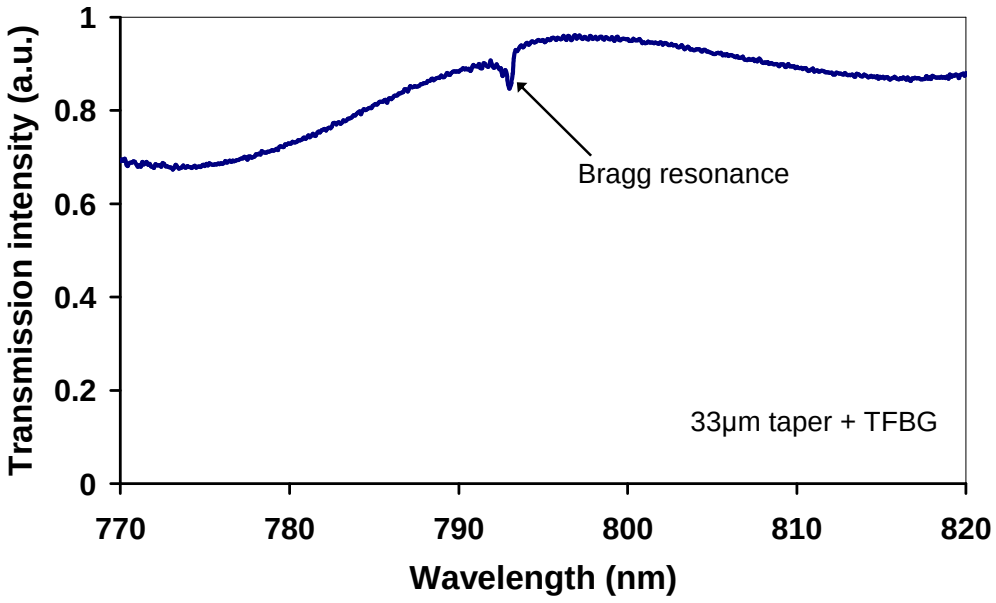

(a)

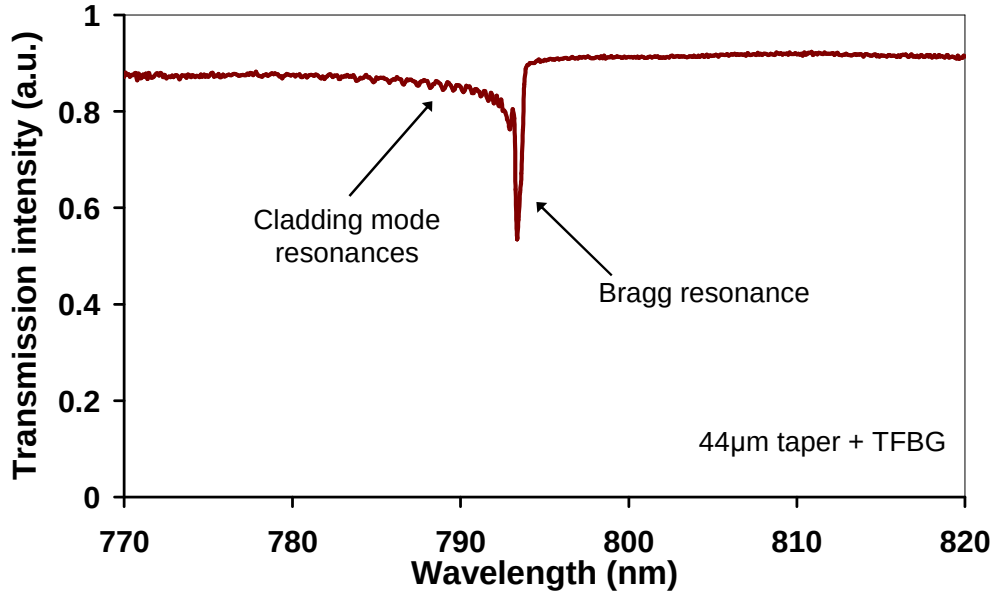

(b)

Fig. 5.30 (a)(b). Transmission spectra (with the baseline correction applied) of (a) 33µm, (b) 44µm taper. TFBG photo written in single mode, hydrogen-loaded fibre.

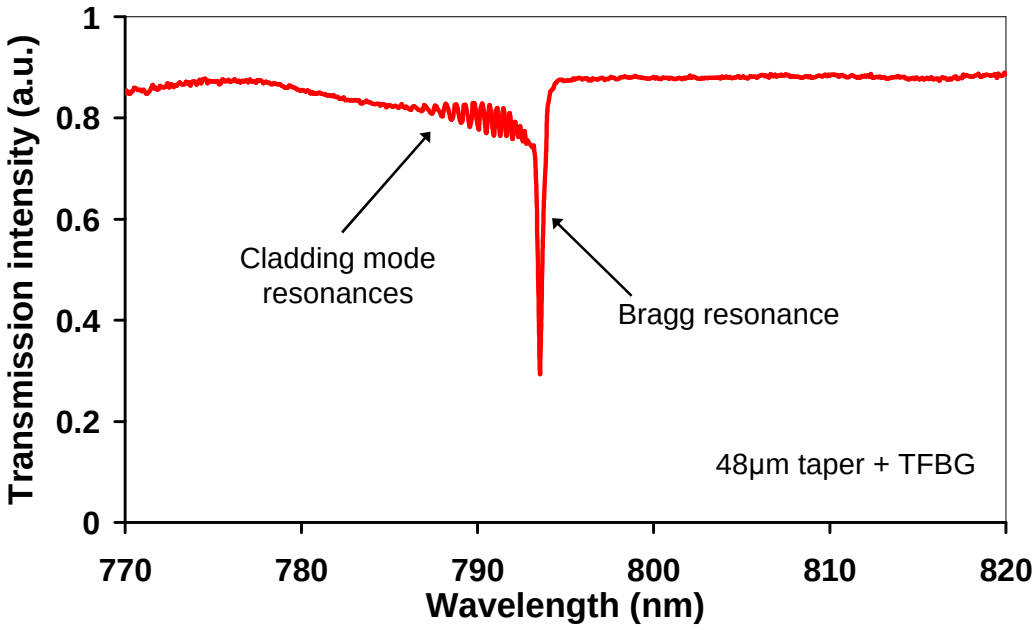

(c)

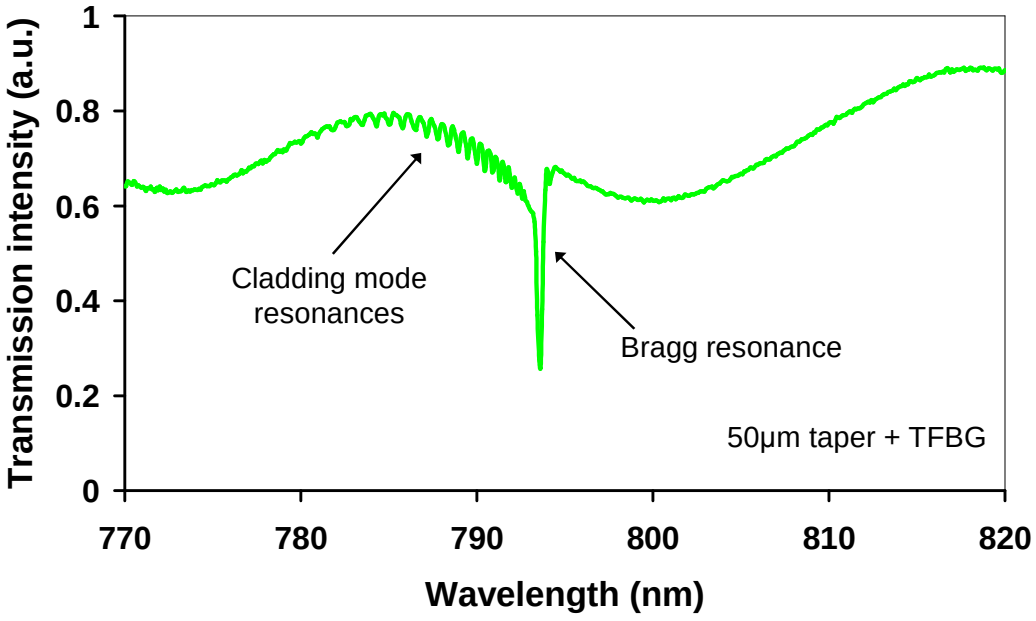

(d)

Fig. 5.30(c)(d). Transmission spectra (with the baseline correction applied) of (c) 48µm, (d) 50µm taper. TFBG photo written in single mode, hydrogen-loaded fibre.

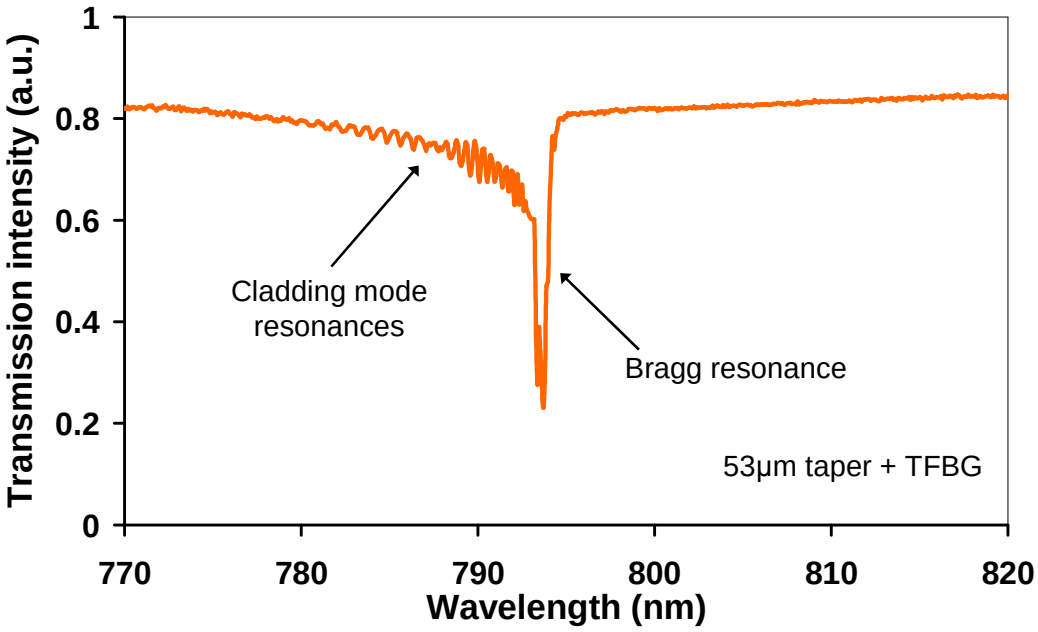

(e)

Fig. 5.30(e). Transmission spectra (with the baseline correction applied) of 53μm tapered fibre. TFBG photo written in single mode, hydrogen-loaded fibre.

When a TFBG is written in untapered fibre at a small tilt angle of the order of 1.5° a single cladding mode resonance is usually observed, which corresponds to coupling from the core mode to a cladding mode. This cladding mode resonance referred to as a ghost mode exhibits weak sensitivity to surrounding external refractive index while the Bragg wavelength resonance exhibits no sensitivity. In case of TFBGs written tapers the ghost mode resonance is not visible, numerous cladding mode resonances are present instead. TFBGs fabricated in the tapered region of the fibre can be anticipated to provide improved sensibility to external refractive index for both the cladding and Bragg resonances as they are more exposed to the external environment. In order to study the spectral response of the TFBGs written tapers to the change of refractive index of an external medium the LB technique can be used, where a fibre is coated with an overlay of a chosen material. Further studies might concern sensors fabrication using TFBG written coated tapers which are sensitive to an arbitrary chosen specimen.

5.6 Computational results

The response of the transmission spectrum of tapered fibre to the deposition of the nanostructured coating can be predicted using slab waveguide approximation for the tapered region, as described in section 3.3. For the calculation of the transmission spectrum a structure described in section 4.5 in Fig. 4.20 was analysed and calculation scheme depicted in Fig. 4.21 applied. Results for two different taper waist diameters are presented: 5μm and 35μm. The cladding refractive index was 1.458 while studied external medium refractive index for 200 layers of coating. Wavelength range was 600-800nm. The result is shown in Fig. 5.31. For the comparison the theoretical result is followed by experimental result shown in Fig. 5.32.

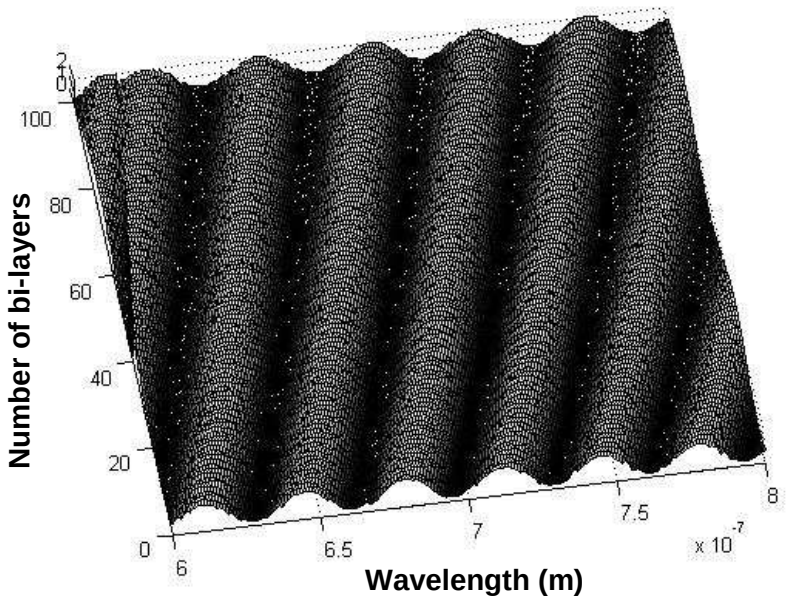

Fig. 5.31. The evolution of the transmission spectrum of a 5μm diameter fiber taper in response to an increase in the nanocoating thickness predicted using slab waveguide approximation.

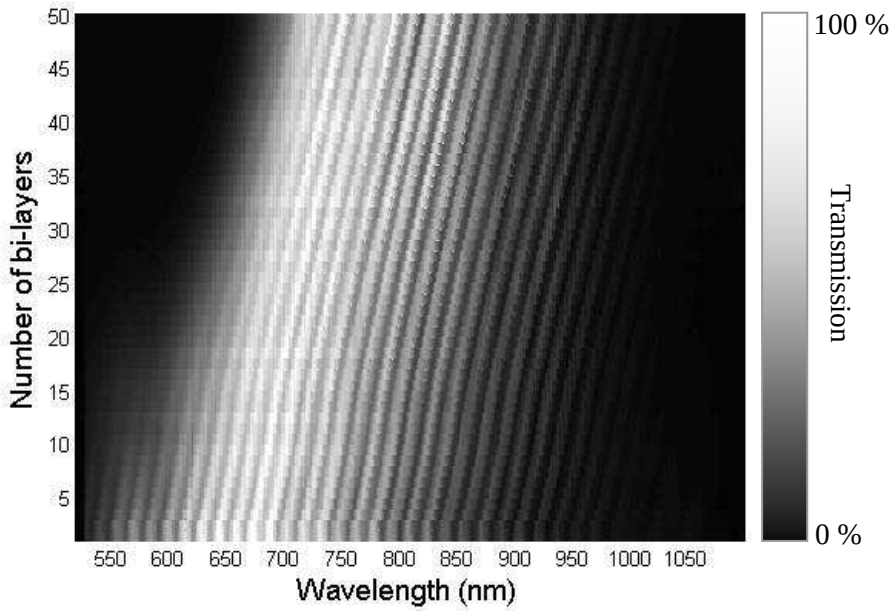

Fig. 5.32. Evolution of the transmission spectrum of a 5μm diameter fiber taper in response to an increase in the nanocoating thickness – experimental result.

In the presented results in Fig. 5.31 and 5.32 a small discrepancy between both figures can be observed. The divergence between predicted and experimentally obtained results is probably due to not exact fit between theoretical and experimental values of taper waist and/or refractive indices of overlay material. Also contracting zones of a taper have not been taken into account and any consequent coupling has not been included into calculations. These results indicate that the model predicts well the trend regarding optical throughput as a function of an overlay thickness. Introduction of the taper geometry and exact values of variables into computations would bring the theoretical results closer to experimental ones.

References

Anderson, D. Z., Mizrahi, V., Erdogan, T., White, A. E., "Production of in-fiber gratings using a diffractive optical-element", *Electronics Letters*, Vol. 29, No. 6, pp. 566-568, 1993

Beychok, M. R., "Fundamentals of Stack Gas Dispersion", M. R. Beychok, 2005 (4^{th} edition)

Cao, Y., Andreatta, A., Heeger, A. J., Smith, P., "Influence of chemical polymerization conditions on the properties of polyaniline", *Polymer*, Vol. 30, No. 12, pp. 2305-2311, 1989

Caucheteur, C., Chen, C., Albert, J., Megret, P., "Use of weakly tilted fiber Bragg gratings for strain sensing purposes", *Proceedings of the Society of Photo-Optical Instrumentation Engineers (SPIE)*, Vol. 7003, pp. 307-307, Optical Sensors Conference 2008, France, 2008

Chehura, E., James, S. W., Tatam, R. P., "Temperature and strain discrimination using a single tilted fibre Bragg grating", *Optics Communications*, Vol. 275, No. 2, pp. 344-347, 2007

Flannery, D., James, S. W., Tatam, R. P., Ashwell, G. J., "Fibre optic chemical sensing using Langmuir-Blodgett overlay waveguides", *Applied Optics*, Vol. 38, No. 36, pp. 7370-7374, 1999

Gonzalez-Segura, A., Cruz, J. L., Andres, M. V., Barrios, P. Rodriguez, A., "Fast response vibration sensor based on Bragg gratings written in tapered core fibres", *Measurement Science & Technology*, Vol. 18, No. 10, pp. 3139-3143, 2007

Guan, B.-O., Tam, H.-Y., Tao, X.-M., Dong, X.-Y., "Highly stable fiber Bragg gratings written in hydrogen-loaded fiber", *IEEE Photonics Technology Letters*, Vol. 12, No. 10, pp. 1349-1351, 2000

Hill, K. O., Malo, B., Bilodeau, F., Johnson, D. C., Albert, J., "Bragg gratings fabricated in monomode photosensitive optical-fiber by uv exposure through a phase mask", *Applied Physics Letters*, Vol. 63, No. 3, pp. 424-424, 1993

Huy, M. C. P., Laffont, G., Dewynter, V., Ferdinand, P., Labonte, L., Pagnoux, D., Roy, P., Blanc, W., Dussardier, B., "Tilted fiber Bragg grating photowritten in microstructured optical fiber for improved refractive index measurement", *Optics Express*, Vol. 14, No. 22, pp. 10359-10370, 2006

Jin, Z., Su, Y., Duan, Y., "An improved optical pH sensor based on polyaniline", *Sensors and Actuators B*, Vol. 71, No. 1-2, pp. 118-122, 2000

Kashyap, R. "Fibre Bragg Gratings", Academic Press, New York, 1999

Laffont, G., Ferdinand, P., "Tilted short-period fibre-Bragg-grating-induced coupling to cladding modes for accurate refractometry", *Measurement Science & Technology*, Vol. 12, No. 7, pp. 765-770, 2001

Lee, K. S., Erdogan, T., "Fiber mode coupling in transmissive and reflective tilted fiber gratings", *Applied Optics*, Vol. 39, No. 9, pp. 1394-404, 2000

Love, J. D., Henry, W. M., Stewart, W. J., Black, R. J., Lacroix, S., Gonthier, F., "Tapered single-mode fibres and devices. Part1: Adiabaticity criteria", *IEE Proceedings-J Optoelectronics*, Vol. 138, No. 5, pp. 343-354, 1991

Meltz, G., Morey, W. W., Glenn, W. H., "Formation of Bragg gratings in optical fibers by a transverse holographic method", *Optics Letters*, Vol. 14, No. 15, pp. 823-825, 1989

Mora, J., Villatoro, J., Diez, A., Cruz, J. L., Andres, M.V., "Tunable chirp in Bragg gratings written in tapered core fibers", *Proceedings Of The Society Of Photo-Optical Instrumentation Engineers (SPIE)*, 4th Iberoamerican Meeting On Optics And 7th Latin

American Meeting On Optics, Lasers, And Their Applications, Vol. 4419, pp. 338-341, 2001

Neudeck, A., Petr, A., Dunsch, L., "The redox mechanism of polyaniline studied by simultaneous ESR-UV-vis spectroelectrochemistry", *Synthetic Metals*, Vol. 107, No. 3, pp. 143-158, 1999

Rahimi, S., Ban, D. Y., Xiao, G. Z., Zhang, Z. Y., Albert, J., "Temperature and Strain Sensors Based on Integration of Tilted Fiber Bragg Gratings With a Free Spectral Range Matched Interrogation System", *IEEE Sensors Journal*, Vol. 9, No. 7, pp. 858-861, 2009

Topliss, S. M., James, S. W., Davis, F., Higson, S. P. J., Tatam, "Optical fibre long period gratings based selective vapour sensing of volatile organic compounds", *Sensors and Actuators B: Chemical*, Vol. 143, pp. 629-634, 2009 (article in press)

DISCUSSION AND SUGGESTIONS FOR FUTURE WORK

6

The fabrication of sensors based on uniform-waist single mode fibre tapers has been demonstrated. The repeatability of the uniform taper waist is promising parameter for the subsequent experiments of functional multilayers of nanocoatings. Three deposition techniques have been used for a functional overlay creation. The potential application of coated tapered optical fibres as chemical sensors – both in liquid and gaseous environment - has been demonstrated. Sensing capability of nano-coated tapered fibres has been reported. Finally, the novel sensor's precursor based on the tilted Bragg grating written in the narrowed section of a tapered optical fibre.

6.1. Properties of manufactured tapered fibres

The setup presented for manufacturing tapered optical fibres allows for fabrication of any desired waist diameter from the original size, typically 125μm, down to 2μm. The setup allows for tapers to be manufactured with 1μm accuracy. The uniform waist, measured using ESEM, of fabricated tapers is ensured. The tapering process affects minimally the light transmission intensity within a fibre. The intensity decrease has been observed to be larger for more abrupt tapers, for those with shorter transition zones, in comparison to the ones with longer transition zones.

In order to improve the tapering process an automatic system with pulling speed control and heat source control is required. As a heat source a CO_2 laser with output power control and motorized stages with "on-the-fly" velocity control are recommended. All together integrated in computer controlled system. The advantage of the CO_2 laser over a gas burner is invulnerability to air currents in the experiment environment. It would allow for better taper geometry control – i.e. length of transition zones – and thus smaller transmission intensity decrease.

6.2. Properties of tapered fibres coated with functional layers

Three techniques for the deposition of a chemically sensitive material have been investigated: (i) the Langmuir-Blodgett technique, (ii) the chemical deposition approach and (iii) electrostatic-self-assembly technique. Each of the methods imposes different overlay material deposited onto tapered fibres as well as different sensing application potential.

L-B coating

Here tapered fibres coated with the functional materials: quinolinium dye and calix[4]resorcinarene using the L-B technique are discussed. Results for the L-B deposited tapers with the waist diameter bigger than 20μm show the evolution of features within the transmission spectra in response to the layer thickness. The 37μm diameter taper response indicates the forming of a coupled waveguide between the taper and the coating. A resonance bands were developed, which showed strong dependence on the thickness of a coating layer. It has been shown that features tend to appear in pairs. This phenomenon can be explained based on the theory presented in Theoretical section: the scalar analysis and coupled-mode theory with hybrid modes – HE - taken into consideration, where the phenomenon is explained as a reorganization of modes. There is finite number of allowed effective refractive indices states of modes in a non-coated tapered fibre. Deposition of a thin layer causes the perturbation of the refractive

index which leads to appearance of not-allowed (in non-coated) states of modes. This allows for transition to guidance of one cladding mode in the overlay. Guidance occurs at a specific thickness. With the increase of the thickness the distribution of modes recovers it original state. Phenomenon repeats periodically as the thickness increase. Appearance of pairs of features suggests the two-step transition of refractive indices of modes, what according to the theory is the refractive index of each HE_{1j} mode shifting to immediate lower order cladding mode: to EH mode before it is definitely shifted to the HE. The present resonance bands in the spectrum of L-B coated tapers were used as response indicators to a chemical stimulus.

The 5μm diameter taper exhibited a channeled spectrum that was indicative of interference between two modes of the tapered region. The phase of the channeled spectrum was dependant on the thickness of the overlay. Also with the increase of coating thickness the transmission spectrum within the wavelength range of presented experiments decreases, and after a certain number of layers reappears with lower intensity. This phenomenon occurs periodically with the overlay deposition. This can be explained by the same theory as for the 37μm taper case: the forming of a coupled waveguide between the taper and the coating. Broad resonance bands were developed, which showed strong dependence on the thickness of a coating layer. The reduction in intensity and disappearance of the channelled spectrum results from increased attenuation of one of the modes, as the phase matching decreases with the coating thickness increase. In case of 5μm tapered fibres the phase channeling in the spectrum showed big sensitivity to the overlay thickness increase, which occurred as a transmission spectrum shift. Therefore study of the application potential of 5μm tapers were based on the channeled spectrum phase shift phenomenon.

Electrostatic-self-assembly

Tapered fibres coated with functional layers composed of three different pairs of materials: 1) PAH and TSPP, 2) TiO_2 nanoparticles imprinted with NPAN ((1-(4-Nitrophenylazo)-2-naphthol (NPAN) compound), 3) PAH and cyclodextrine, are

discussed here. The first pair of compounds showed the biggest response of the transmission spectrum of a taper to the increase of number of layers. Therefore the biggest interest was devoted for this type of coating and for further ammonia sensing potential study of tapers PAH /TSPP coated. Results show the transmission intensity decrease and spectrum shift in response to the coating thickness increase. No resonance band forming during the deposition was recorded for 20μm fibre tapers and above because of strong light absorption by the overlay during the deposition of more than 10 bi-layers. A strong transmission intensity decrease was observed for the 5μm tapers coated with one bi-layer of an overlay. Therefore tapers with waist diameters from the range: 9 - 12μm were studied. The recorded shift of the transmission spectrum due to the number of bi-layers increase is attributed to the phase change of cladding modes.

Chemical coating

Tapered fibres coated with the polyaniline film using chemical deposition technique are discussed here. Based upon the deposition of a coating a red-ox sensor was developed. A change in response to an external stimulus was shown. Results show the decrease of the transmission intensity with the growing polyaniline layer thickness. No resonance band forming during the deposition was recorded. This can be attributed to the optical quality of the formed overlay. The chemical deposition does not assure the molecular ordering thus enabling the film morphology control. During the coating process polymers polyaniline chains are being created which precipitate in the solution and deposit onto a fibre. During whole process already existing molecules are elongated in polymer chains and new created. Thus a randomly formed overlay is created. Therefore the coating does not form a waveguide structure, which would support the mode guidance. Sensing application of polyaniline coated tapers was based on the material absorption phenomenon.

6.3. Application potential of tapered fibres coated with functional layers

L-B coated tapers

Based on the results observation the L-B coated tapers offer greater potential for the sensors development. It is due to the layer thickness control possibilities of the technique. The LB method allows for precise and easy to set process control. There were two different overlay coatings studied within the project: quinolinium iodide for pH application in water environment, and calix[4]resorcinarene for ammonia gas sensing application. Two different waist diameters of tapered fibres were chosen for investigation for both materials: 37 and 5μm and 6μm. The size of tapers was used based upon different phenomenon underlying their sensing.

Quinolinium iodide coated tapers

The results for tapers resolution of $\Delta pH = 0.04$ for 37μm and $\Delta pH = 0.05$ for 6μm taper show promising potential. The comparison with commercially used pH meters is shown in the Table 6.1. The resolution of our sensors is competitive to the commercial ones. In order to enhance tapers' performance a coating material which is more sensitive to the pH change is suggested. Application of a higher resolution spectrum analyzer would also improve the sensing capability of the setup.

pH meter model	Resolution	pH range
Hanna pH Meter model HI 9024	0.01	0-14
37μm taper with L-B coating	0.04	2-10(*)
5μm taper with L-B coating	0.05	4-10
Lehman Scientific pH meter, model 57	0.10	0-14

Table. 6.1. Comparison of chosen commercially used pH meters with tapered fibres coated with calix[4]resorcinarene overlay; (*) the pH range was limited to the range of available buffer solutions used for experiments.

Calix[4]resorcinarene coated tapers

The sensing resolution of the calix[4]resorcinarene coated tapers for ammonia was determined as: ΔC=1.96kppmv for 37μm and ΔC = 2.8 kppmv for 6μm taper. The low resolution of the presented sensors may be attributed to the accuracy of the used setup, which did not have gas concentration control system. The long time response of the sensor to the ammonia is caused by the length time of interaction of the calix[a]resorcinarene with ammonia molecules. The use of a system with gas concentration control would allow for more precise measurements.

ESA coated tapers

Based on the results observation tapers coated with bi-layers of PAH/TSPP using the layer-by-layer electrostatic self assembly method offer great potential for the ammonia gas sensors development. Unlike the ammonia sensing experiments performed on calix[4]resorcinarene coated tapers, here the sensing principle is the absorption phenomenon of the TSPP molecules. The sensitivity of the 10μm taper coated with 5 PAH/TSPP bi-layers was 0.28ppmv, measured within the 10 – 104ppmv concentration range, and fast response time – 100ms - makes the sensor commercially

applicable. The comparison with commercially used ammonia sensors is shown in Table 6.2.

Ammonia detector type	**Detection range (ppmv)**	**Response time (ms)**	**Sensitivity**
10μm taper coated with PAH/TSPP overlay	10 - 104	100	0.320 ± 0.002
Honeywell Vulcain, type Manning EC-F9-NH3 (diffusion based sensor)	0 - 100	Less than 1000	Not given
Figaro, type TGS 826 (semiconductor based sensor)	30 - 300	Not given	0.55 ± 0.15

Table 6.2. Comparison of chosen commercially used ammonia gas detectors with tapered fibre coated with 5 bi-layers of PAH/TSPP.

The presented comparison is based upon the three chosen parameters, which were experimentally measured. In order to achieve ammonia gas sensor competitive to the commercial ones more parameters must be estimated. Application of a higher resolution spectrum analyzer would improve the sensing capability of the setup.

PANI coated tapers

Polyaniline coated tapered fibres show optical response to the red-ox change in the environment which is due to the absorption change of the coating. The immediate response of the sensor is an advantage however the red-ox sensing as well as pH sensing capabilities of PANI are known, broadly studied and described. The aim of the study was to obtain a waveguide formed by polyaniline overlay supporting propagation of cladding modes and thus enabling resonance bands appear in the transmission spectrum and study application potential. It has not been achieved. The reason is believed to be the poor film thickness and structure control of the deposition technique. Thus the

method is not recommendable for an overlay waveguide deposited onto tapered fibres formation.

Based on the results observation the L-B and ESA coated tapers offer greater application potential for the sensors development over the polyaniline coated tapers.

6.4 Tapered optical fibres imprinted with tilted fibre Bragg gratings (TFBGs)

The initial results for tapered optical fibres imprinted with tilted fibre Bragg gratings show promising prospect for sensing applications. The high reflectivity of imprinted gratings is an advantage here. The tapered region of a fibre exposes more the fibre core to the external environment than it is in not tapered fibres. The TFBG being closer to the surrounding is more prone to induce the change in transmission spectrum of a fibre due to change of refractive index. Therefore a suggestion for the future study is coating TFBG written tapers with a functional overlay in order to study optical properties of such system, see Fig. 6.1.

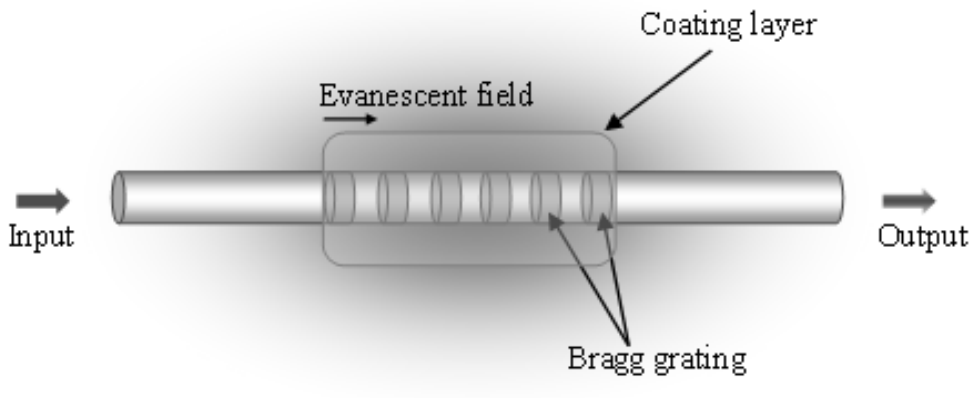

Fig. 6.1. Schematic diagram of a tapered part of as optical fibre with Bragg grating imprinted under a coating layer.

In response to a particular stimulus the absorption spectrum of the coating material will change and thus the change of refractive indices of cladding modes induced, which

results in change of the transmission spectrum. The coating material can be chose so it is specific to chosen compounds.

Summarizing, it has been shown that the presented setup allows for uniform waist diameter tapered fibres fabrication and low transmission loss. Suggestion for the future work in manufacture process would be the development of the fibre taper fabrication system, i.e. application of a CO_2 laser as a heat source and development of the program to facilitate process control, data acquisition and processing. The manufactured tapers are easy to apply to different deposition techniques. Coated tapered fibres proved to have a great application potential in liquid as well as in gaseous environment. The applicability of manufactured sensors depends on the deposition technique utilized while the sensitivity of manufactured sensors strongly depends on the coating material used. Therefore in order to improve the sensing capabilities of coated tapers, other from the presented above functional materials can be used. Suggestion for the future work in application potential would be further study of coated tapers in L-B and ESA deposition process using different coating materials. Imprinting of the tilted period fibre Bragg grating (TFBG) within the tapered region and coating with a functional material to obtain a sensing system for an arbitrary chosen compounds.

APPENDIX A

Maxwell's equations for a source-free medium are the following:

$$\begin{aligned} \nabla \cdot \vec{E} &= 0 \\ \nabla \cdot \vec{H} &= 0 \\ \nabla \times \vec{E} &= -\mu \frac{\partial \vec{H}}{\partial t} \\ \nabla \times \vec{H} &= \varepsilon \frac{\partial \vec{E}}{\partial t} \end{aligned} \tag{A.1}$$

where ∇ is del operator, $\vec{E}$ the electric field, $\vec{H}$ the magnetic field, μ magnetic permeability which is very nearly equal to the free space value μ_0, ε dielectric constant, which is related to the refractive index *n* by $\varepsilon = n^2 \varepsilon_0$ where ε_0 is dielectric constant of free space. Electric and magnetic field in the cylindrical polar coordinates (see Equation A.3) have the form:

$$\begin{aligned} \vec{E}(r, \Phi, z) &= \vec{E}_0(r, \Phi) \exp[i(\omega t - \beta z)] \\ \vec{H}(r, \Phi, z) &= \vec{H}_0(r, \Phi) \exp[i(\omega t - \beta z)] \end{aligned} \tag{A.2}$$

where $\omega = 2\pi f$ is the light frequency, β is the propagation constant, the remaining quantities are depicted in Fig. A.1.

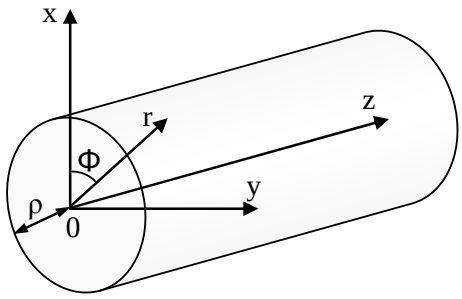

Fig. A.1. Section of circularly symmetric fibre unbound in r- and z-direction. ρ is a core radius; z-axis coincides with the fibre axis of symmetry

For fields defined by equations (A.4), the transverse field components in a circular waveguide are determined to be:

$$E_r = \begin{cases} \dfrac{-i\rho^2}{U^2}\left[\dfrac{\beta U}{\rho}AJ_l'\left(\dfrac{Ur}{\rho}\right)+\dfrac{\omega\mu l}{r}BJ_l\left(\dfrac{Ur}{\rho}\right)\right]\cos(l\Phi+\Psi_l) & r\le\rho \quad \text{(core)} \\ \dfrac{i\rho^2}{W^2}\left[\dfrac{\beta W}{\rho}CK_l'\left(\dfrac{Wr}{\rho}\right)+\dfrac{\omega\mu l}{r}DK_l\left(\dfrac{Wr}{\rho}\right)\right]\cos(l\Phi+\Psi_l) & r\ge\rho \quad \text{(cladding)} \end{cases}$$

$$H_r = \begin{cases} \dfrac{-i\rho^2}{U^2}\left[\dfrac{\omega\varepsilon_1 l}{r}AJ_l\left(\dfrac{Ur}{\rho}\right)+\dfrac{\beta U}{\rho}BJ_l'\left(\dfrac{Ur}{\rho}\right)\right]\sin(l\Phi+\Psi_l) & r\le\rho \quad \text{(core)} \\ \dfrac{i\rho^2}{W^2}\left[\dfrac{\omega\varepsilon_2 l}{r}CK_l\left(\dfrac{Wr}{\rho}\right)+\dfrac{\beta W}{\rho}DK_l'\left(\dfrac{Wr}{\rho}\right)\right]\sin(l\Phi+\Psi_l) & r\ge\rho \quad \text{(cladding)} \end{cases} \qquad \text{(A.3)}$$

$$E_\Phi = \begin{cases} \dfrac{i\rho^2}{U^2}\left[\dfrac{\beta l}{r}AJ_l\left(\dfrac{Ur}{\rho}\right)+\dfrac{\omega\mu U}{\rho}BJ_l'\left(\dfrac{Ur}{\rho}\right)\right]\sin(l\Phi+\Psi_l) & r\le\rho \quad \text{(core)} \\ \dfrac{-i\rho^2}{W^2}\left[\dfrac{\beta l}{r}CK_l\left(\dfrac{Wr}{\rho}\right)+\dfrac{\omega\mu W}{\rho}DK_l'\left(\dfrac{Wr}{\rho}\right)\right]\sin(l\Phi+\Psi_l) & r\ge\rho \quad \text{(cladding)} \end{cases}$$

$$H_\Phi = \begin{cases} \dfrac{-i\rho^2}{U^2}\left[\dfrac{\omega\varepsilon_1 U}{\rho}AJ_l'\left(\dfrac{Ur}{\rho}\right)+\dfrac{\beta l}{r}BJ_l\left(\dfrac{Ur}{\rho}\right)\right]\cos(l\Phi+\Psi_l) & r\le\rho \quad \text{(core)} \\ \dfrac{i\rho^2}{W^2}\left[\dfrac{\omega\varepsilon_2 W}{\rho}CK_l'\left(\dfrac{Wr}{\rho}\right)+\dfrac{\beta l}{r}DK_l\left(\dfrac{Wr}{\rho}\right)\right]\cos(l\Phi+\Psi_l) & r\ge\rho \quad \text{(cladding)} \end{cases}$$

Where J_l is lth-order Bessel function, K_l is lth-order modified Bessel function, J_l' and K_l' are their derivatives respectively; l is the azimuthal mode number (positive integral); Ψ_l is a constant; ω is the light frequency. The quantities $U=\sqrt{n_1^2k_0^2-\beta^2}$ and $W=\sqrt{\beta^2-n_2^2k_0^2}$ are dimensionless modal parameters and often are referred to eigenvalues of the core and cladding, respectively; $k_0=\omega\sqrt{\varepsilon_0\mu_0}=\omega/c$ is the vacuum wavenumber. Coefficients A-D can be determined when the fields are subjected to

boundary conditions. The solution of the above equations exists when the determinant of the coefficients equals zero.

$$\begin{vmatrix} J_l & 0 & -K_l & 0 \\ \frac{\beta l}{U^2} J_l(U) & \frac{\omega\mu}{U} J_l'(U) & \frac{\beta l}{W^2} K_l(W) & \frac{\omega\mu}{W} K_l'(W) \\ 0 & J_l(U) & 0 & -K_l(W) \\ \frac{\omega\varepsilon_1}{U} J_l'(U) & \frac{\beta l}{U^2} J_l(U) & \frac{\omega\varepsilon_2}{W} K_l'(W) & \frac{\beta l}{W^2 K_l(W)} \end{vmatrix} = 0 \qquad \text{(A.4)}$$

Calculation of this determinant leads to the eigenvalue equation, which is the characteristic for the step-index circular fibre:

$$\left[\frac{J_l''(U)}{UJ_l(U)} + \frac{K_l'(W)}{WK_l(W)}\right]\left[n_1^2 \frac{J_l'(U)}{UJ_l(U)} + n_2^2 \frac{K_l'(W)}{WK_l(W)}\right] = l^2 \frac{\beta^2}{k_0^2}\left(\frac{1}{U^2} + \frac{1}{W^2}\right)^2 . \qquad \text{(A.5)}$$

The solutions of this equation are the modes of a fibre, which are represented by values of β. Modes which does not have the axial component of the electric field $E_z = 0$ are called transverse electric (TE). Modes with $H_z = 0$ are called transverse magnetic (TM). In optical waveguides, in general, modes are hybrid, having both E_z and H_z components. They are marked HE_{lm} and EH_{lm} modes, depending on whether H_z or E_z makes larger contribution. HE and EH modes are polarization degenerate, whilst TE and TM modes are not. The electric field distribution in six lower order modes is presented in Fig. A.2.

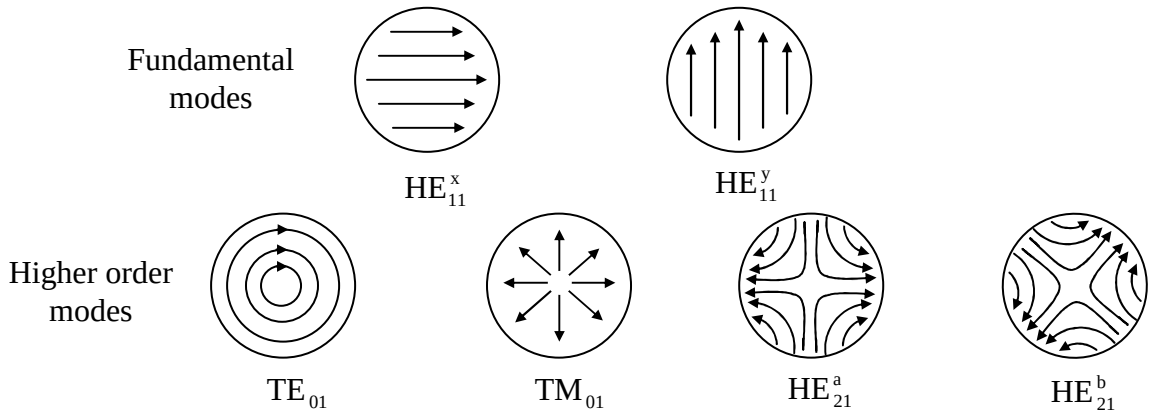

Fig. A.2. Electric field distribution of first six lower order modes, including the polarization degeneration of the modes HE_{11} and HE_{21} (insert after [Hunsperger, R.G. 1994]).

Modal fields of an optical waveguide depend on physical quantities such as geometry of the fibre cross-section, refractive index profile, radius and wavelength of the light source. From these quantities the dimensionless parameter V is formed, which is called the normalized frequency, waveguide or fibre parameter:

$$V = \frac{2\pi\rho}{\lambda}\sqrt{n_{\mathrm{co}}^2 - n_{\mathrm{cl}}^2} \tag{A.6}$$

where n_{co} is the refractive index of the core, n_{cl} is the refractive index of the cladding. The V parameter is proportional to the frequency via $f = c/\lambda$, but it is more convenient to define it in terms of λ, since wavelength is more easily measured. The number N of possible modes that can propagate in a step-index fibre can be estimated from the equation:

$$N = \frac{V^2}{2} \tag{A.7}$$

This equation is valid for large values of V. For small values of V the exact of modes must be determined.

The next parameter, which is used to determine guidance properties of fibre, is the profile height parameter Δ defined as:

$$\Delta = \frac{n_{co}^2 - n_{cl}^2}{2n_{co}^2} \cong \frac{n_{co} - n_{cl}}{n_{co}} = \frac{\Delta n}{n_{co}} \quad \text{(A.8)}$$

Standard telecommunication fibres usually satisfy the condition $\Delta \ll 1$. Fibres with such properties are called weakly-guiding fibres hence large portion of light is carried in the cladding.

The modes of weakly guiding circular fibre are sometimes represented as LP modes after [Gloge. D. 1971]. It has been shown by [Synder, A. *et al*. 2000; Gloge. D. 1971] that, for weakly guiding fibres, the higher order exact modes are degenerate. Linear combination of these modes can be chosen to yield linearly polarized LP modes. Nomenclature emphasizes that the field is polarized in one direction everywhere along a waveguide. The combinations of the degenerate modes into LP_{lm} ones show common intensity pattern, although there is field configuration difference, see Fig. A.3.

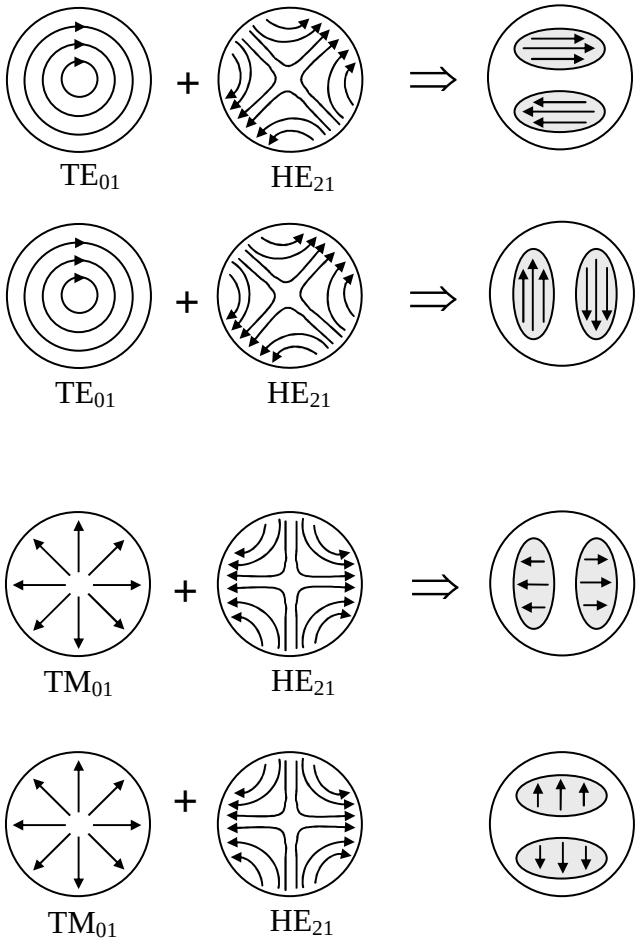

Fig. A.3. Composition of four LP_{11} modes from the exact modes. Intensity distribution and electric field direction depicted (insert after [Hunsperger, R.G. 1994]).

If the propagation constants of the contributing modes slightly differ, then the field superposition changes as the mode propagates along the fibre.

APPENDIX B

```
   Tapered fibre performance modelling - effective index vs overlay thickness


clear all
close all


Define refractive indices
n1=1;                          %air
nlb=1.57;                      %refractive index of the overlay material
dclad =2e-6;
nclad=1.458;

n2=nlb;
n3=nclad;
n4=nlb;
n5=n1;
n=[n1,n2,n3,n4,n5];


Define thickness
thick=40;
dlb=linspace(0e-9,300e-9,thick);    %array for the thickness of the LB
                                       overlay



Define the wavelength range
points=100;
lambda=linspace(600e-9,700e-9,points);


Electric field amplitudes in the layers of the waveguide structure
Ep=[0,0,0,0,1];
Em=[0,0,0,0,0];

Define the wavevector
ko=2*pi./lambda;


Array of values of effective index in the 1st layer (air)
theta=zeros(1,5);
dlb1=2e-7;
neffmid=double((nclad+n1)/2);
neffmax=double(neffmid+0.1);
neffmin=double(neffmid-0.1);
neffmax=1.45;
neffmin=1.0;
pts=10000;neff=linspace(neffmin,neffmax,pts);
```

```
This section scans through the range of effective indices in region 1,
considering refraction at the boundaries, calculates the reflection and
transmission coefficients at each boundary


for h=1:pts                                                %scan of the effective
indicies
    theta(1,h)=double(asin(neff(h)/n(1)));                 %calculates the angle
of propagation in layer 1.

    for l=2:5                                              %l defines the layer in
which the angle is calculated
        theta(l,h)=double(asin(sin(theta(l-1,h))*n(l-1)/n(l)));   %calculates
the angle of propagation in each layer (Snell's law)

    end

    for l=1:5
            if real(cos(theta(l,h)))==0
               theta(l,h)=theta(l,h)+180;
              end
         end

      for l=1:4
         r(l,h)=double((n(l)*cos(theta(l,h))-
n(l+1)*cos(theta(l+1,h)))/(n(l)*cos(theta(l,h))+n(l+1)*cos(theta(l+1,h))));
%reflection coefficient

t(l,h)=double((2*n(l)*cos(theta(l,h)))/(n(l)*cos(theta(l,h))+n(l+1)*cos(theta(l
+1,h))));       %transmission coefficient
      end
end


This section calculates the effective index of each cladding mode as a function
of wavelength and as a function of the thickness of the overlay

 for w=1:thick          %loop through the thicknesses of the LB film

   d=[0,dlb(w),dclad,dlb(w)];


for m=1:points          %wavelength loop
   chk=[w,m]

for h=1:pts             %effective index loop

         for l=1:4      %layer loop


            delta(l)=double(ko(m)*n(l)*d(l)*cos(theta(l,h)));         %phase
change on propagating through the layer
```

```
Calculate matrix elements

S(1,[1,2],l)=double([(exp(i*delta(l)))/t(l,h),r(l,h)/t(l,h)*exp(i*delta(l))]);
            S(2,[1,2],l)=double([r(l,h)/t(l,h)*exp(-i*delta(l)),(exp(-
i*delta(l)))/t(l,h)]);
         end

         %the following calculates the electric field in each layer
         for l=4:-1:1
            Ep(l)=S(1,[1 2],l)*[Ep(l+1);Em(l+1)];
            Em(l)=S(2,[1 2],l)*[Ep(l+1);Em(l+1)];

         end

         %calculate the ratio of the electric field amplitude in the cladding
to that in layer 1.
         %generates a series of peaks, each representing a cladding mode
         f1(h)=(abs(Ep(3)/Ep(1)))^2;
         f2(h)=(abs(Em(3)/Em(1)))^2;

    end


Search though the peaks generated in the previous section to identify the
effective index of each cladding mode


    q=1;
 flag=1;

   for h=pts:-1:2

    if h==pts
       fcheck=f1(h);

   else if f1(h)>fcheck
         fcheck=f1(h);
         flag=1;
      end
   end

   if f1(h)<fcheck
      if flag==1
          neff(h-1)
          neffective(q,m,w)=neff(h-1);
          flag=-1;
          q=q+1;
      end
       fcheck=f1(h);
    end

    end
```

```
end

 end
for i=1:thick
    i
Intensity(:,:,i)=1+cos((2*pi./lambda).*(neffective(2,:,i)-
neffective(3,:,i))*1e-3);
end


Plot dispersion curves for selected cladding modes

figure(1);
plot(lambda,neffective(1,:,1),lambda,neffective(2,:,1),lambda,neffective(3,:,1)
,lambda,neffective(4,:,1))
figure(2)
plot(dlb,squeeze(neffective(2,1,:)))
figure(3)
plot(lambda,squeeze(Intensity(1,:,:)))
%wk1write('nanowire index 157 3-300nm.wk1',squeeze(neffective(:,1,:))')
%wk1write('dlb.wk1',1e9*dlb)
figure(4)
colormap gray
X=1:300/thick:300;
surf(lambda',X,squeeze(Intensity(1,:,:))')
```

APPENDIX C

List of publications

1. R. Jarzebinska, C. S. Cheung, S. W. James, G. J. Ashwell and R. P. Tatam, ”Response of the transmission spectrum of tapered optical fibres to the deposition of nanostructured coating”, *International Conference on Optical Fibre Sensors (OFS) Proceedings*, 2008

2. R. Jarzebinska, C. S. Cheung, S. W. James, G. J. Ashwell and R. P. Tatam, ”Response of the transmission spectrum of tapered optical fibres to the deposition of nanostructured coating”, *Measurement Science and Technology*, Vol. 034001- 034007 , 2009